AD 787 313

AD-787 313

A STUDY OF RHEOLOGIC PROPERTIES OF ESTUARIAL SEDIMENTS

R. B. Krone

California University

Prepared for:

Committee on Tidal Hydraulics (Army)

September 1963

DISTRIBUTED BY:

NTIS

National Technical Information Service
U. S. DEPARTMENT OF COMMERCE

US-CE-C Property of the United States Government

GC 303
C6t
no. 7

TECHNICAL BULLETIN NO. 7

A STUDY OF RHEOLOGIC PROPERTIES OF ESTUARIAL SEDIMENTS

by

R. B. Krone

September 1963

Prepared for

Committee on Tidal Hydraulics
CORPS OF ENGINEERS, U. S. ARMY

Under

Contract No. DA-22-079-civeng-61-7

by

Hydraulic Engineering Laboratory

and

Sanitary Engineering Research Laboratory
University of California
Berkeley

PRESENT MEMBERSHIP OF
COMMITTEE ON TIDAL HYDRAULICS

Members

J. B. Tiffany	Waterways Experiment Station	Chairman
J. C. Lockett	North Pacific Division	Recorder
J. M. Caldwell	Coastal Engineering Research Center	
A. B. Davis, Jr.	Galveston District	
T. Saville, Jr.	Coastal Engineering Research Center	
J. R. Johnston	North Atlantic Division	
C. P. Lindner	South Atlantic Division	
J. B. McAleer	New England Division	
E. A. Schultz	San Francisco District	
H. B. Simmons	Waterways Experiment Station	
P. A. Becnel, Jr.	New Orleans District	

Liaison

J. H. Douma	Office, Chief of Engineers

Consultants

Dr. Arthur T. Ippen	Massachusetts Institute of Technology
Dr. G. H. Keulegan	Waterways Experiment Station
Dr. D. W. Pritchard	Johns Hopkins University
Mr. C. F. Wicker	Consulting Engineer, Philadelphia

U. S. ARMY ENGINEER WATERWAYS EXPERIMENT STATION
CORPS OF ENGINEERS
OFFICE OF THE DIRECTOR
VICKSBURG, MISSISSIPPI 39181

REFER TO WESAR

28 January 1965

Errata Sheet

Committee on Tidal Hydraulics, Technical Bulletin No. 7

A STUDY OF RHEOLOGIC PROPERTIES OF

ESTUARIAL SEDIMENTS, by R. B. Krone

September 1963

Please make the following changes in the text of the report.

1. Page xi, List of Figures: Change page 71 for Figure 38 to page 69.
2. Page 1, top paragraph: Add to last line, after United States and, for comparison, from an inland fresh-water stream, the White River.
3. Page 3, Sample Sources: Two samples of Delaware River sediment were used in this study. Sample one, shown at the bottom of the list, was provided by the Beach Erosion Board for use in an earlier study. Sample Two, shown at the top of the list, was furnished by the Wilmington, Delaware, field office of the Philadelphia District, not the Wilmington District. The latter sample is designated "Wilmington District" throughout the report to distinguish it from Sample One.
4. Page 4, Figure 1: Ordinate Value: Change 0.1 to 0.2.
   Abscissa Designation: Delete 10 between d and μ so that it reads ... STOKE'S DIAMETER, d, μ.
5. Page 36, Table V, Middle Column Heading: Change the unit Energy of Cohesion from dynes/cu cm to dyne cm/cu cm.

6. Page 46, Lines 27, 30, and 34: Change Figure No. 22 to 23.
7. Page 47, Lines 13 and 15: Change Figure No. 22 to 23.
8. Page 47, Lines 19 and 37: Change Figure No. 23 to 24.
9. Page 49, Line 1: Change Figure No. 22 to 23; and 23 to 24.
10. Page 49, Line 10: Change Figure No. 24 to 25; and 29 to 30.
11. Page 49, Line 11: Change Figure No. 30 to 31.
12. Page 49, Line 20: Change Figure No. 23 to 24.
13. Page 49, Line 24: Change Figure No. 24 to 25.
14. Page 49, Line 29: Change Figure No. 25 to 26.
15. Page 49, Line 32: Change Figure No. 25 to 26.
16. Page 51, Figure 25: The ordinate values, representing the Relative Differential Viscosity, should range from a low of 1.0 to a high of 10.0 (not 0.1 to 1.0).
17. Page 52, Figure 26: The ordinate values, representing the Relative Differential Viscosity, should range from a low of 1.0 to a high of 30.0 (not 0.1 to 3.0).
18. Page 54, Figure 28: The units for RELATIVE DIFFERENTIAL VISCOSITY as ordinates are shown incorrectly as η_d , dyne sec/sq cm Replace this with η_d/η_1.
19. Page 68, Lines 7 and 8: Change Figure No. 24 to 25; and 29 to 30.
20. Page 71, Mismatch: Change Figures 30 through 36 to read 31 through 36.

A STUDY OF RHEOLOGIC PROPERTIES OF ESTUARIAL SEDIMENTS

FINAL REPORT

Prepared for the Committee on
Tidal Hydraulics under Contract
DA-22-079-CIVENG-61-7 with the
Waterways Experiment Station,
Corps of Engineers, U.S. Army

By

R. B. Krone

Faculty Investigators

H. A. Einstein
W. J. Kaufman
G. T. Orlob

D D C
OCT 1974
D

September 1963

Hydraulic Engineering Laboratory
and
Sanitary Engineering Research Laboratory
University of California
Berkeley

SERL Report No. 63-5

DISTRIBUTION STATEMENT A
Approved for public release;
Distribution Unlimited

FOREWORD

A laboratory study on properties of sediment, such as this one, is a necessary step toward understanding the behavior of the material in any of the complex environments in streams, estuaries, or oceans. The reason for conducting a study in the laboratory stems from the need for controlling the conditions under which the measurements are made. Before the results of a laboratory study can be utilized to obtain knowledge of sediment behavior in any particular location, means are required for describing sediment behavior from knowledge of the environment and of the sediment properties. In addition to reporting measurements on properties of cohesive sediments, therefore, an effort was made to present means of applying the resulting data. The measurements and appropriate discussions are presented in Chapters II, III, and IV. Methods of application are presented in Chapter V. Further application awaits more detailed knowledge of the transporting environment.

40220

TABLE OF CONTENTS

	Page
FOREWORD	iii
LIST OF TABLES	vii
LIST OF FIGURES	ix
LIST OF SYMBOLS	xiii
Chapter	
I. INTRODUCTION	
Objective of Study	1
Acknowledgments	1
II. SEDIMENTS USED FOR STUDY	
Particle Size Distribution	3
Cation Exchange Capacities	5
Mineral Compositions	5
III. RHEOLOGICAL MEASUREMENTS USING A CAPILLARY VISCOMETER	
The Capillary Viscometer	9
Theory of Capillary Viscometer	9
Calibration of Capillary Viscometer	11
Measurements on Suspensions of Cohesive Sediments	13
Relative Differential Viscosities	13
Bingham Yield Strengths	25
Viscous Properties of Suspensions at Low Salinities	25
Discussion	34
Conclusions	38
IV. RHEOLOGICAL MEASUREMENTS USING A ROTATING CYLINDER VISCOMETER	
The Rotating Cylinder Viscometer	39

TABLE OF CONTENTS (continued)

Chapter		Page
	Theory of Rotating Cylinder Viscometer	41
	Calibration of Rotating Cylinder Viscometer	42
	Viscous Behavior of Suspensions of Cohesive Sediments	46
	Measurement Procedure	46
	Data Obtained from Sediment Suspensions	47
	Discussion	65
	Relative Differential Viscosity Data	68
	Bingham Shear Strength Data	70
	Conclusions	73
V.	APPLICATIONS OF RHEOLOGICAL DATA	
	The Shoal Surface	77
	The Suspended Aggregate	79
	Aggregation	79
	Particle Size	80
	Particle Shear Strength	81
	Particle Density	83
	Particle Settling Velocity	83
	Shoaling	84
	Conclusions	86
VI.	SUMMARY AND CONCLUSIONS	89
REFERENCES		91

LIST OF TABLES

Table	Title	Page
I.	Cation Exchange Capacities of Sediments Studied	5
II.	Mineral Composition of Sediment Samples Determined from X-Ray Diffraction Analysis	6
III.	Description of Capillary Viscometer	11
IV.	Densities of Flocs in the Capillary Viscometer	24
V.	Particle Aggregate Shear Strengths	36
VI.	Description of Rotating Cylinder Viscometer with Air Bearings	44
VII.	Observed and Calculated Coefficients for the Shear Strength-Sediment Concentration Relation	72
VIII.	Integers N and (n-2), Shown as N,(n-2)	73
IX.	Properties of Sediment Aggregates	74
X.	Average Shearing Rates in a Channel 30 Feet Deep	84

LIST OF FIGURES

Figure	Title	Page
1.	Particle Size Distributions of Sediments Investigated . .	4
2.	Plot of Viscometer Data for Determination of Capillary Radius and Internal Head	12
3.	Plot of Viscometer Data to Determine Differential Viscosities and Bingham Shear Strengths	14
4.	Relative Differential Viscosities of Wilmington District Sample from Capillary Viscometer Measurements	15
5.	Relative Differential Viscosities of Brunswick Harbor Sample from Capillary Viscometer Measurements	16
6.	Relative Differential Viscosities of Gulfport Channel Sample from Capillary Viscometer Measurements	17
7.	Relative Differential Viscosities of San Francisco Bay Sample from Capillary Viscometer Measurements	18
8.	Relative Differential Viscosities of Delaware River Sample from Capillary Viscometer Measurements	19
9.	Relative Differential Viscosities of Potomac River Sample from Capillary Viscometer Measurements	20
10.	Relative Differential Viscosities of White River Sample from Capillary Viscometer Measurements	21
11.	Shear Strengths of Wilmington District Sample from Capillary Viscometer Measurements	26
12.	Shear Strengths of Brunswick Harbor Sample from Capillary Viscometer Measurements	27
13.	Shear Strengths of Gulfport Channel Sample from Capillary Viscometer Measurements	28
14.	Shear Strengths of San Francisco Bay Sediment from Capillary Viscometer Measurements	29
15.	Shear Strengths of Delaware River Sample from Capillary Viscometer Measurements	30
16.	Shear Strengths of Potomac River Sample from Capillary Viscometer Measurements	31
17.	Shear Strengths of White River Sample from Capillary Viscometer Measurements	32

LIST OF FIGURES (continued)

Figure	Title	Page
18.	Bingham Shear Strength Changes with Salinity	35
19.	Relation between Shear Strength and Cation Exchange Capacity for Sediment Samples	37
20.	Essential Parts of Rotating Cylinder Viscometer	40
21.	Plot for Determination of Torque Constant of Torsion Wire	43
22.	Check for Laminar Flow in Rotating Cylinder Viscometer . .	45
23.	A Plot of Raw Viscometer Data Obtained from the Wilmington District Sample	48
24.	Data Obtained from Repeated Sequences of Measurements on a San Francisco Bay Sample	50
25.	Relative Differential Viscosities of Wilmington District Sample from Rotating Cylinder Viscometer Measurements .	51
26.	Relative Differential Viscosities of Brunswick Harbor Sample from Rotating Cylinder Viscometer Measurements .	52
27.	Relative Differential Viscosities of Gulfport Channel Sample from Rotating Cylinder Viscometer Measurements .	53
28.	Relative Differential Viscosities of San Francisco Bay, Sample Two, from Rotating Cylinder Viscometer Measurements	54
28a.	Relative Differential Viscosities of San Francisco Bay, Sample One, from Rotating Cylinder Viscometer Measurements	55
29.	Relative Differential Viscosities of White River Sample in Salt Water from Rotating Cylinder Viscometer Measurements	56
30.	Relative Differential Viscosities of White River Sample in Tap Water from Rotating Cylinder Viscometer Measurements	57
31.	Shear Strengths of Wilmington District Sample from Rotating Cylinder Viscometer Measurements	58
32.	Shear Strengths of Brunswick Harbor Sample from Rotating Cylinder Viscometer Measurements	59

LIST OF FIGURES (continued)

Figure	Title	Page
33.	Shear Strengths of Gulfport Channel Sample from Rotating Cylinder Viscometer Measurements	60
34.	Shear Strengths of San Francisco Bay, Sample Two, from Rotating Cylinder Viscometer Measurements	61
34a.	Shear Strengths of San Francisco Bay, Sample One, from Rotating Cylinder Viscometer Measurements	62
35.	Shear Strengths of White River Sample in Salt Water from Rotating Cylinder Viscometer Measurements	63
36.	Shear Strengths of White River Sample in Tap Water from Rotating Cylinder Viscometer Measurements	64
37.	A Two-Dimensional Representation of a Particle Aggregate Aggregate Aggregate Aggregate, p4a	66
38.	Test of Equation 16	71

LIST OF SYMBOLS

Descriptive symbols are used where possible, with appropriate subscripts wherever similar units need to be distinguished. Only cgs units are used in formulas.

Symbol	Definition
c	concentration by weight
d	diameter
D	dial reading
E_v	energy of cohesion per unit volume
E_m	energy of cohesion per unit mass
g	acceleration of gravity
h	head or thickness of layer of sediment
H	height of fluid in annulus
k	relative differential viscosity constant, cu cm/g
K	empirical constant
K_s	hydrostatic pressure ratio
ℓ	length of capillary
N	rotation rate of outer cylinder, rpm
p	pressure required to overcome shear strength of suspension in capillary
P	driving pressure
q	tangential velocity
Q	discharge
r	radius
R	radius of capillary or floc
ΔR	interpenetration of colliding flocs
t	time
T	torque
u	velocity in x direction
v	average velocity
V	volume
z	distance in z direction

LIST OF SYMBOLS (continued)

Symbol	Definition
ϵ	void ratio
ρ	density
σ	compressive stress
Φ	volume fraction
η	viscosity
η_d	differential viscosity
τ	shear stress
τ_B	Bingham yield stress
ω	angular velocity

General Subscripts

ℓ	liquid
s	suspension
p	primary particle
a	aggregate
pa	particle aggregate
paa	particle aggregate aggregate
f	floc

I. INTRODUCTION

Studies of estuarial sediment transport processes have been limited to a few estuaries where expensive maintenance has motivated investigation. Such studies of sediment transport in portions of San Francisco Bay, and laboratory studies using Bay sediments, were conducted by the University prior to 1961 for the San Francisco District, Corps of Engineers. During the course of these studies several laboratory measurements of physical properties of the sediments were found useful for characterizing the sediment's transport properties, particularly the properties that determine the stability of deposits. These laboratory measurements are used in the present study to extend the knowledge of estuarial sediment transport to other estuaries. This report presents laboratory measurements made on sediments from five estuaries selected by the Committee on Tidal Hydraulics, C. E., as representative of important estuaries of the United States.

Objective of Study

The objective of this study includes the determination of rheological properties of sediments from a variety of estuaries for the purposes of obtaining information on the stability of deposits and on the character of sediment during transport. Such information is needed for descriptions of shoaling processes.

Acknowledgments

Sediments studied during this investigation were provided by personnel in several branches of the Corps of Engineers. Their interest and services materially aided the study. The construction and operation of one of the viscometers used during the study was supported by the National Science Foundation for an associated study. The simultaneous need for information on sediment properties by the Corps of Engineers, the desire of the National Science Foundation for basic knowledge of the behavior of fine sediment materials, and the general need for advance in rheology enhanced the desirability of conducting this study. The interest and support of members of branches of the Corps of Engineers and of the National Science Foundation are gratefully acknowledged.

Students who assisted with the measurements include Messrs. S. Nola, K. Moaveni, A. Lubeschitz, and G. Terzides. Secretarial and report preparation services were provided by the staff of the Sanitary Engineering Research Laboratory. The enthusiastic and diligent participation in this study by members of the staff is acknowledged and is sincerely appreciated.

Special acknowledgment is due Professor H. A. Einstein. His enthusiasm, frequent stimulating discussions, counsel, and review of the manuscript are gratefully acknowledged and sincerely appreciated.

II. SEDIMENTS USED FOR STUDY

Samples of sediments causing shoaling problems were provided by branches of the Corps of Engineers from various rivers and estuaries as follows:

Delaware River Estuary*	Wilmington District
Brunswick Harbor	Savannah District
Gulfport Channel	Mobile District
San Francisco Bay	San Francisco District
White River	Omaha District
Potomac River**	Beach Erosion Board
Delaware River**	Beach Erosion Board

These sediments were maintained in a wet condition and transmitted in sealed containers. At no time have the sediments been allowed to dry. No attempt has been made to prevent consolidation during storage, however.

The character of each of the sediment samples was determined by particle size distribution analysis, X-ray diffraction measurements, and determination of cation exchange capacities. These data are shown below.

Particle Size Distribution

Analysis of the samples for particle size distributions was done by the sedimentation method using a hydrometer. The samples were kept wet during pretreatment. Organic matter was oxidized by hydrogen peroxide and dispersed with Calgon.

Particle size distributions of the sediment samples are presented in Figure 1. The plots in Figure 1 show that except for the Brunswick Harbor sediment each of the sediments has a wide, fairly uniform size distribution. The distributions are similar but vary in predominant particle size. The clay fraction (less than 2 microns) ranges from 0.30 to 0.76 of the sediment materials; all of the sediments can be described as clayey.

---

*The Delaware River Estuary sample is hereinafter called the "Wilmington District" sample to distinguish it from the Delaware River sample.

**Samples provided for use in an earlier study.

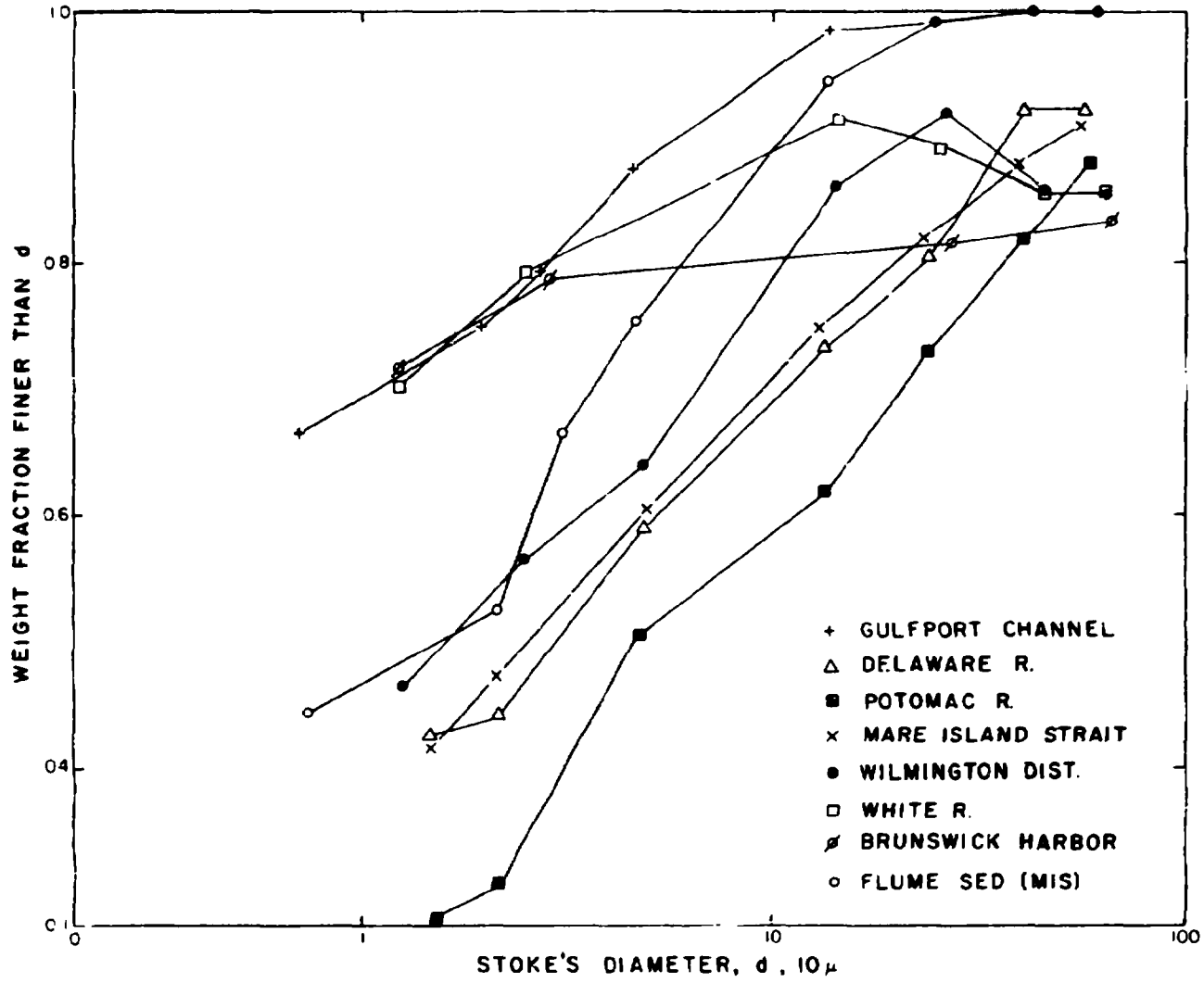

FIGURE 1. PARTICLE SIZE DISTRIBUTIONS OF SEDIMENTS INVESTIGATED

Cation Exchange Capacities

Measurements of cation exchange capacities, by a method described in a previous report [1], were made on whole samples. The measured values are presented in Table I.

TABLE I

CATION EXCHANGE CAPACITIES OF SEDIMENTS STUDIED

Sediment	Cation Exchange Capacity me/100g
Wilmington District	25.5
Brunswick Harbor	30.5
Gulfport Channel	46.8
Mare Island Strait	24.5
Flume Sediment	28.9
Delaware River	15.6
Potomac River	9.1
White River	53.5

The wide range of cation exchange capacities shown in Table I can be due to variations in the amounts of clay mineral kinds in the several sediments. The cation exchange capacities are discussed further in the next section.

Mineral Compositions

Qualitative analyses of the mineral compositions of the sediment samples were made by X-ray diffraction methods on whole samples. The minerals found in the samples are listed in order of abundance in Table II. The order of abundance was taken from the relative amplitudes of the diffraction peaks, and is not completely reliable. The peak heights for montmorillonite and kaolinite were about the same for the Gulfport Channel, Wilmington District, and Mare Island Strait samples, but had a ratio of 1:2 for the Brunswick Harbor sample.

The mineral compositions presented in Table II show that sediments from all of the estuaries sampled are mixtures of minerals. All of the samples contain montmorillonite, and all except the White River sediment contain kaolinite, with other minerals occurring in smaller amounts.

TABLE II

MINERAL COMPOSITION OF SEDIMENT SAMPLES DETERMINED FROM X-RAY DIFFRACTION ANALYSIS

Sample	Mineral Composition	Cation Exchange Capacity, me/100g of < 10μ Fraction
Wilmington District	kaolinite montmorillonite vermiculite quartz	32
Brunswick Harbor	kaolinite montmorillonite chlorite illite vermiculite (?) quartz feldspar	38
Gulfport Channel	montmorillonite kaolinite illite chlorite quartz	49
Mare Island Strait	kaolinite montmorillonite illite chlorite feldspar quartz	34
Delaware River	illite montmorillonite kaolinite quartz	23
Potomac River	kaolinite montmorillonite illite quartz	15
White River	montmorillonite illite quartz feldspar	60

In order further to describe the clay mineral fraction, an estimate of the exchange capacity of the clay mineral fraction was made by dividing the exchange capacities of the whole sediment samples by the fraction having a size less than ten microns. These values are tabulated

in column three, Table II. Past experience [1] indicated that clay minerals occur in sizes larger than two microns, and the ten-micron upper limit was selected to include such minerals. The values in column three, together with the compositions given in Table II, can be used further to characterize the sediments by noting that the predominant clay minerals have widely different exchange capacities. They are, commonly: montmorillonite, 80 to 150 me/100g; illite, 10 to 40 me/100g; kaolinite, 5 to 15 me/100g; and vermiculite, 100 to 150 me/100g. For example, Gulfport Channel, Potomac River, and Mare Island Strait have similar mineral composition but the relative abundances of kaolinite, montmorillonite, and illite are shown by the exchange capacities to be very different.

Figure 1 and Table II show that although the sediments all contain mixtures of the common clay minerals the amount of clay and the relative abundances of the minerals differ widely.

III. RHEOLOGICAL MEASUREMENTS USING A CAPILLARY VISCOMETER

Measurements of flow characteristics on suspensions of San Francisco Bay sediments have been found to provide both insight into the transport processes of these sediments and quantitative descriptions of the shear strength and viscous behavior of sediment suspensions [2]. Such measurements are well suited to study of these properties of sediments from different estuaries for comparative purposes, and for examining the ranges of shear strengths that occur in problem estuaries.

Measurements of rheological properties of the sediments provided for this study, using an Ostwald capillary viscometer, are described in this chapter.

The Capillary Viscometer

The viscometer used for this study and the method of operation have been described in detail in earlier reports and papers [2,3]. A brief description is given here, however, to facilitate presentation of the measurement results. The viscometer consists of a glass U tube, one arm of which is a straight capillary with a small chamber at its upper end. The other arm has an inside diameter of about one centimeter and serves as a reservoir. Marks are engraved in the tubing above and below the small chamber to define a volume. In operation, a measured volume of sediment suspension is placed in the reservoir arm of the tube, and a portion of this suspension is drawn from the reservoir arm through the capillary to fill the small chamber. The time required for the chamber to empty is measured with a stop watch. Variable driving pressures were provided for these studies by means of a vacuum pump and vacuum reservoir connected to the larger arm of the viscometer. A water manometer was also connected to the larger arm to indicate the driving head. The temperature of the viscometer was controlled by a water bath.

Theory of Capillary Viscometer. Capillary viscometers have been used for precise determination of viscosities of liquids for more than half a century. Relations between the driving pressure and flow through a capillary were found by Poiseuille [4] for Newtonian liquids and by Bingham [5] for plastic suspensions. These theories enable interpretation of rheological properties of materials from measurements made using a capillary viscometer, and are summarized to facilitate presentation and discussion of measurements made on estuarial sediments.

Clay-water systems at low clay concentrations have properties of liquids and at high concentrations have properties of plastic solids. The distinction depends on the existence of a shear strength in the plastic solid that must be exceeded by the applied shear before flow can be

Preceding page blank

maintained. Bingham described the shear stress-shearing rate relation for plastic solids as

$$\tau - \tau_B = \eta_d \frac{du}{dz} , \tag{1}$$

where τ is the applied shear, τ_B is the yield value of shear, η_d is a constant herein called the differential viscosity, and du/dz is the shearing rate.* For materials having no shear strength, such as unassociated liquids, Equation 1 reduces to Newton's hypothesis.

Bingham derived his description of flow through a capillary on the assumption of the applicability of Equation 1. Within a central core, bounded by the radius at which $\tau = \tau_B$, material moves as a slug. Shearing takes place in the material between the slug and the capillary wall, with a shearing rate depending on the excess of shear above the yield value. Bingham's relation is

$$\frac{V}{t} = \frac{\pi R^4}{8\eta_d \ell} \left(P - \frac{4}{3}p + \frac{p^4}{3P^3} \right) . \tag{2}$$

V is the volume of the small chamber in the viscometer; t is the time to empty the small chamber; R and ℓ are the radius and length of the capillary; P is the driving pressure; and p is the driving pressure necessary to initiate flow in the capillary by shearing at the wall.

For Newtonian liquids p is zero, and Equation 2 reduces to Poiseuille's Equation. Pressures were measured during these studies by means of a manometer. For convenience, and following custom, the pressures are expressed as pressure heads. The driving head was the resultant of the applied head, a velocity head lost at the downstream end of the capillary, and the average head difference between the arms of the viscometer. Rearranging Equation 2 and putting the pressures in terms of head gives

$$\left(h - \frac{\rho_s}{\rho_\ell} \frac{v^2}{2g} \right) = \left(\frac{8V\ell}{\pi R^4 \rho_\ell g} \right) \frac{\eta_d}{t} + \frac{4}{3} h_B - \frac{\rho_s}{\rho_\ell} h_o . \tag{3}$$

The applied head, h; the velocity head, $v^2/2g$; the head required to overcome the yield strength of the suspensions, h_B; and the average head in the viscometer, h_o, are arranged to facilitate reduction of data. The densities of the suspension, ρ_s, and of the liquid in the manometer, ρ_ℓ, are used to change all heads into heads of water. The bracketed term

*Symbols used in this report are defined on page xiii.

on the right side of Equation 3 contains constants of the system which are lumped together for convenience.

There are no terms in Equation 3 corresponding to $p^4/3P^3$ in Equation 2. The values of P in this work were much larger than p, and the term $p^4/3P^3$ was always less than 0.018 of the applied pressure, so that it was reasonable to neglect the term.

A plot of the left side of Equation 3 against 1/t gives a straight line with an intercept at the 1/t = 0 ordinate of $4h_B/3 - \rho_s h_o/\rho_\ell$ and a slope of $(8V\ell/\pi R^4\rho_\ell g)\eta$. If the system constants h_o and $(8V\ell/\pi R^4\rho_\ell g)$ are known, and if the material behaves according to Bingham's relation, both h_B and η can be determined from measurements on sediment suspensions using a capillary viscometer.

Calibration of Capillary Viscometer. Water has virtually no shear strength, at least not sufficient to be significant in a capillary having the dimensions of the one used in this study. For water, therefore, h_B in Equation 3 is zero. Water has well-known viscosities and its use in the manometer makes $\rho_s/\rho_\ell = 1$. Further, water is the lower limit of the suspension concentration. For these reasons water was selected to calibrate the viscometer.

The volume of the small chamber, V, and the length of the capillary, ℓ, was measured directly. The values of the radius of the capillary, R, and of the average head difference between arms of the viscometer, h_o, was found from measurements using water in the viscometer. Measurements of the time, t, to empty the small chamber were made at several driving pressures. A plot of the left side of Equation 3 vs. 1/t can be found by iteration of R or by trial values of R that give a straight line with a slope of $8V\ell/\pi R^4\rho g$, and an intercept of $-h_o$. Such a plot is shown in Figure 2. The measured and derived characteristics of the capillary viscometer used for this study are listed in Table III.

TABLE III

DESCRIPTION OF CAPILLARY VISCOMETER

Volume of chamber, V	3.3 cu cm
Length of capillary, ℓ	8.5 cm
Radius of capillary, R	0.0286 cm
Average internal head, h_o	11.9 cm of water
$8V\ell/\pi R^4\rho_\ell g$	1.08 cu cm/dyne

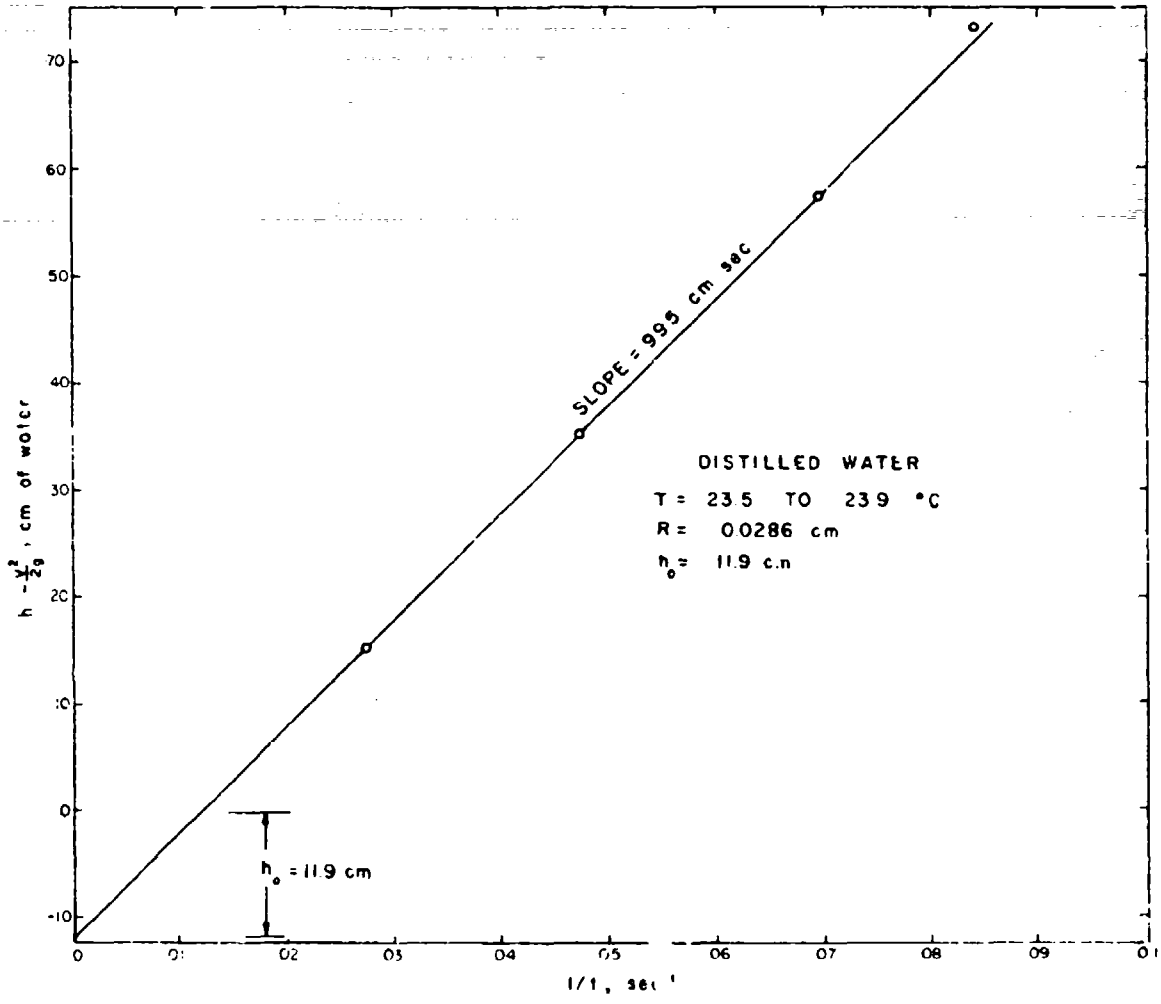

FIGURE 2. PLOT OF VISCOMETER DATA FOR DETERMINATION OF CAPILLARY RADIUS AND INTERNAL HEAD

Measurements on Suspensions of Cohesive Sediments

Samples of the sediments, except that from the White River, were suspended in settled San Francisco Bay water and passed through a 170-mesh sieve to remove bits of wood, shell, and other debris that might clog the capillary. Approximate dilutions of the suspensions were made from measurement, and a portion of each dilution was taken for suspended solids analysis. Five milliliters of a suspension was placed in the reservoir arm of the capillary, and four measurements were made of time for the volume of suspension in the small chamber to flow through the capillary. Stirring between successive measurements was maintained by bubbling air through the suspension. Each suspension was measured at four driving heads. Appropriate values of $h - v^2/2g$ and of $1/t$ were calculated from the manometer readings and the measured times, and were plotted as shown in Figure 3. Intercepts and slopes of the lines of best fit were then used to calculate the yield shear strengths and the differential viscosities of the suspensions at the several suspension concentrations, according to Equation 3, as described above.

Figure 3 is typical of the plots in its fit of plotted points to straight lines. The slopes of the lines can be determined with precision. The intercepts on some of the plots were close together; therefore, the relation between the concentration and yield strength could not be determined with precision.

The range of shearing rates over which the measurements were made are not easily described. The shearing rate is zero in the core and maximum at the capillary wall. Values at the capillary wall, calculated from Equation 1, ranged from 280 to 1400/sec. Average shearing rates calculated as $[(\text{power dissipated per cu cm})/(\text{differential viscosity})]^{1/2}$, ranged from 100 to 440/sec. A wide range of shearing rates having high average values existed in the viscometer. The fit of points to straight lines, as shown in Figure 3, indicates that the suspensions had constant sediment volume fractions over the range of shearing rates prevailing in the capillary viscometer.

Differential viscosities obtained from the slopes of the $h - v^2/2g$ vs. $1/t$ plots are presented in Figures 4 through 10, and the Bingham shear strengths obtained from the intercepts are presented in Figures 11 through 17. For any sediment concentration in the measured range, η_d and τ_B can be obtained from the figures for the appropriate sediment and inserted in Equation 1 to obtain the shear—shearing rate relation. It is more useful, however, to consider the differential viscosity plots and the Bingham shear strength plots themselves for information they provide on cohesive sediment properties.

Relative Differential Viscosities. The plots of relative differential viscosities, presented in Figures 4 through 10, show a logarithmic increase with sediment concentration for the values measured at the maximum salinity. An explanation of the logarithmic relationship will assist interpretation of these plots.

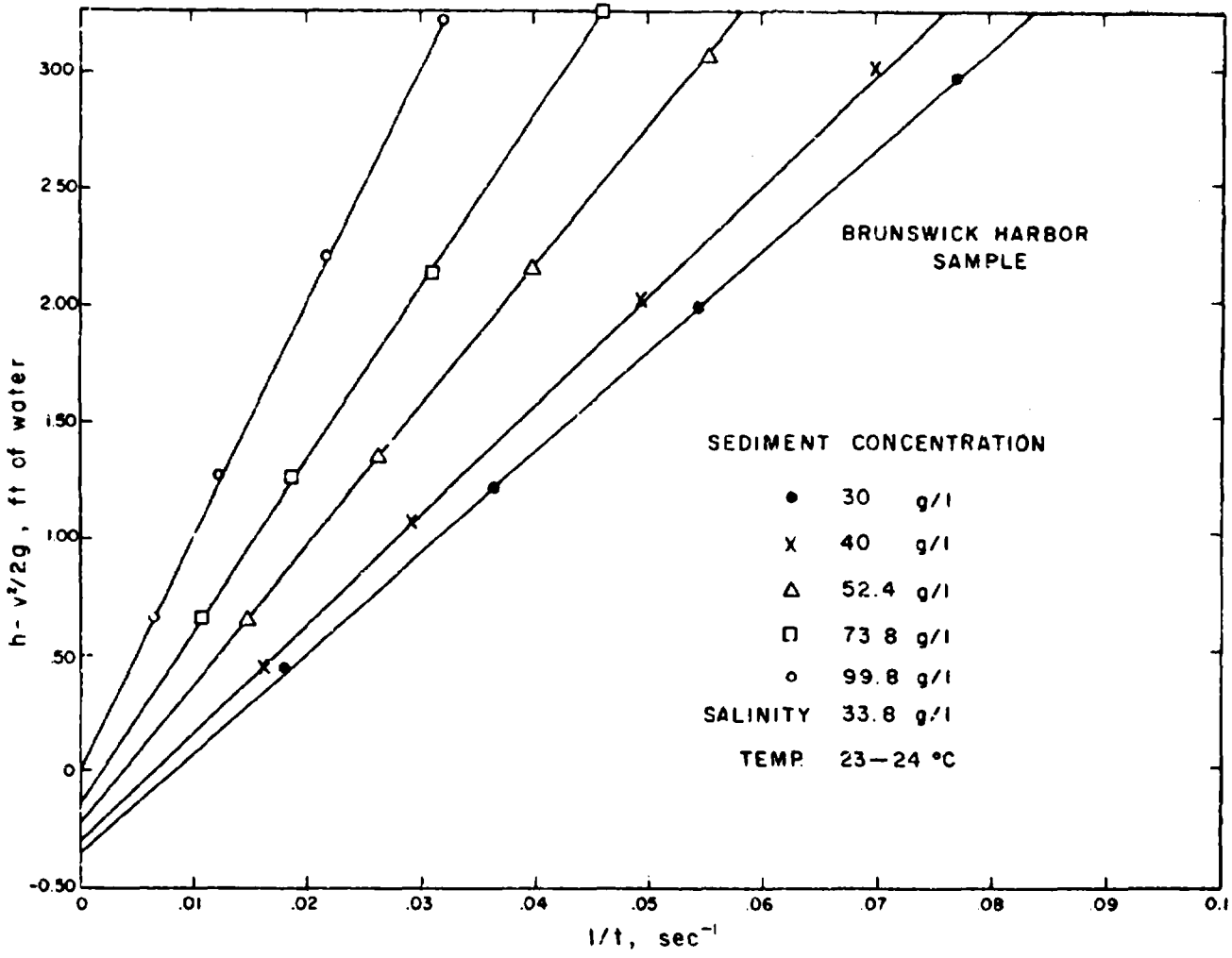

FIGURE 3. PLOT OF VISCOMETER DATA TO DETERMINE DIFFERENTIAL VISCOSITIES AND BINGHAM SHEAR STRENGTHS

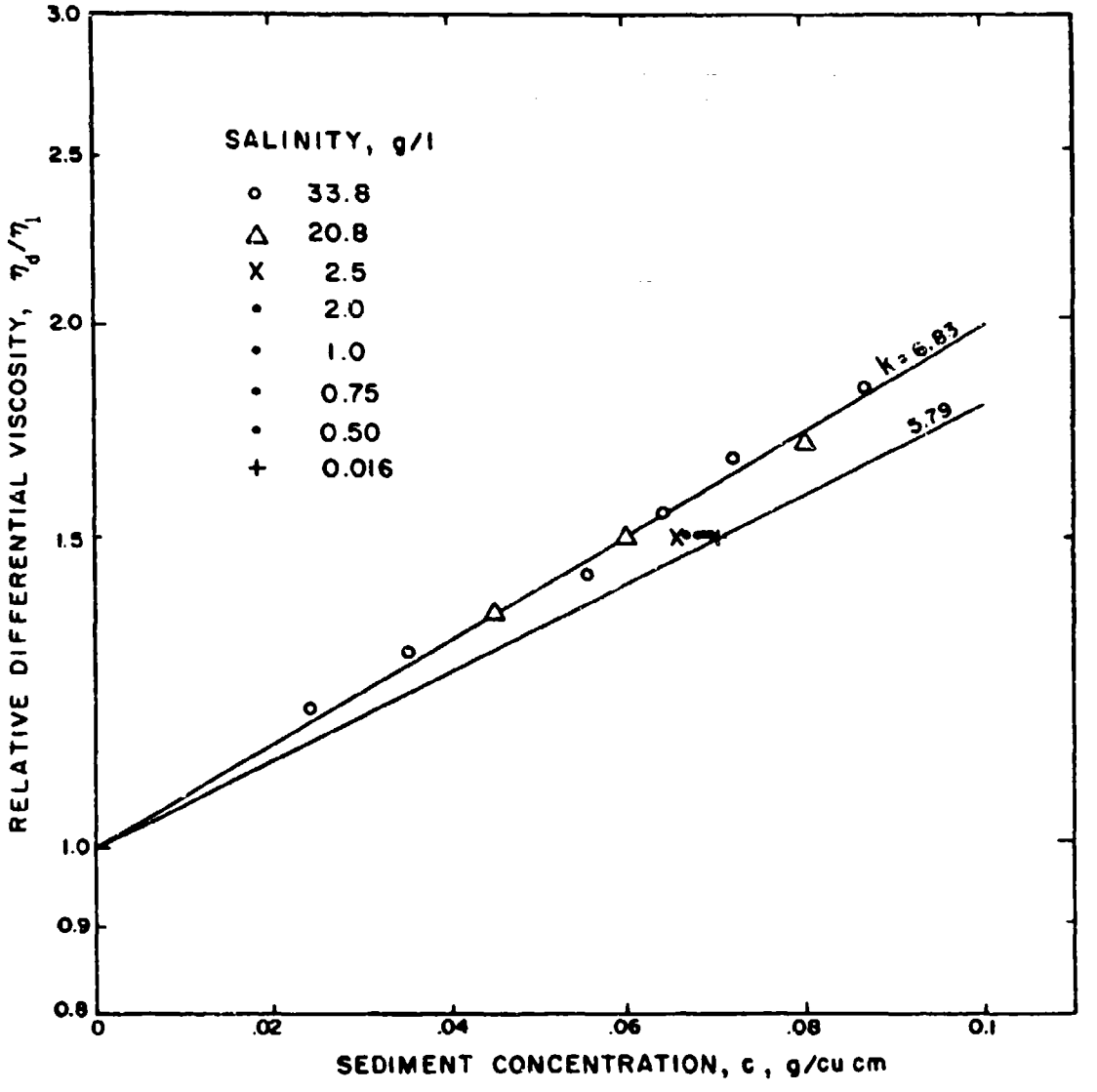

FIGURE 4. RELATIVE DIFFERENTIAL VISCOSITIES OF WILMINGTON DISTRICT SAMPLE FROM CAPILLARY VISCOMETER MEASUREMENTS

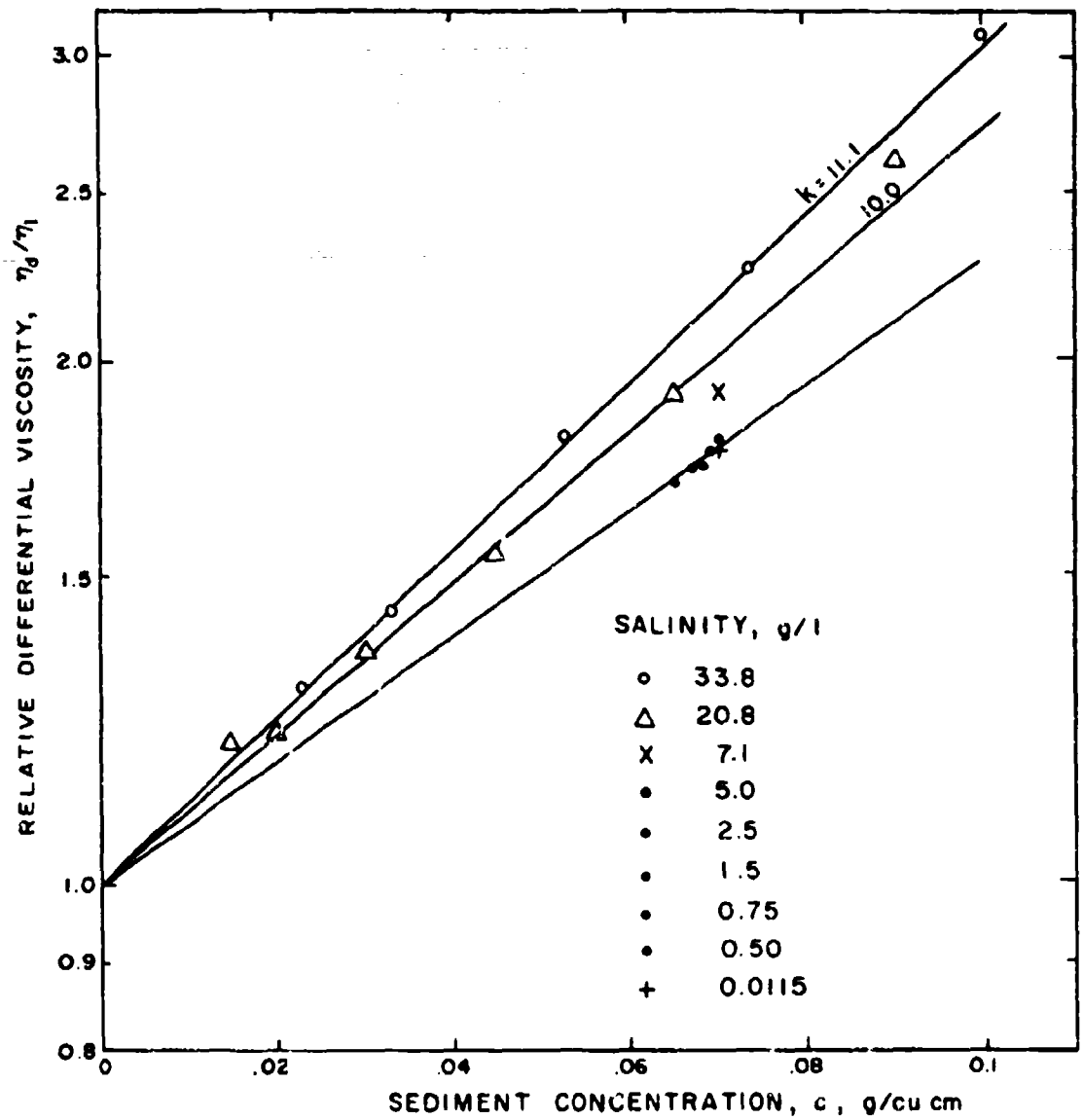

FIGURE 5. RELATIVE DIFFERENTIAL VISCOSITIES OF BRUNSWICK HARBOR SAMPLE FROM CAPILLARY VISCOMETER MEASUREMENTS

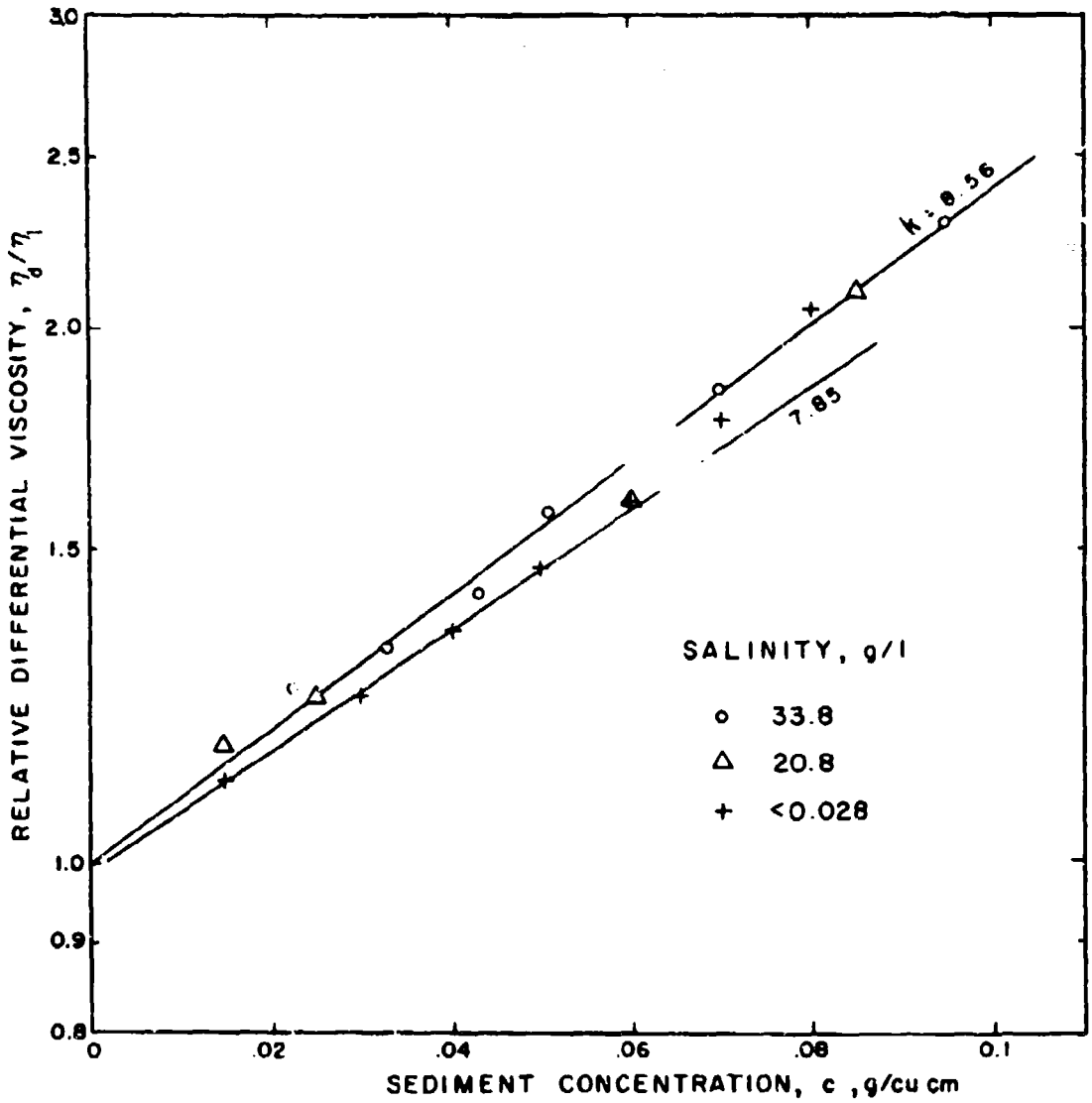

FIGURE 6. RELATIVE DIFFERENTIAL VISCOSITIES OF GULFPORT CHANNEL SAMPLE FROM CAPILLARY VISCOMETER MEASUREMENTS

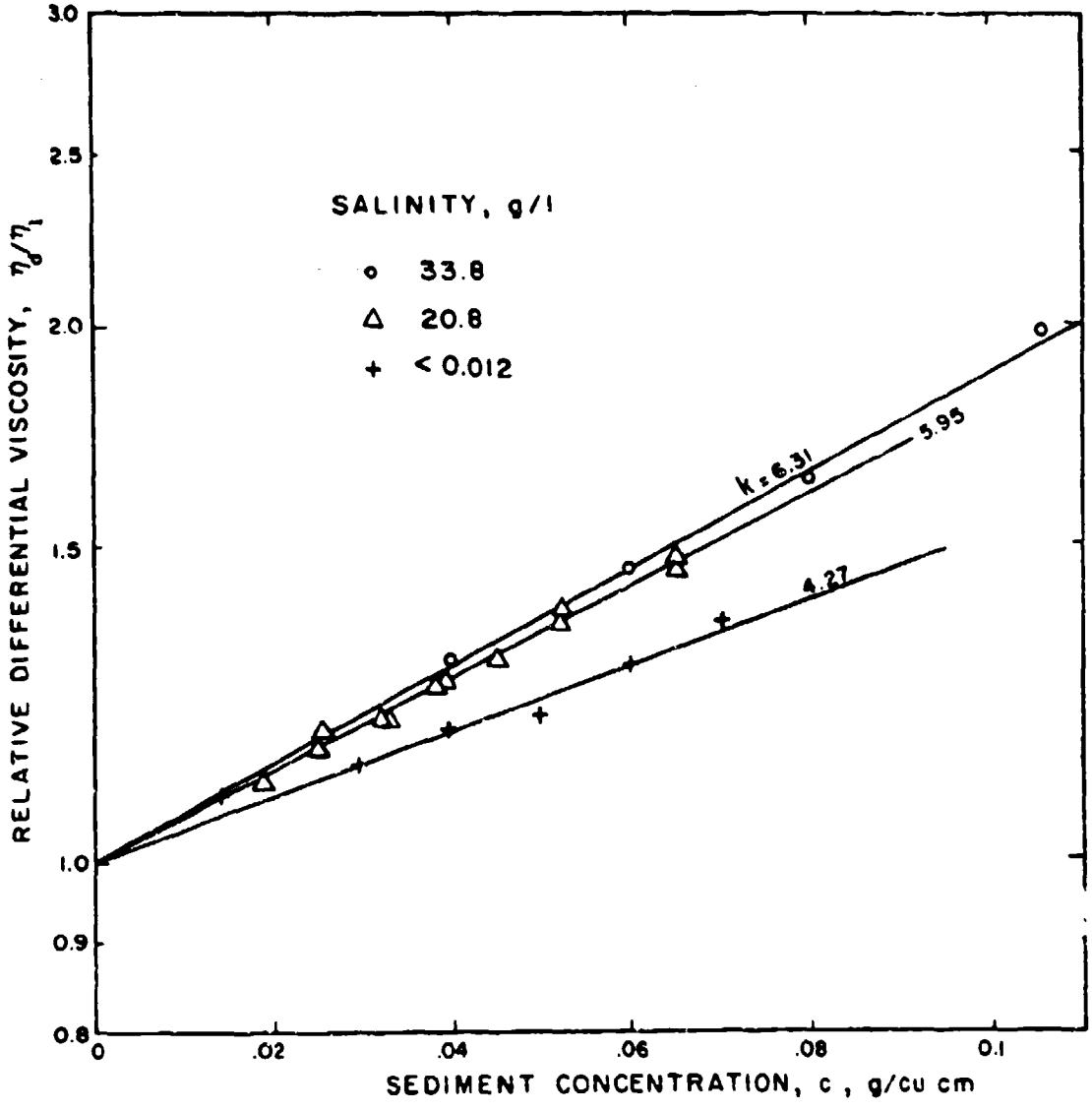

FIGURE 7. RELATIVE DIFFERENTIAL VISCOSITIES OF SAN FRANCISCO BAY SAMPLE FROM CAPILLARY VISCOMETER MEASUREMENTS

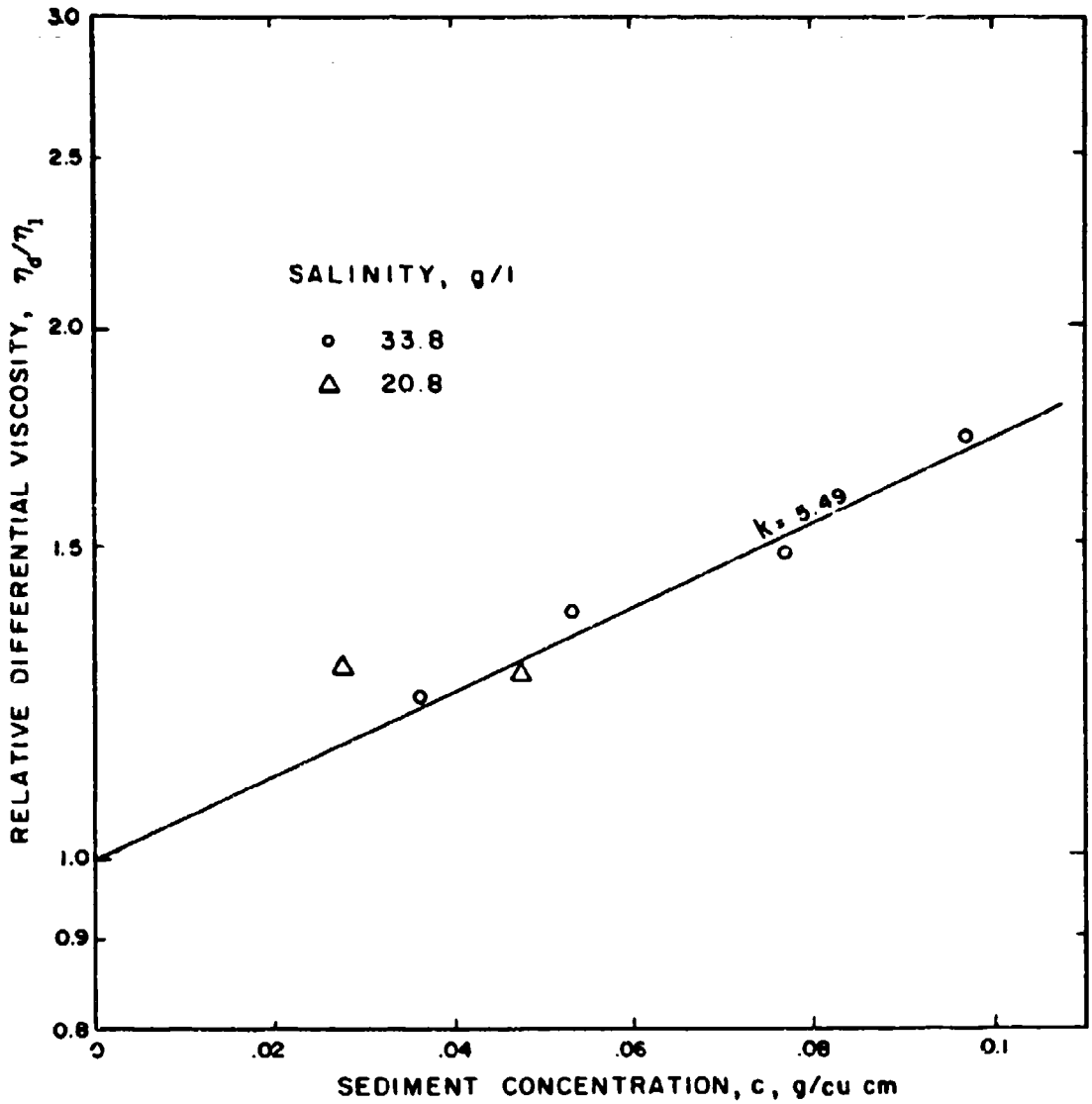

FIGURE 8. RELATIVE DIFFERENTIAL VISCOSITIES OF DELAWARE RIVER SAMPLE FROM CAPILLARY VISCOMETER MEASUREMENTS

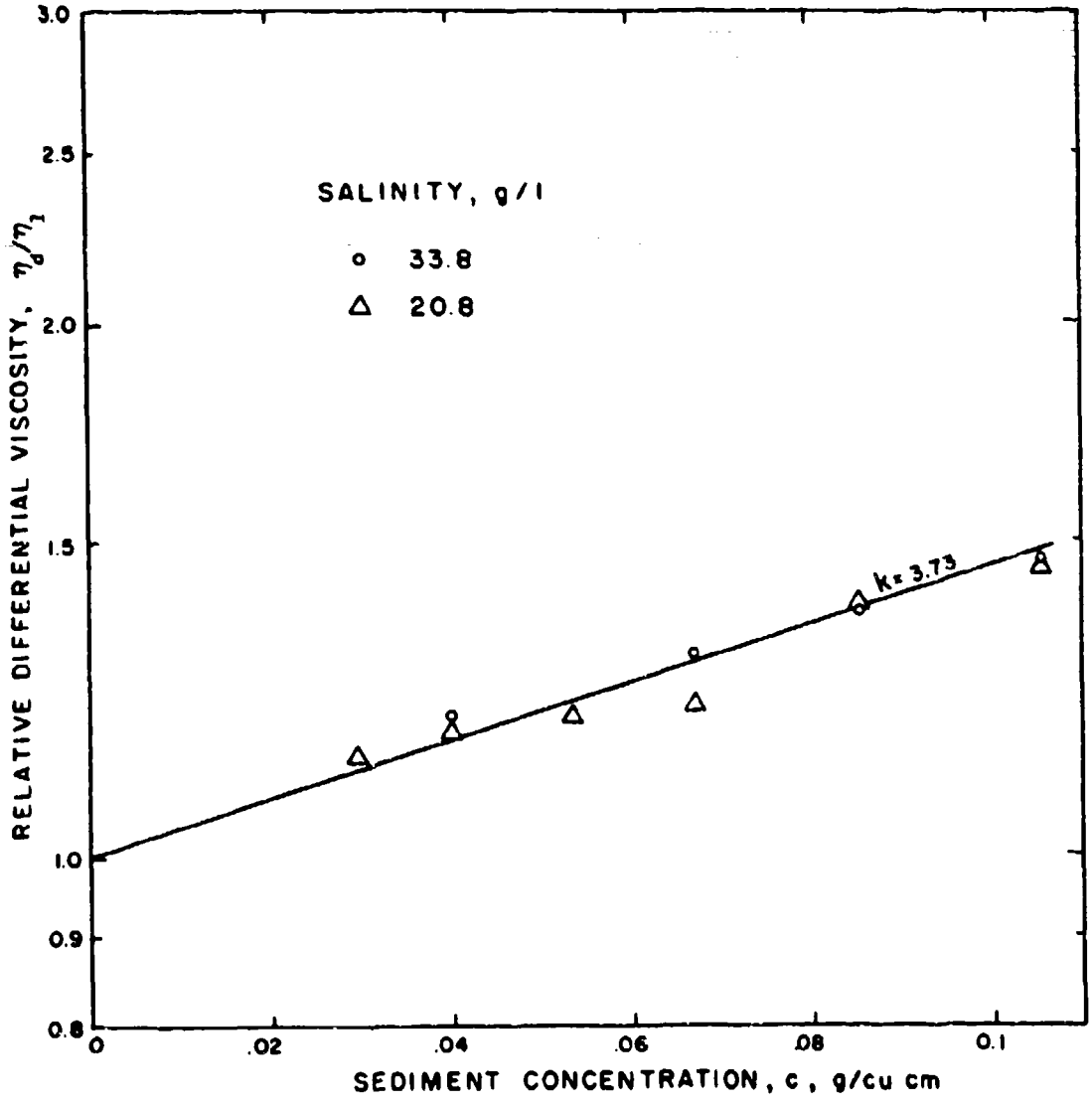

FIGURE 9. RELATIVE DIFFERENTIAL VISCOSITIES OF POTOMAC RIVER SAMPLE FROM CAPILLARY VISCOMETER MEASUREMENTS

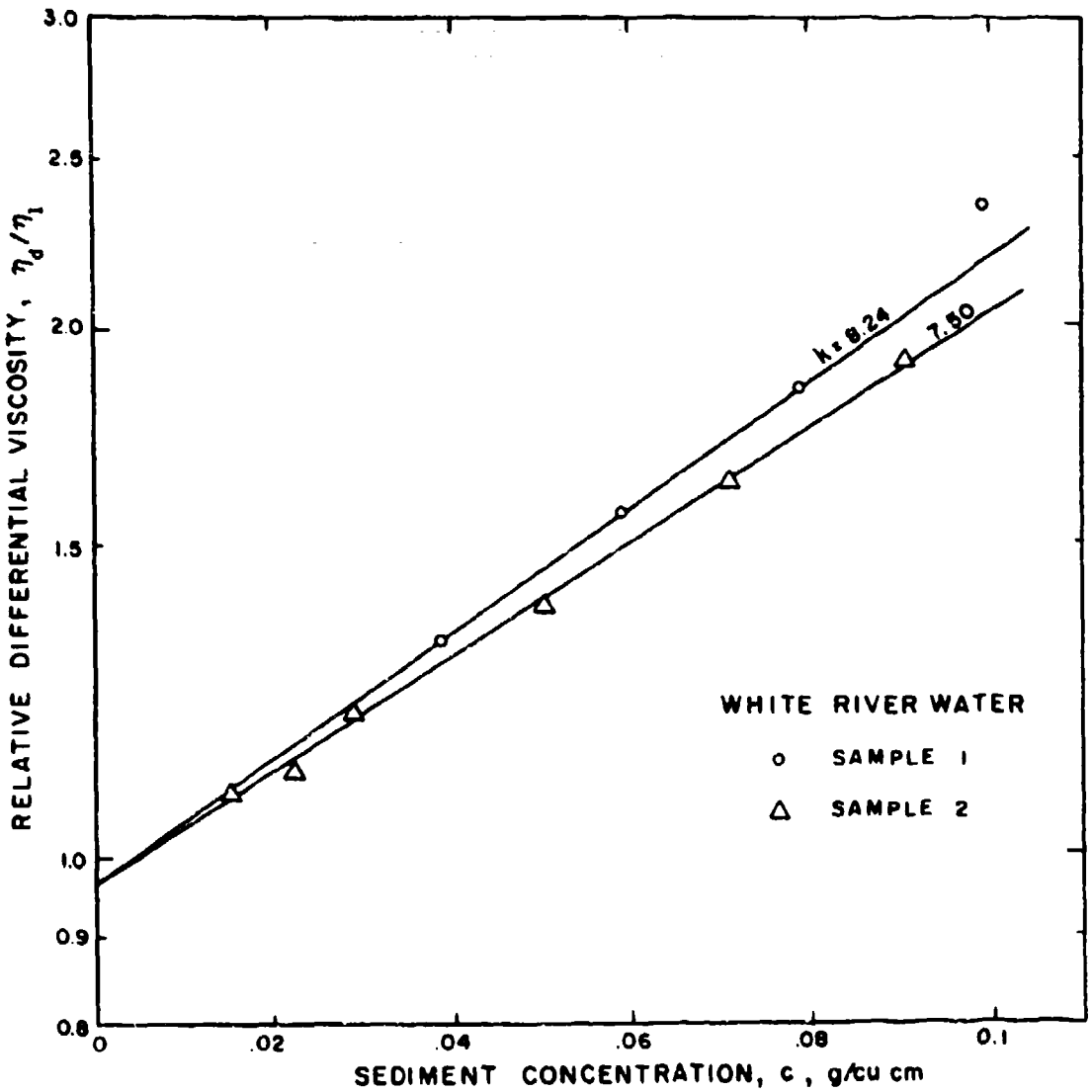

FIGURE 10. RELATIVE DIFFERENTIAL VISCOSITIES OF WHITE RIVER SAMPLE FROM CAPILLARY VISCOMETER MEASUREMENTS

A relation for the viscosity of a dilute suspension of rigid, inert, wetted spheres in an incompressible liquid was derived by Einstein [6]. His conditions are that the disturbance to the flow pattern around one sphere does not affect the flow pattern around adjacent spheres, and that inertia effects and turbulence are negligible. The relation is

$$\frac{\eta_s}{\eta_\ell} = 1 + 2.5\,\Phi \quad , \tag{4}$$

where Φ is the fraction of the suspension volume occupied by spheres. This elegant relation has the remarkable feature of being independent of the sizes and numbers of spheres. The factor 2.5 depends on the shape of the suspended particles, however, and is generally greater than 2.5 for shapes other than a sphere.

The sediment suspensions used for study had concentrations ranging up to the maximum that the viscometer would accommodate. Particle cohesion was the basis given for the existence of a static shear strength. Interaction of flow patterns around particles or flocs must occur, and the observed logarithmic relation, rather than a linear one, between differential viscosity and sediment concentration is attributed to this interaction. The observed relation can be explained on the basis of interactions of flow disturbances as follows:

Consider a suspension having only one small spherical floc per unit of volume. The viscosity can be approximated by Equation 4,

$$\eta_1 = \eta_\ell\,(1 + 2.5\,\Phi') \ ,$$

where η_1 is the viscosity of the suspension, η_ℓ is the viscosity of the liquid, and Φ' is the volume fraction of the increment of suspended particles. If a second particle is added to the suspension the viscosity can be put in terms of that of the first suspension,

$$\eta_2 = \eta_1\,(1 + 2.5\,\Phi') \ .$$

A third increment, Φ', can be added and the new viscosity given in terms of η_2, as above, $\eta_3 = \eta_2\,(1 + 2.5\,\Phi')$, and so on. Substituting the value for η_1 in the relation for η_2; then that value of η_2 in the relation for η_3, and so on, leads to

$$\eta_n = \eta_\ell\,(1 + 2.5\,\Phi')^n \ ,$$

where n is the number of increments of Φ' added. For a suspension, n is Φ/Φ', however, and the viscosity is

$$\eta_s = \eta_\ell \left(1 + 2.5\,\Phi'\right)^{\frac{\Phi}{\Phi'}}$$

which by definition of e, the base of natural logarithms, approaches

$$\eta_s = \eta_\ell \exp\left(2.5\,\Phi\right) \tag{5}$$

for $\Phi' \ll \Phi$. This relation expands to

$$\eta_s = \eta_\ell \left[1 + 2.5\,\Phi + \frac{(2.5\,\Phi)^2}{2!} + \frac{(2.5\,\Phi)^3}{3!} + \ldots\right],$$

which can be visualized as a weighted sum of interactions of 1, 2, 3, . . . particles at a time. The derivation assumes that the effect of each particle on the viscosity of the suspension can be described by Equation 4. Einstein's value of the constant, 2.5, was retained because photographs of flocs have shown them to have the shape of rough spheres [2, pp. 16 and 64].

The data for the most saline suspensions presented in Figures 4 through 10 clearly show an exponential relation between η_d/η_ℓ and c. The effect of interparticle cohesion on shear is separated from the effect of viscosity on shear by Bingham's hypothesis (Equation 1), and η_d should be equivalent to η_s. In view of Equation 5 and the observed exponential relation between η_d/η_ℓ and c, therefore, the floc shape and density must have remained constant with $2.5\,\Phi_f = k_1 c$, where k_1 is obtained from slopes of the lines plotted in Figures 4 through 10.

Assuming that the mineral particles and the water have uniform density throughout the suspension,

$$\rho_f - \rho_\ell = \frac{c}{\Phi_f\,\rho_p}\left(\rho_p - \rho_\ell\right), \tag{6}$$

where ρ_f is the floc density; ρ_ℓ, the liquid density; Φ_f, the floc volume fraction; and ρ_p, the mineral particle density.

The value of $c/\Phi_f = 2.5/k_1$ can be found from the η_d/η_ℓ vs. c plots. Taking mineral density as 2.65 g/cu cm, and the liquid density as 1.025 g/cu cm, values of the floc density can be calculated from Equation 6. Values calculated in this way are presented in Table IV.

TABLE IV

DENSITIES OF FLOCS IN THE CAPILLARY VISCOMETER

Sample	k_1, cu cm/g[a]	c/Φ_f, g/cu cm	Φ_p/Φ_f	ρ_f, g/cu cm for ρ_ℓ = 1.025
Wilmington District	6.83	0.366	0.138	1.250
Brunswick Harbor	11.1	0.225	0.085	1.164
Gulfport Channel	8.56	0.292	0.110	1.205
San Francisco Bay	6.31	0.396	0.150	1.269
Delaware River	5.49	0.455	0.172	1.305
Potomac River	3.73	0.670	0.253	1.437
White River	8.24	0.304	0.115	1.212

[a]From η_d/η_ℓ vs. c plots. Salinity 33.8 g/l.

The numbers in column 2 of Table IV are the values of k_1 obtained from the slopes of the lines in Figures 4 through 10. The numbers in column 3 are obtained from column 2, $c/\Phi_f = 2.5/k_1$, and are the sediment concentrations within the flocs. The numbers in column 4, $\Phi_p/\Phi_f = c/\rho_p\Phi_f$, are the fractions of the flocs that are composed of mineral particles. The values in column 4 show that the flocs are mostly water, with only a skeleton of clay particles. The calculated floc densities are tabulated in the last column, and have values commonly found for in-place densities of muds.

At salinities below 33.8 g/l the η_d/η_ℓ values are also logarithmic functions of c, but have flatter slopes which indicate a greater floc or particle density. At least at very low salinities the particles were largely dispersed, so that the constant in Equation 5 is larger than 2.5, which would require the particles to be much denser. In Figures 5 and 6, the lower salinity values shift to the line for the highest salinity values at sediment concentrations above 0.06 g/cu cm, suggesting a bunching of particles at concentrations sufficient to cause mutual interference in particle rotations. "Bunches" of particles resulting from crowding might have only transient existence, but would affect the viscosity as long as the bunched particles move as a group. If bunching is the cause, it appears from Figure 6 that the bunches have about the same density as do flocs.

The differential viscosity data obtained from the capillary viscometer provides descriptions of the flocs at high shearing rates. Because the floc densities are comparable to those for sediment deposits, and because of the range of high shearing rates at which the flocs exist, it can be concluded that the flocs in the capillary are uniform primary particle aggregates, and not aggregates of particle aggregates.

Bingham Yield Strengths. The lines of the plots of $h - v^2/2g$ vs. $1/t$ were extrapolated to $1/t = 0$ and the differences between the intercepts for the distilled water plot and those for the sediment suspensions were used to calculate the Bingham shear strength as indicated by Equation 3. Corrections were applied to the average internal head in the viscometer for the density of the suspension, and the Bingham shear strength was calculated as $h_B \rho_\ell g r/2\ell$.

Values of internal shear strengths, plotted in Figures 11, 12, 13, and 17, show considerable scatter but appear to fit arithmetic plots over most of the sediment concentration range observed. The linear plots indicate that the particle arrangement is the same over the concentration range examined. The remaining plots have lower shear strengths and appear to be linear over only a short concentration range. Extrapolation of these curves toward either of the axes is inadvisable because at some lower concentration limit a suspension should have almost no shear strength. A tendency for the shear strength to fall off at low concentrations is shown in Figures 14 and 15.

Figures 11 through 17 show that the shear strengths of the suspensions are appreciable.

Viscous Properties of Suspensions at Low Salinities. In order to obtain information on the effect of salinity on properties of sediment-water mixtures the washed sediments were suspended in water having increasing salinities and subjected to measurement. Dilutions with salt water were made of a 0.070 g/cu cm suspension to obtain the desired salinities. This dilution resulted in a variation of suspended sediment concentrations between 0.065 and 0.070 g/cu cm with the lowest at 0.070 g of sediment per cu cm.

Bingham shear strengths found for these suspensions are plotted in Figure 18, together with values for suspensions having salinities of 20.8 and 33.8 g/ℓ. Figure 18 shows that the shear strengths observed at high salinities were equaled or exceeded, within the precision of measurement, at the salinity of 1 g/ℓ or less. All except the Brunswick Harbor sample indicated a higher shear strength at 2 g/ℓ salinity than that at 33.8 g/ℓ. This exceptional strength might be due either to dispersal resulting from the washing procedure or to a denser structure of the floc. In either case, the observation should apply to sediments in an estuary.

The shear strength at very low salinities suggests cohesion of the particles. "Non-salt" flocculation, attributed to weak positive edge to negative face attraction, has been observed. Such attraction together with

40220

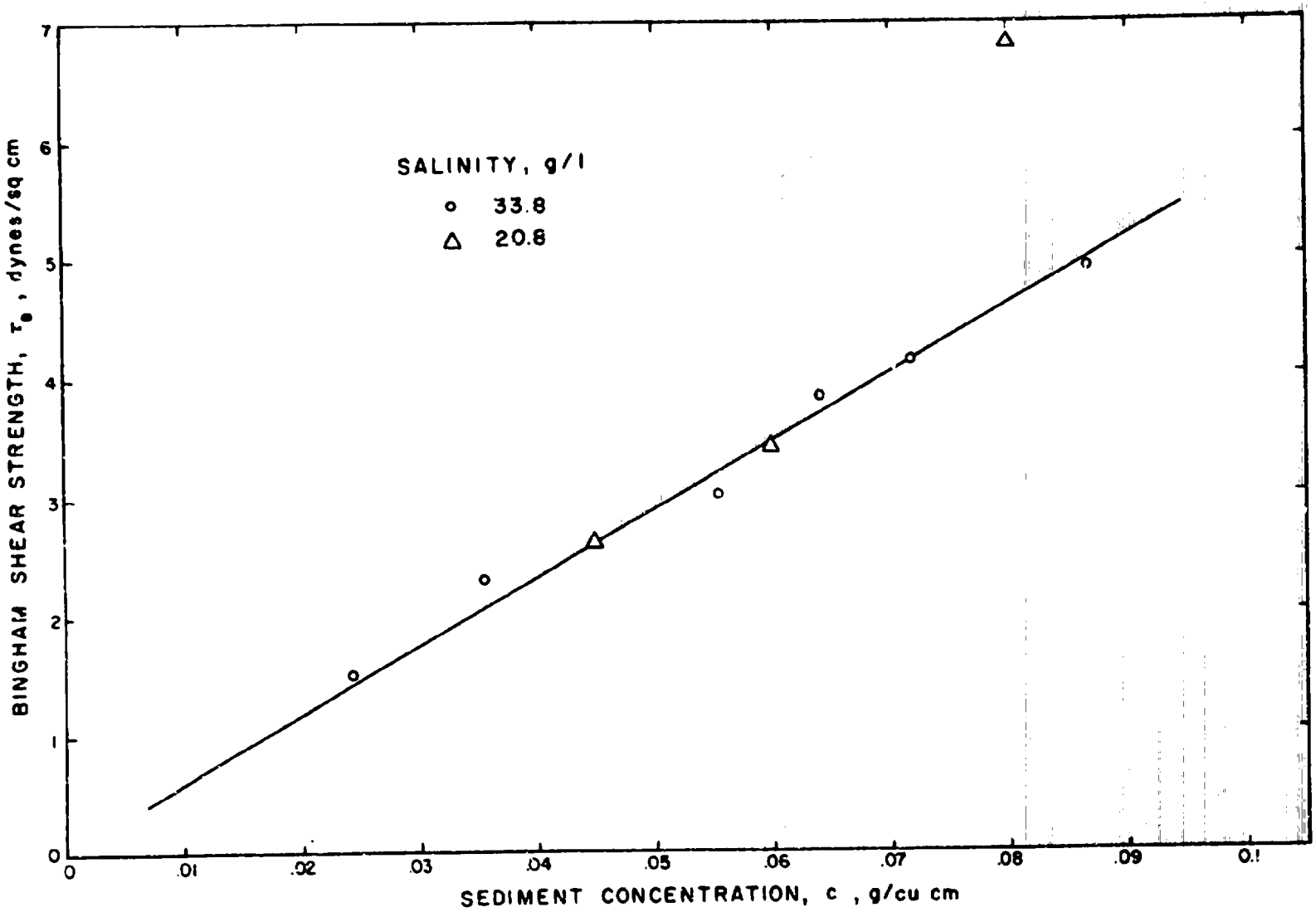

FIGURE 11. SHEAR STRENGTHS OF WILMINGTON DISTRICT SAMPLE FROM CAPILLARY VISCOMETER MEASUREMENTS

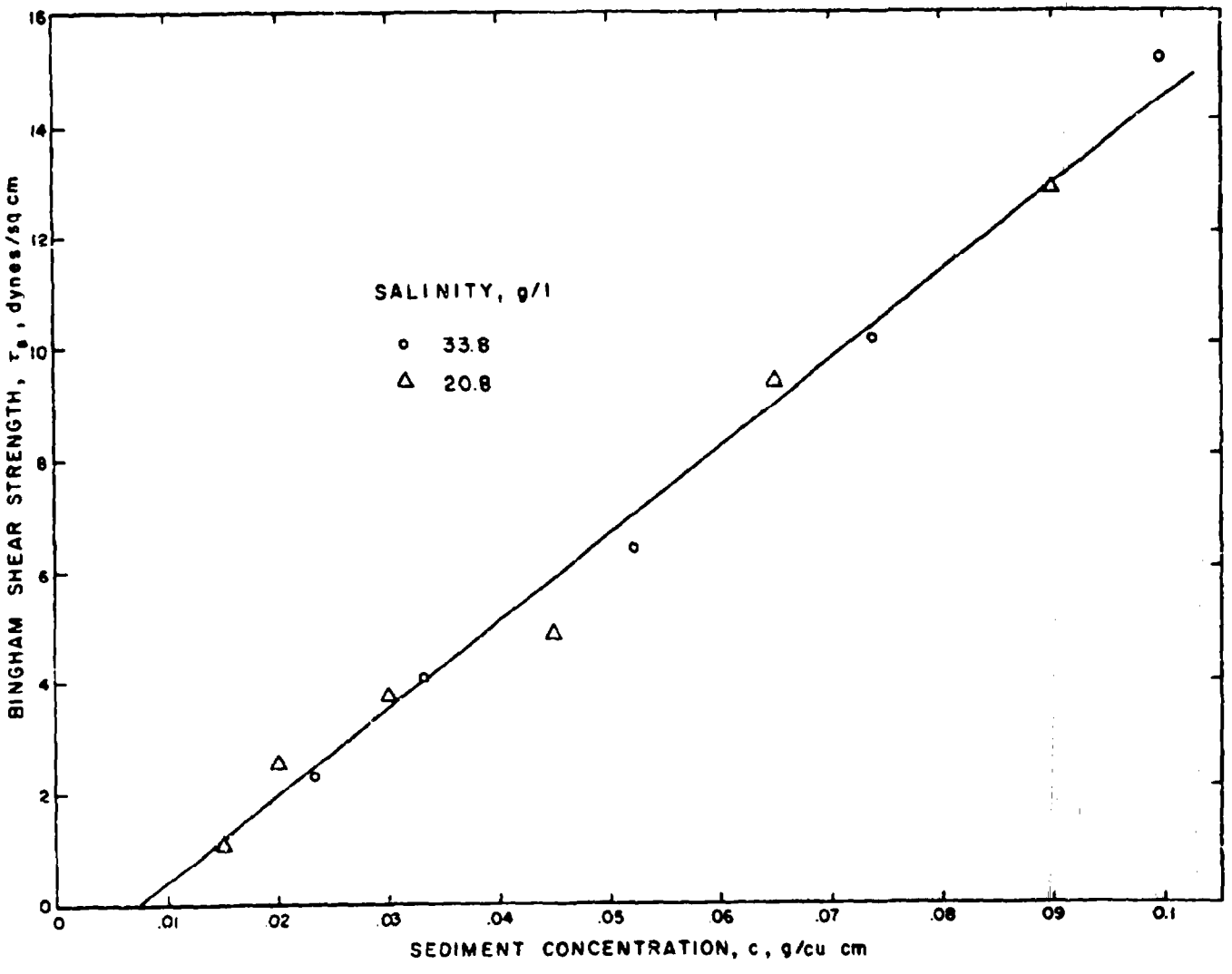

FIGURE 12. SHEAR STRENGTHS OF BRUNSWICK HARBOR SAMPLE FROM CAPILLARY VISCOMETER MEASUREMENTS

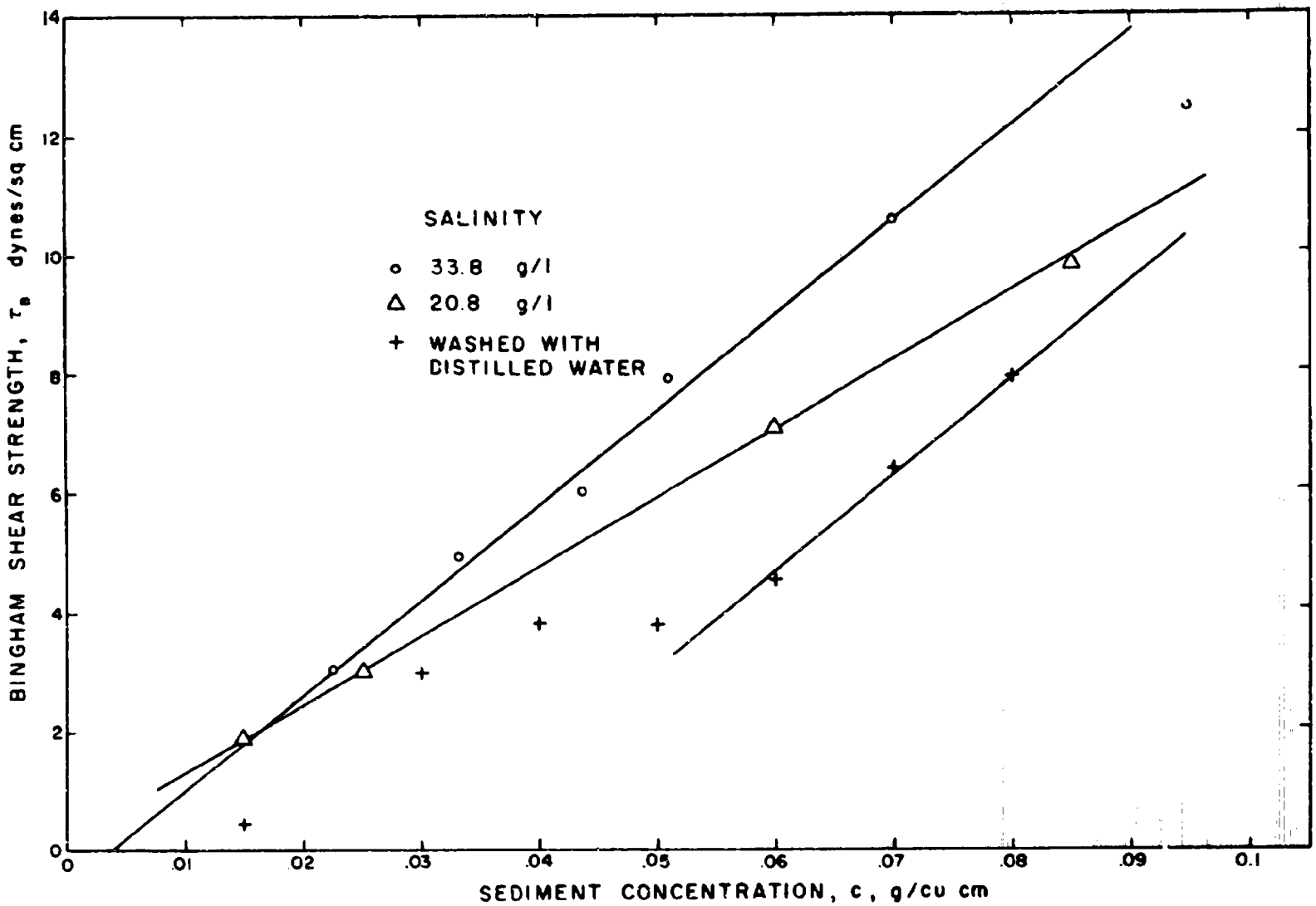

FIGURE 13. SHEAR STRENGTHS OF GULFPORT CHANNEL SAMPLE FROM CAPILLARY VISCOMETER MEASUREMENTS

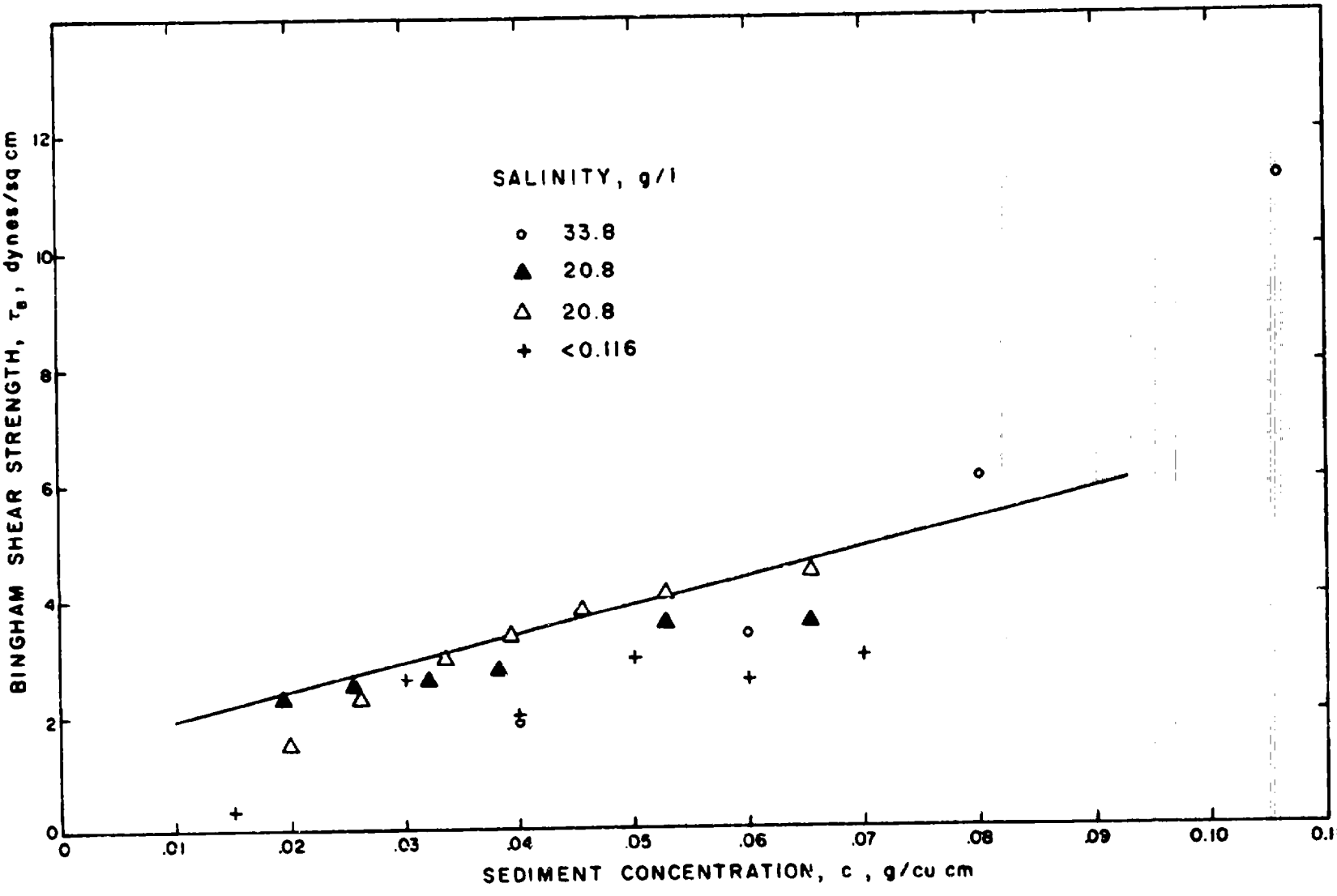

FIGURE 14. SHEAR STRENGTHS OF SAN FRANCISCO BAY SEDIMENT FROM CAPILLARY VISCOMETER MEASUREMENTS

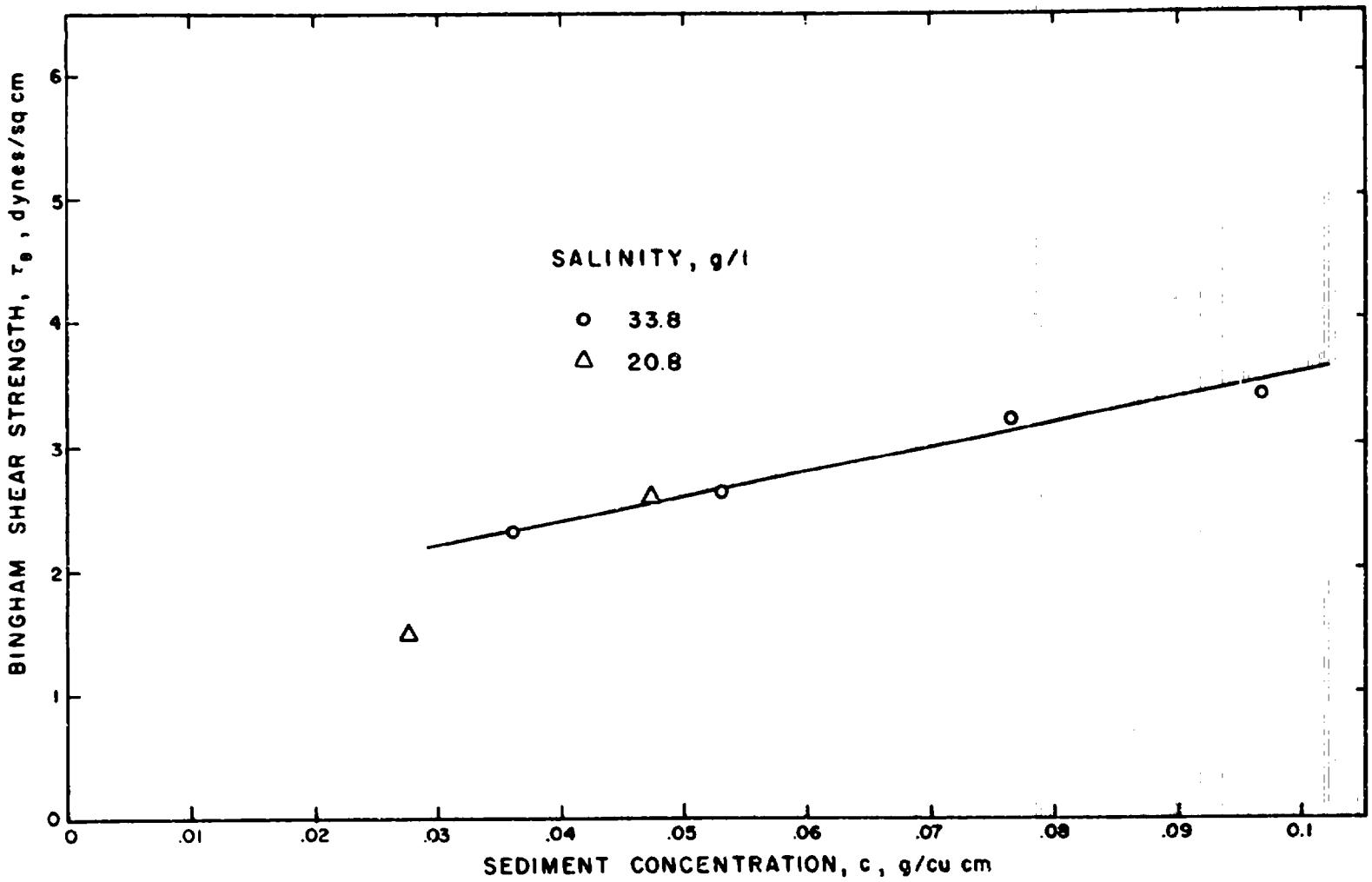

FIGURE 15. SHEAR STRENGTHS OF DELAWARE RIVER SAMPLE FROM CAPILLARY VISCOMETER MEASUREMENTS

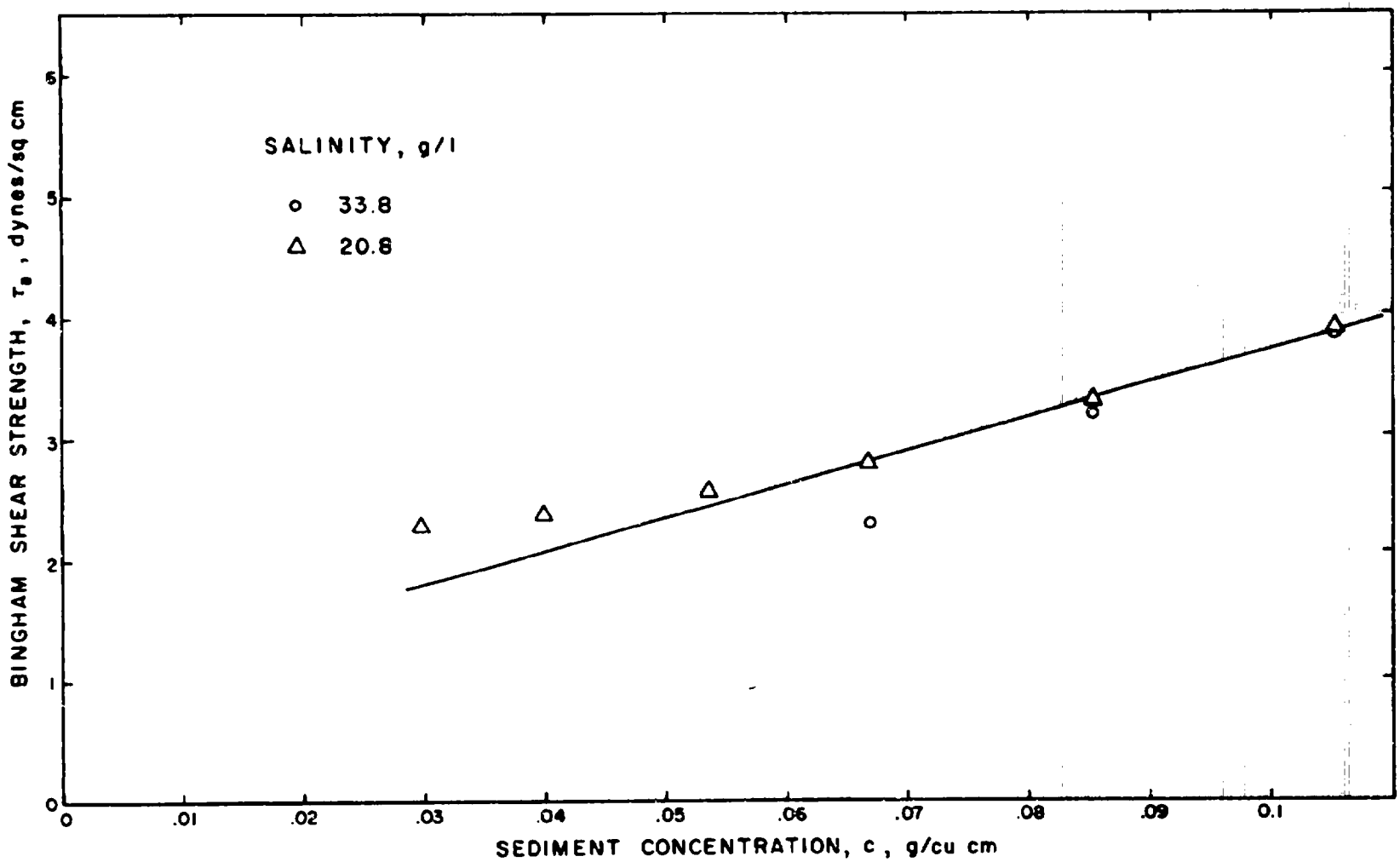

FIGURE 16. SHEAR STRENGTHS OF POTOMAC RIVER SAMPLE FROM CAPILLARY VISCOMETER MEASUREMENTS

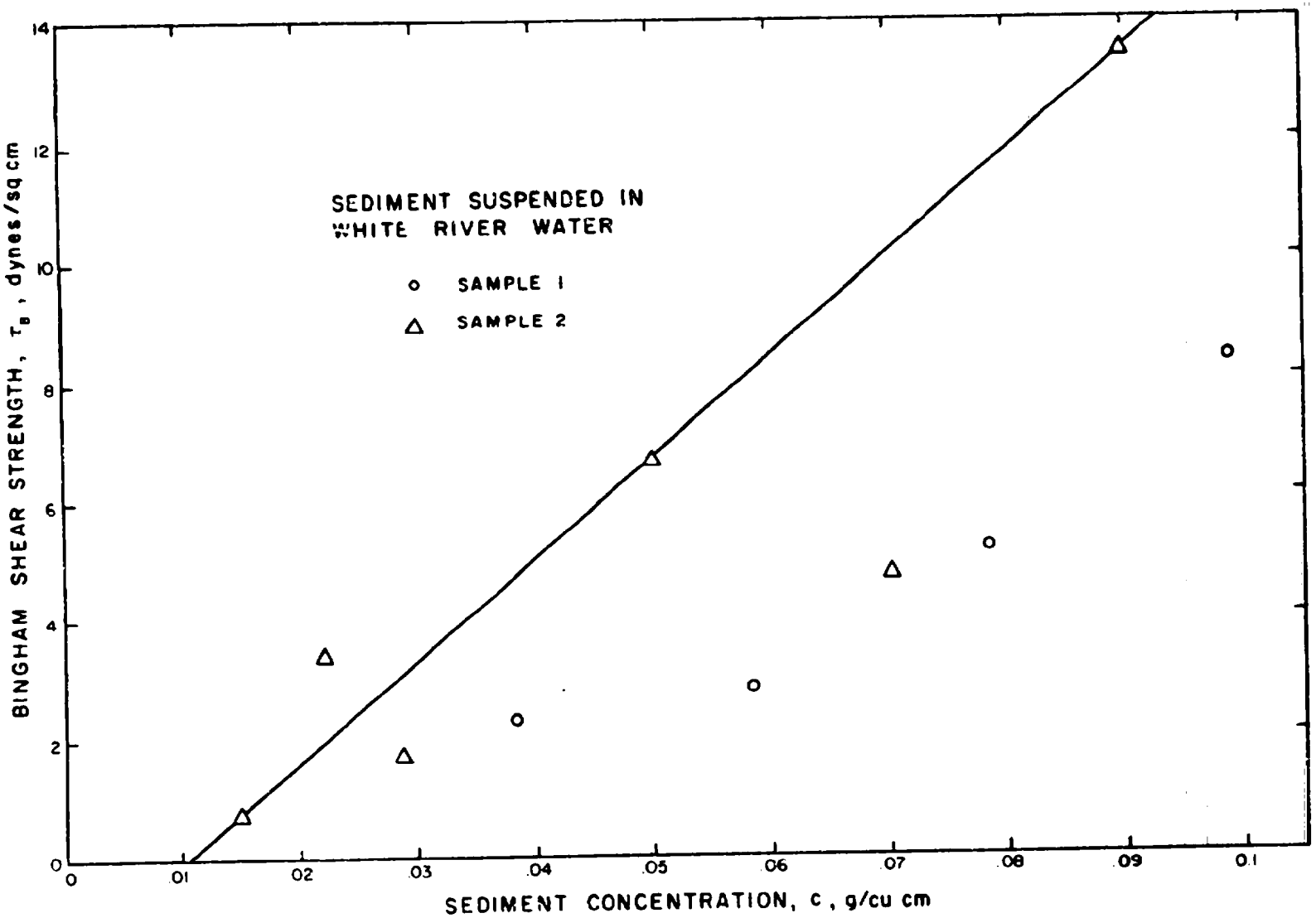

FIGURE 17. SHEAR STRENGTHS OF WHITE RIVER SAMPLE FROM CAPILLARY VISCOMETER MEASUREMENTS

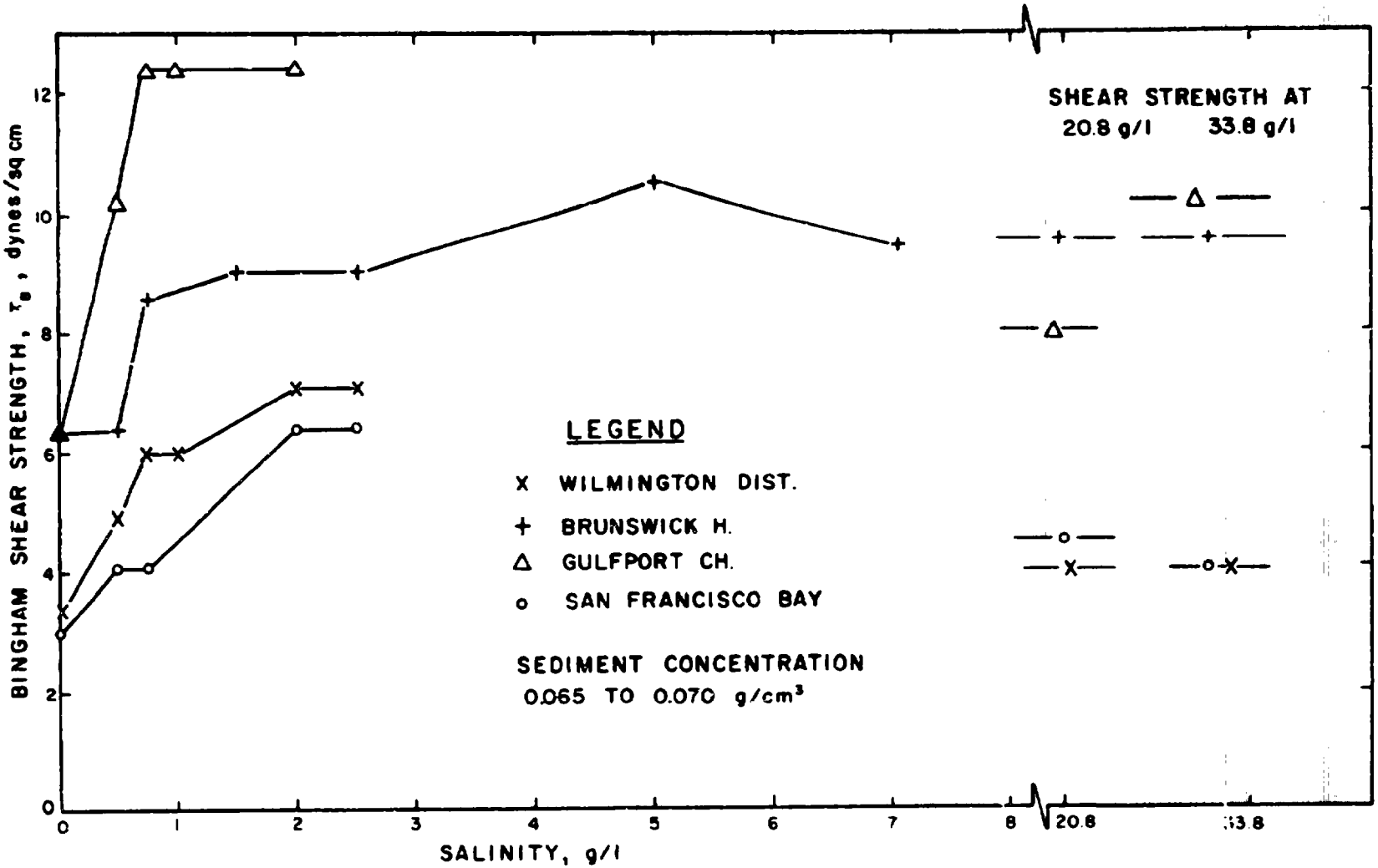

FIGURE 18. BINGHAM SHEAR STRENGTH CHANGES WITH SALINITY

crowding can account for the bunching of particles mentioned earlier, as well as for the observed higher shear strength at very low salinity [7].

Discussion

In the preceding sections data on suspensions determined with the capillary viscometer were treated by application of Bingham's hypothesis and relation and Einstein's relation to obtain fundamental properties of particle aggregates. It is useful to discuss these foundations for the interpretation of data and the method of measurement before presenting a discussion of the results.

Bingham's hypothesis is a superposition of the shear required by fluid friction, $\eta_d\, du/dr$ (Newton's hypothesis), and the shear necessary to overcome interparticle friction, τ_B. This powerful hypothesis facilitates separate consideration of interparticle friction and fluid friction as well as provides a basis for mathematical descriptions of flow. The constant η_d characterizes the macroscopic viscosity of a suspension which Einstein calculated for spherical particles to be a function only of the fluid viscosity and the solids volume fraction. The shear τ_B needed to overcome friction must include any form of interparticle friction, including cohesion and mutual interference of particle movements, that would require driving pressure to overcome.

Bingham's derivation of Equation 3, using the assumption of a solid core within the radius where $\tau \leq \tau_B$, parallels that of Poiseuille's. Telescoping concentric tubes of fluid in the annular space between the core and the capillary wall are assumed, with the shear between them given by Bingham's hypothesis. This model appears to give the correct macroscopic velocity distribution in the direction of the capillary axis for both Newtonian fluids and suspensions flowing through a capillary. It should not be inferred from the model, however, that a particle is constrained to remain at a constant radius. Both rotation and radial movement must occur in the presence of shearing and interparticle collisions so that any one particle can experience the entire range of shearing rates existing in the flow from the core to the wall. Equation 3 and the constancy of η_d and τ_B over the range of shearing rates employed are substantiated by the measured values plotted in Figure 3.

The differential viscosities of the saline suspensions appear to follow Einstein's relation, as applied, over the range of concentrations studied. The value of the constant used, 2.5, is based on the spherical shape of aggregates of smaller spherical aggregates observed in photographs of San Francisco Bay sediments. If an open structure of the aggregates prevails, a spherical shape would result from random collisions of mineral particles and the absence of strong orienting forces in the flow. If the shape were markedly different from spherical the calculated densities would be greater. The calculated values, shown in Table IV, are already close to those of consolidated sediment, and it is unlikely that aggregates would have a closer pack. It might be argued that the particles are moving separately, and that because of their platy shapes the constant is much higher and compensates for the relatively high

density of the minerals. The slopes of the η_d/η_ℓ vs. c curves (Figures 4 through 10) for low salinities are lower than those for high salinities, however, indicating at least a change in structure of aggregates, if not dispersal, with reduction of salinity. The particles are therefore believed to be aggregated at the higher salinities.

The uniformity of aggregate density over the range of shearing rates and concentrations studied indicates that the aggregates are either stable or form quickly. The high values of shearing rate included in the conditions of measurement and the densities observed lead to the conclusion that the aggregates are simple aggregations of primary mineral particles, that the aggregations might change their size but not change their density with shearing rate, and that they are not aggregates of particle aggregates.

The shear strength vs. concentration plots shown in Figures 11, 12, and 13 for Wilmington District, Brunswick Harbor, and Gulfport Channel samples are linear with an intercept on the concentration axis. A similar plot was presented by Bingham [5] who suggested that the intercept concentration (or volume fraction) was a fundamental property of the suspension. The lines that best fit the next three sediments do not pass through the concentration axis, however, making a further explanation necessary.

Figure 13 shows a plot of shear strength vs. concentration for washed Gulfport Channel sediment. This plot has a shear strength "plateau" between 3 and 4 dynes/sq cm ranging from a concentration of 0.03 to above 0.05 g/cu cm, followed by an apparently linear increase in shear strength with concentration that has a slope parallel to that for the most saline suspension. Such a shear strength vs. concentration relation can be explained in terms of particle behavior. Clays exhibit a "non-salt" cohesion resulting from positive mineral edge sites and negative mineral faces when the salt concentration in the suspension is low. This cohesion accounts for the existence of shear strength beginning at about 0.015 g of sediment per cu cm. As the sediment concentration increases, crowding impairs freedom of orientation and a decreasing portion of the particles experience edge-to-face cohesion; increasing numbers are forced into a more parallel arrangement, resulting in the plateau shown in Figure 13. When crowding is sufficient to cause several particles to cohere at once "bunching" like that in a log jam occurs, and as sediment concentration increases, larger and larger fractions of the particles move as clusters. The material then has the characteristics of a strongly flocculated material. In this concentration range weak cohesion is supplemented by crowding.

The relative differential viscosity of the washed Gulfport Channel sample, shown in Figure 6, supports this interpretation. At the sediment concentration of about 0.06 g/cu cm, where "bunching" is indicated in Figure 13, the relative differential viscosity deviates from the curve for the lower concentrations toward the curve for the saline suspension. Plots of the differential viscosity and of shear strength vs. concentration indicate a change in suspended particle character for the washed sample.

Figures 14, 15, and 16, and the lower plot in Figure 17 are similar to the plot just described. In these plots, plateaus occurred when additional particles no longer contributed to shear strength, because there was not a sufficiently strong orienting force to maintain an open structure with increasing particle numbers in the presence of high shearing rates. The White River sample showed both kinds of behavior, suggesting a metastable structure of the material entering the capillary.

The shear strengths of the particle aggregates themselves can be calculated by extrapolating the shear strength plots to the concentrations of the aggregates shown in column three, Table IV. Floc shear strengths calculated in that manner are shown in Table V.

TABLE V

PARTICLE AGGREGATE SHEAR STRENGTHS

Sample	Bingham Shear Strength dynes/sq cm or Energy of Cohesion dynes/cu cm	Energy of Cohesion dyne cm/g
Wilmington District	21.0	57
Brunswick Harbor	33.7	150
Gulfport Channel	45.[illegible]	160
San Francisco Bay	21.8	55
Delaware River	11	23
Potomac River	19	29
White River	48.6	160

These shear strengths are approximate, but are much greater than the shears existing at the bottom of ordinary estuarial channels. The flocs subject to destruction in such channels must be aggregates of particle aggregates with more open structures and consequently lower strengths.

The calculated shear strengths of the particle aggregates are plotted against the cation exchange capacities of the sediments in Figure 19. The cation exchange capacity is proportional to the surface area of the clay mineral fraction, so that Figure 19 shows the effect of cohesion on shear strength. The scatter at the low exchange capacities is due to the variety of clay minerals that can combine to result in those exchange capacities. Cohesion depends on mineral shapes and sizes as well as on total surface area. As the exchange capacity of a sediment increases, the possible number of mineral kinds is reduced, and a more direct relation can be expected.

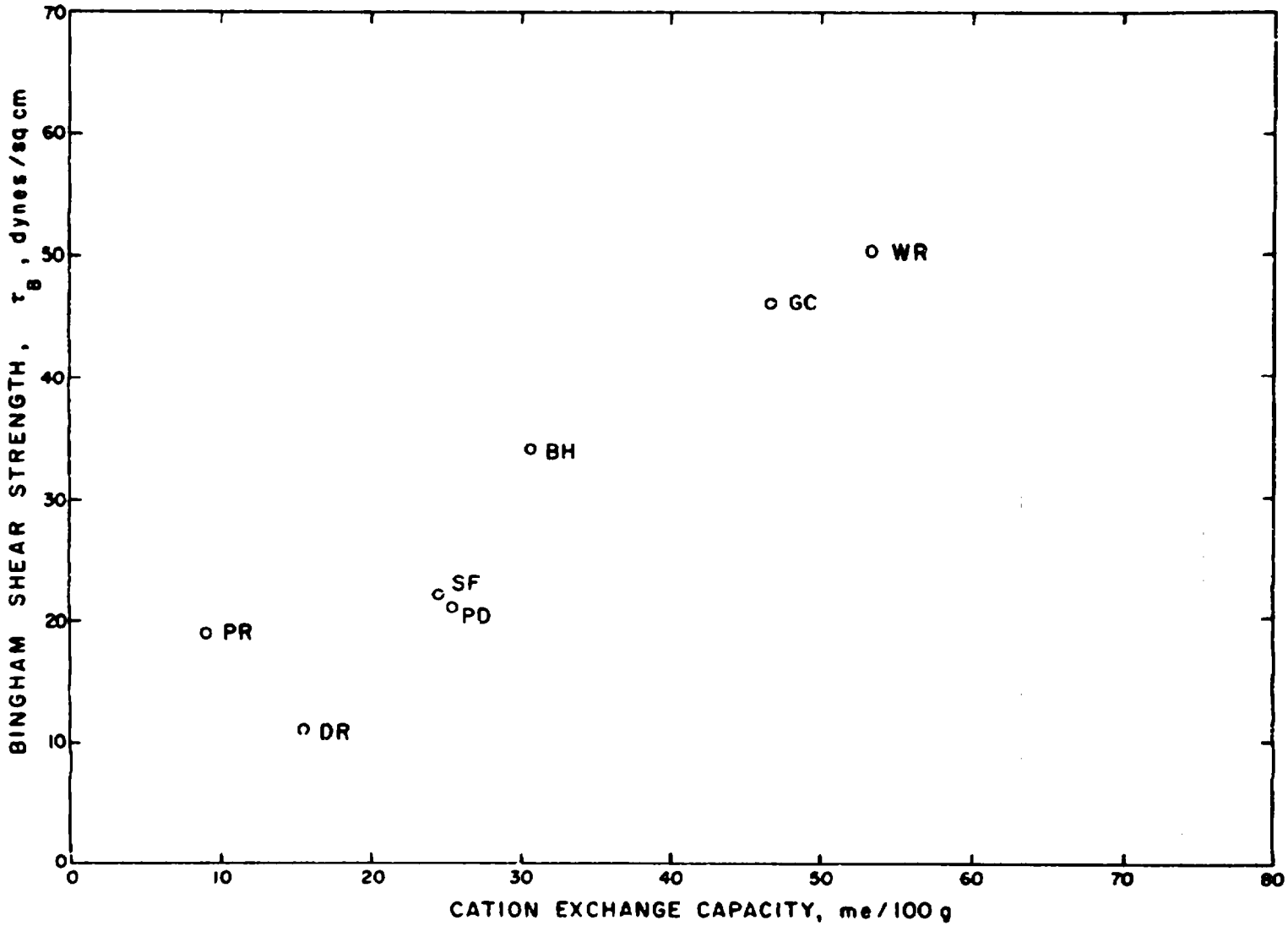

FIGURE 19. RELATION BETWEEN SHEAR STRENGTH AND CATION EXCHANGE CAPACITY FOR SEDIMENT SAMPLES

Conclusions

Data from the measurements of the rheological properties of suspensions of the sediment samples made using a capillary viscometer provided information on the character of the material. In addition to the reduced data, presented as figures and tables, several characteristics of sediment material from the sampled estuaries became evident:

1. Sediments from all of the estuaries are cohesive. Cohesion was shown by the existence of Bingham shear strengths and by the low densities of suspended flocs.

2. Cohesion is high at the salinity of one g/ℓ and higher, as shown in Figure 18.

3. At the shearing rates prevailing in the capillary viscometer, 100/sec or more, particles existed as separate mineral particles or as primary aggregations of mineral particles. This conclusion results from the densities of the particles in the saline suspensions, calculated using the slopes of the relative differential viscosity vs. concentration curves, and from the flatter slopes of the curves for suspensions of washed sediments.

4. Two general relations between shear strength and sediment concentrations exist under the conditions in the capillary: a simple linear relation, and a relation including a transition from an initial shear strength to a linear relation at higher sediment concentrations.

5. The shear strengths of the flocs themselves, as determined by extrapolation of measured values shown in Table V, are higher than the shears at the bed commonly observed in estuaries. Erosion must therefore involve rupture of inter- (primary) aggregate bonds.

Application of the data and conclusions presented in this chapter are made in subsequent pages, where their significance to understanding estuarial sediment behavior is also described.

IV. RHEOLOGICAL MEASUREMENTS USING A ROTATING CYLINDER VISCOMETER

The capillary viscometer has the virtues of simplicity, ease of operation, and a well-developed theoretical foundation--all of which have recommended its use for study of suspensions. It has the serious disadvantages, however, of small dimensions and wide ranges of shearing rates within the capillary at any one flow rate. The small dimensions prohibit the study of aggregations of primary particle aggregates, and the wide range of shearing rates in the capillary inhibits the study of floc structure as a function of shearing rate. In order to facilitate the study of larger flocs it was necessary to construct a viscometer having a relatively large thickness of shearing suspension, a narrow range of shearing rates, and sufficient sensitivity to provide shear-shearing rate data for sediment suspensions. A rotating cylinder viscometer design similar to the one described by Mallock [8] was selected.

The Rotating Cylinder Viscometer

A diagram of the essential parts of the viscometer is shown in Figure 20. The outer cylinder was a 1-liter pyrex glass graduated cylinder held on a turntable by springs. The turntable was equipped with leveling screws arranged so that the cylinder could be aligned and made concentric with the turntable support shaft. The edge of the turntable was grooved and the turntable driven by a belt from stepped pulleys mounted on the shaft of a variable-speed motor. A cam and switch mounted on the turntable shaft actuated a counter during a 1-minute interval, controlled by an electric timer, so that the rpm of the turntable was measurable for any speed of the drive motor. The range of turntable speed employed during the study was 8 to 180 rpm.

The inner cylinder was made of pyrex glass rigidly mounted on a metal fitting that included a collett for fastening the end of a steel torsion wire and a positioning tube for maintaining the alignment of the inner cylinder with respect to the outer. The positioning tube was restrained by two bearings. These bearings were gyroscope-type ball bearings equipped with a "keep alive" vibrator during the early part of the study. Air bearings were installed later to reduce friction. A mirror was mounted at the upper end of the positioning tube to facilitate a light lever null-position indicator. An aluminum plate magnetic damper was also mounted on the upper end of the positioning tube to reduce torsional oscillations of the inner cylinder. The entire assembly, including the inner cylinder, positioning tube, mirror, and aluminum plate of the magnetic damper, was rigidly connected. A rubber stopper was installed a few centimeters above the open lower end of the inner cylinder so that air was trapped and an air-water interface formed the bottom of the inner cylinder. Lead weights (450 g total) were placed in the inner cylinder to compensate its buoyancy.

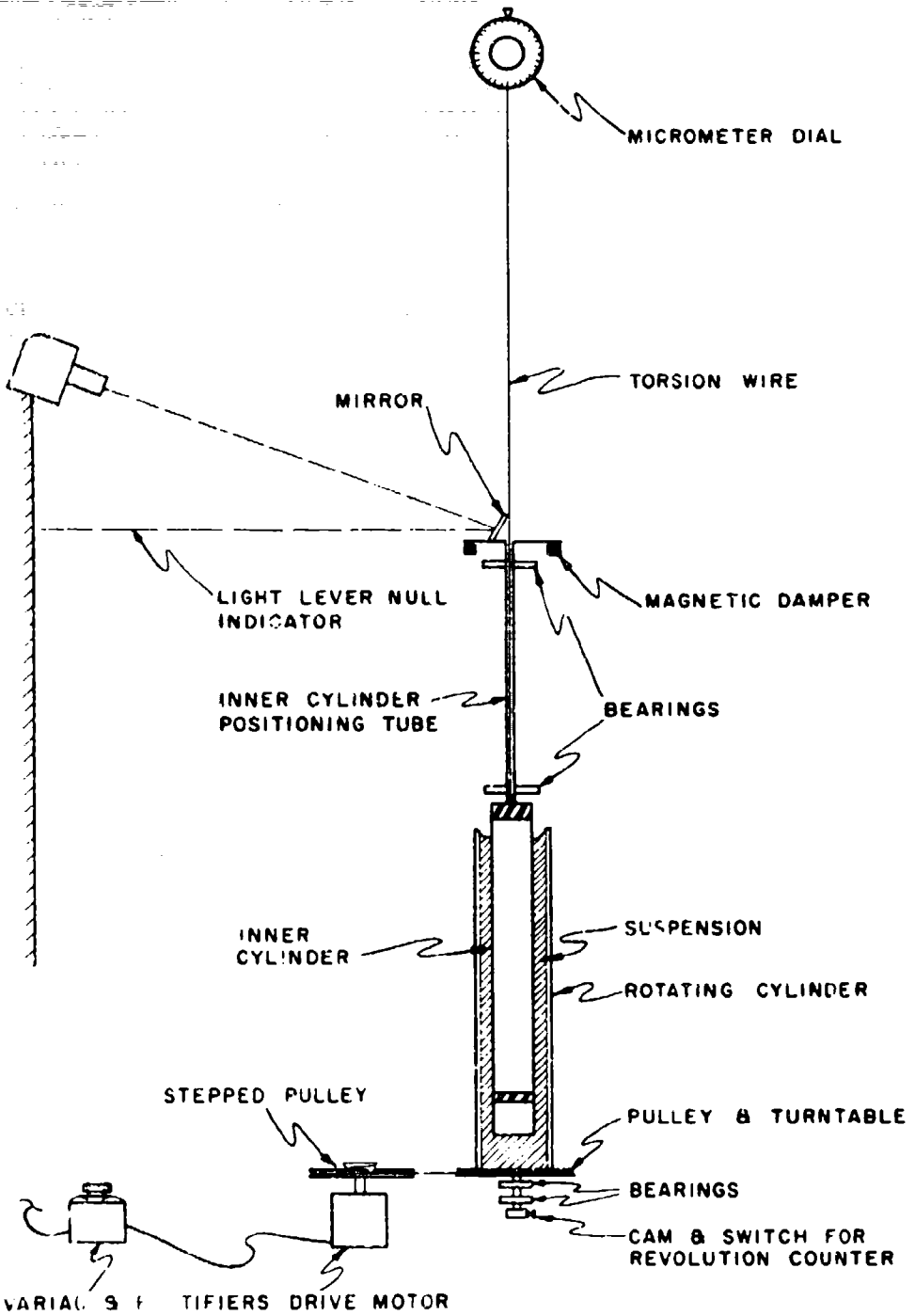

FIGURE 20. ESSENTIAL PARTS OF ROTATING CYLINDER VISCOMETER

The steel torsion wire was 0.079 cm in diameter and 133 cm long during the early parts of the study. A 0.050-cm diameter wire of the same length was installed later to increase the sensitivity of the torque measurement. The wire was fastened to the collett on the inner cylinder at one end and to a collett on a "zero-backlash" worm drive reduction gear assembly at the other end. The worm gear was rotated by a micrometer-type dial so that the dial and gear assembly provided 1000 1/4-in. divisions in one rotation of the wire end.

The bearings on the inner cylinder positioning tube, the worm gear and dial assembly, and the magnets of the magnetic damper were mounted on a telescoping frame arranged so that the entire inner cylinder with its connected assemblies could be lifted to facilitate removal of the outer cylinder.

The viscometer was located in a multistory concrete building with common thermostatic temperature controls. The temperatures at the beginning and end of each series of runs were measured with a mercury thermometer.

The viscometer was simple, flexible, and all parts were easily accessible. It had the additional feature that calibration and measurements were made in fundamental units.

Theory of Rotating Cylinder Viscometer

The drag on the inner cylinder caused by a Bingham fluid was derived for this study by H. A. Einstein as follows: Using cylindrical coordinates with the coordinate axis located at the cylinder axis, Bingham's hypothesis can be written

$$\tau = \tau_B + \eta_d \left(\frac{dq}{dr} - \frac{q}{r} \right) , \tag{7}$$

where q is the tangential velocity, r is the radius, and the other symbols are as previously defined. The torque, T, is constant throughout the fluid, and

$$T = 2\pi \, Hr^2 \tau \quad ,$$

where H is the height of fluid in the annular space. Substituting for τ in Equation 7, and rearranging gives

$$\eta_d \frac{dq}{dr} = \frac{T}{2\pi Hr^2} + \eta_d \frac{q}{r} - \tau_B \quad . \tag{8}$$

The solution of Equation 8 for inner and outer cylinders of radii, r_1 and r_2, respectively, with zero angular velocity at the inner cylinder and ω_2 at the outer cylinder is

$$T = \eta_d \left[\frac{4\pi H}{\frac{1}{r_1^2} - \frac{1}{r_2^2}} \right] \omega_2 + \left[\frac{4\pi H \ln \frac{r_2}{r_1}}{\frac{1}{r_1^2} - \frac{1}{r_2^2}} \right] \tau_B \quad . \qquad (9)$$

The terms in brackets are constants that depend on the geometry of the cylinders. Equation 9 is linear. Since T is proportional to the twist of the torsion wire for small twists and ω_2 is proportional to the rpm of the outer cylinder, the measured values themselves were plotted and appropriate factors applied to the intercepts and slopes of the plots to obtain η_d and τ_B.

Calibration of Rotating Cylinder Viscometer

Calibration of the viscometer was done in two ways: First, the dimensions of the system and the torsional constant of the wire were measured; and secondly, measurements were made using water to establish the range of conditions over which laminar flow with negligible end-effects occurred.

The torsional constant of the wire was found by wrapping a light linen cord around the inner cylinder with one end fastened to the cylinder and the other extending horizontally a few centimeters to a weight and then upward to an anchor. A horizontal scale was fixed just below the anchor. Calibration proceeded by moving the anchor in half-centimeter steps, turning the dial to compensate the increment of tangential force as shown by the light lever null-position indicator. The observed dial readings were plotted against the increment in anchor position in Figure 21. The wire constant, K, was calculated from the slope of the line through the points; as shown in Figure 21, K = 23.4 dyne cm/division.

The diameter of the inner cylinder was determined by means of vernier calipers. Readings for five diameters were averaged. The diameter of the graduated cylinder was calculated from the volume and length of the calibrated portion. Because of breakage several cylinders were replaced during the study. Each cylinder was measured, and the small variations were appropriately used. For the measurements immediately to be described the dimensions are as shown in Table VI.

Measurements were made on water placed in the annulus at various depths. At the beginning of every series of measurements at each depth, the outer cylinder was rotated at the maximum speed for five minutes to allow any secondary currents that might occur to develop. The speed of rotation was then lowered in steps and the drag measured after one minute of constant speed. These measurements are plotted at the bottom of Figure 22, and show that at speeds less than 110 rpm, the drag on the

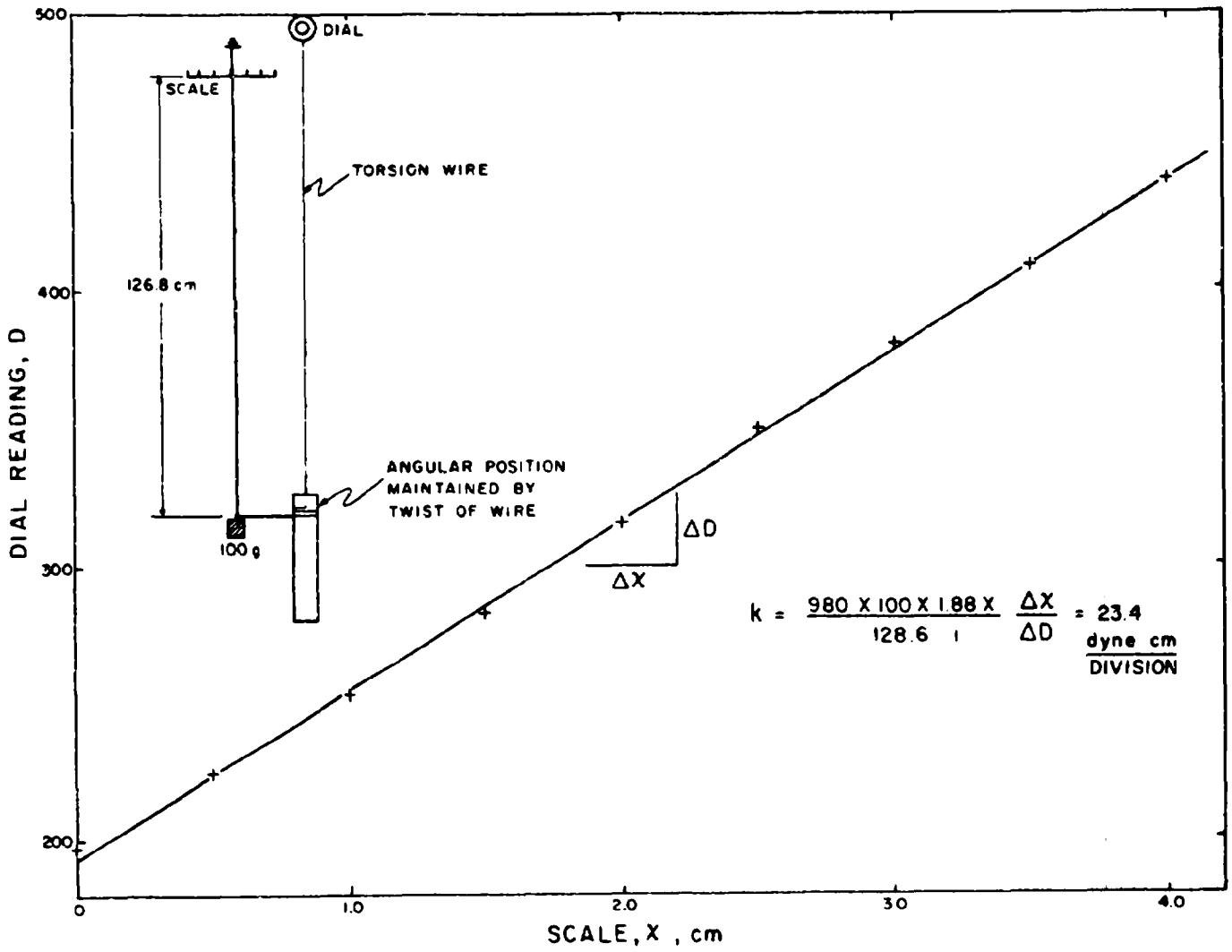

FIGURE 21. PLOT FOR DETERMINATION OF TORQUE CONSTANT OF TORSION WIRE

inner cylinder was linearly related to the speed of rotation of the outer cylinder. It should be noted that the intercept varies between zero and one-half of a dial division. Such variations were believed to be the result of changes in flow patterns in the air bearings.

TABLE VI

DESCRIPTION OF ROTATING CYLINDER VISCOMETER WITH AIR BEARINGS

Radius of inner cylinder, r_1	1.88 cm
Radius of outer cylinder, r_2	3.08 cm
Annular thickness	1.20 cm
Distance between lower ends of cylinders	2.6 cm
Wire constant	23.4 dyne cm/division

The slopes of the rpm vs. Dial Reading curves, divided by the values of viscosity of the water taken from tables for the measured temperatures, are plotted against the height of water in the outer cylinder at the top of Figure 22. A straight line drawn from the origin fits the points reasonably well. The slope of this line can also be used to obtain the calibration constant for the system. It was found that

$$\eta = 2.77 \frac{\Delta D}{H \Delta N} \quad . \tag{10}$$

From Equation 9 and the values in Table VI it can be calculated that

$$\eta = 0.1333K \frac{\Delta D}{H \Delta N} \quad . \tag{11}$$

The value of K determined from measurements using water is 2.77/0.1333 = 20.7 dyne cm/division.

Factors that affect the accuracy of the viscometer are the occurrence of slow secondary currents due to the lower end configuration, variations in air-bearing induced torque, and errors in rpm, torque, dimension, and temperature measurements. Of all these probable factors, slow secondary currents are likely to be the most significant. The linearity of the plots in the lower part of Figure 22 show, however, that the flow geometry was unchanged at speeds less than 100 rpm.

The onset of instability at speeds from 100 to 110 rpm is shown by the appropriate points in Figure 22. Instability at this speed is predicted by Taylor's work with similar systems [9]. In measurements

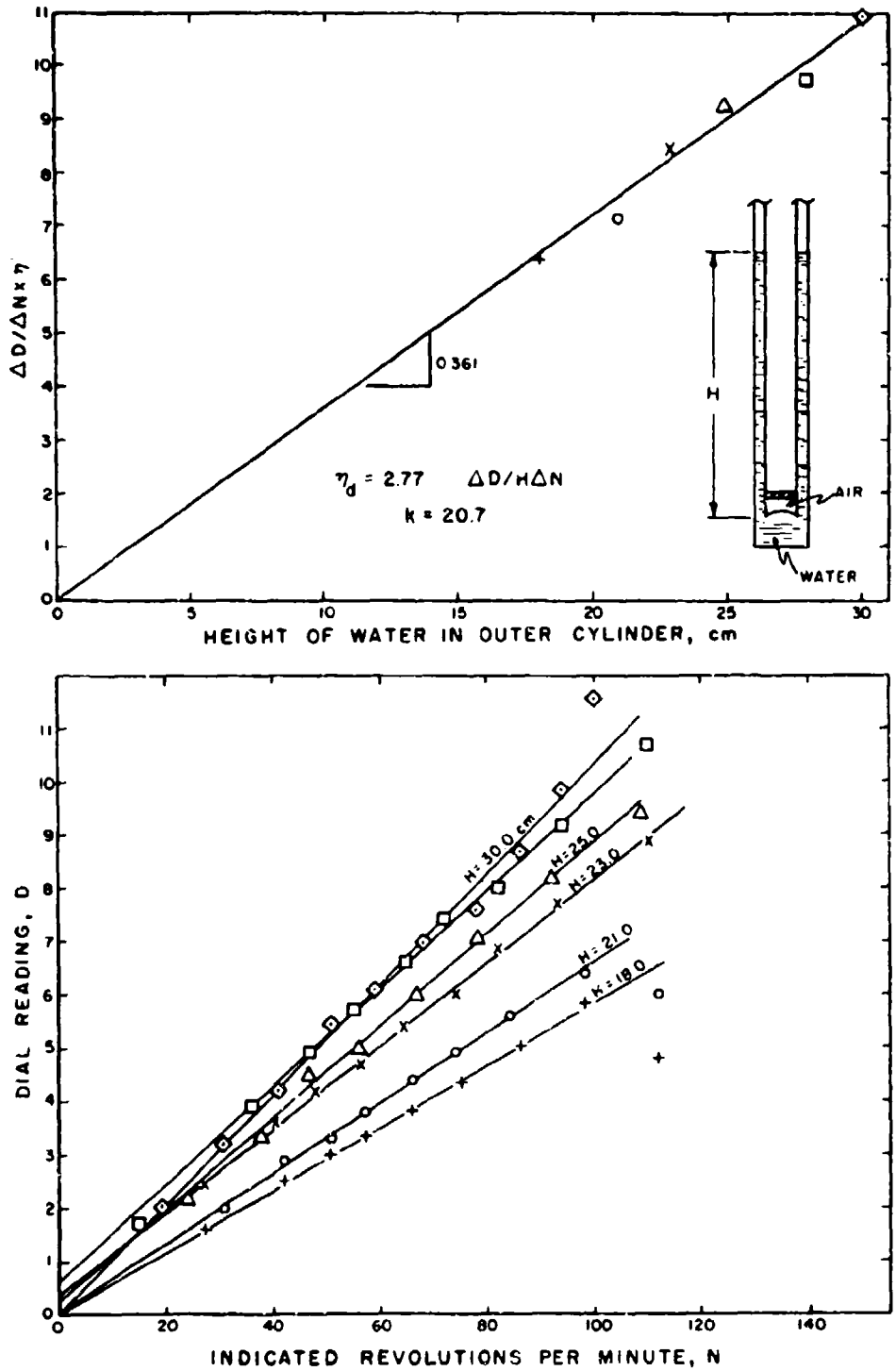

FIGURE 22. CHECK FOR LAMINAR FLOW IN ROTATING CYLINDER VISCOMETER

on clay suspensions to be presented later instability was absent at even higher speeds because of the increase in differential viscosity and the existence of shear strength.

Unless otherwise indicated, the mechanically determined constants are used for determination of differential viscosities and Bingham shear strength from D vs. N plots.

Viscous Behavior of Suspensions of Cohesive Sediments

Measurement Procedure. Suspensions of cohesive sediments change their properties with time, even in the absence of shearing. Both settling of flocs and larger particles, and alteration of floc properties occur. Before undertaking extensive measurements, therefore, it was necessary to select and try measurement procedures that would yield information on properties of the suspension.

It was desired both to determine the character of flocs in the suspension with a minimum amount of shearing and settling, and to observe the character of flocs stable in a given shear field. The following procedure was selected to yield optimum accuracy: Each selected rotation rate was maintained one minute before the drag on the inner cylinder was measured. After determining the drag by means of the dial and torsion wire, the speed was changed to the next selected rotation rate, and the procedure was repeated. Settling of particles during a sequence of measurements was compensated by mixing the contents of the outer cylinder. Mixing was done with a plunger that was lowered and raised 10 times at intervals of a few to perhaps 12 one-minute measurements, depending on the settling velocity of the material.

An example of such a sequence of measurements is presented in Figure 22. The sample was first suspended uniformly, then the inner cylinder was lowered into the outer cylinder and the outer cylinder rotation was started at its lowest speed. After the group of measurements at successively higher speeds, shown as crosses in Figure 22, the suspension was again mixed, and the measurements shown as X's were made. The procedure was continued at increasing, then at decreasing speeds, with stops for mixing as indicated by a change of symbols.

Figure 22 is essentially a rate of strain vs. shear stress plot. It shows the several characteristics commonly observed for sediments in the rotating cylinder viscometer. Several linear portions are apparent, and the dial readings (proportional to shear stresses) found during increasing and decreasing rotation speeds are different, indicating an effect of previous experience on the suspension. The first mixing (at 44 rpm) caused a "jump" from the lower side of the loop to the upper. The second and third mixing (178 and 82 rpm, respectively) caused no change. The fourth mixing, (43 rpm on the decreasing side) caused a "jump" again to the upper side of the loop. Further decrease in rpm produced a well-defined linear portion with a steep slope. There appeared to be at least two stable floc forms in the viscometer shown

on the decreasing rpm portion of the plot. One form persists in the range between 140 and 40 rpm; the other is stable below 40 rpm. The points above 140 rpm suggest the beginning of another region. On plots for some of the samples steep linear portions also appeared at the beginning of the increasing rpm portion. Both of the increasing rpm sections of the plot approach the plots of points for the decreasing rpm data, indicating a breakdown of bonds in the old sediment structure to those of a continuously re-forming structure. During the decreasing rpm conditions, newly forming flocs had the same bonds as those being broken. As the shearing rate decreased, flocs tended to grow in such a way that all parts had similar experience. For the subsequent presentations and interpretations only, data obtained with decreasing rpm were used.

The continuity of the plots in Figure 22 after mixing at 178 and 82 rpm indicated that settling was not a problem.

The evidence of hysteresis shown in Figure 22 raised questions concerning the time of waiting at each speed and the effect of the test on the material. Repeated sequences of measurements were made on a San Francisco Bay sample to obtain information on these questions. A plot of three successive sequences on the same sample is presented in Figure 23. The first sequence was made using the procedure outlined above, with one-minute waits at each speed. The second sequence was made using five-minute waits at each speed; and the third, using one-minute waits at each speed. The plots show that at speeds above 40 rpm the one-minute and five-minute sequences were similar. Below 40 rpm, however, there seemed to be a change in both the increasing and decreasing rpm plots. The shears were generally higher, and the slopes of the decreasing rpm curves steepened. These trends continued in the third sequence, which followed the same procedure as the first, indicating that the change was due to a change in the sediment rather than a difference in procedure. The increase in shear strength is believed to result from the increased numbers of loose particles and particle aggregates produced by shearing. These particles acted as cement by increasing the numbers of bonds at interfloc contacts. This increased strength facilitated larger floc volumes in a shear field, accounting for the steeper slopes below 40 rpm. The slope above 40 rpm did not change, indicating that the aggregate volume had not changed for aggregates stable in that range of shearing. The time at each speed is shown by Figure 23 to have less effect than does shearing of the sediment. The procedure utilizing a one-minute wait at each speed was followed in the remaining measurements to facilitate acquisition of data for a larger number of speeds for a given amount of shearing. Mixing of the suspension was done at about the 40 rpm measurement, and usually after the 180 rpm measurement.

No pretreatment was given the samples other than dilution with water from San Francisco Bay or, in the case of the White River sediment, dilution with tap water.

Data Obtained from Sediment Suspensions. Dilutions of suspensions of each of the estuarial sediments were placed in the viscometer. Sequences of drag vs. rpm measurements were then made and plotted. Straight lines

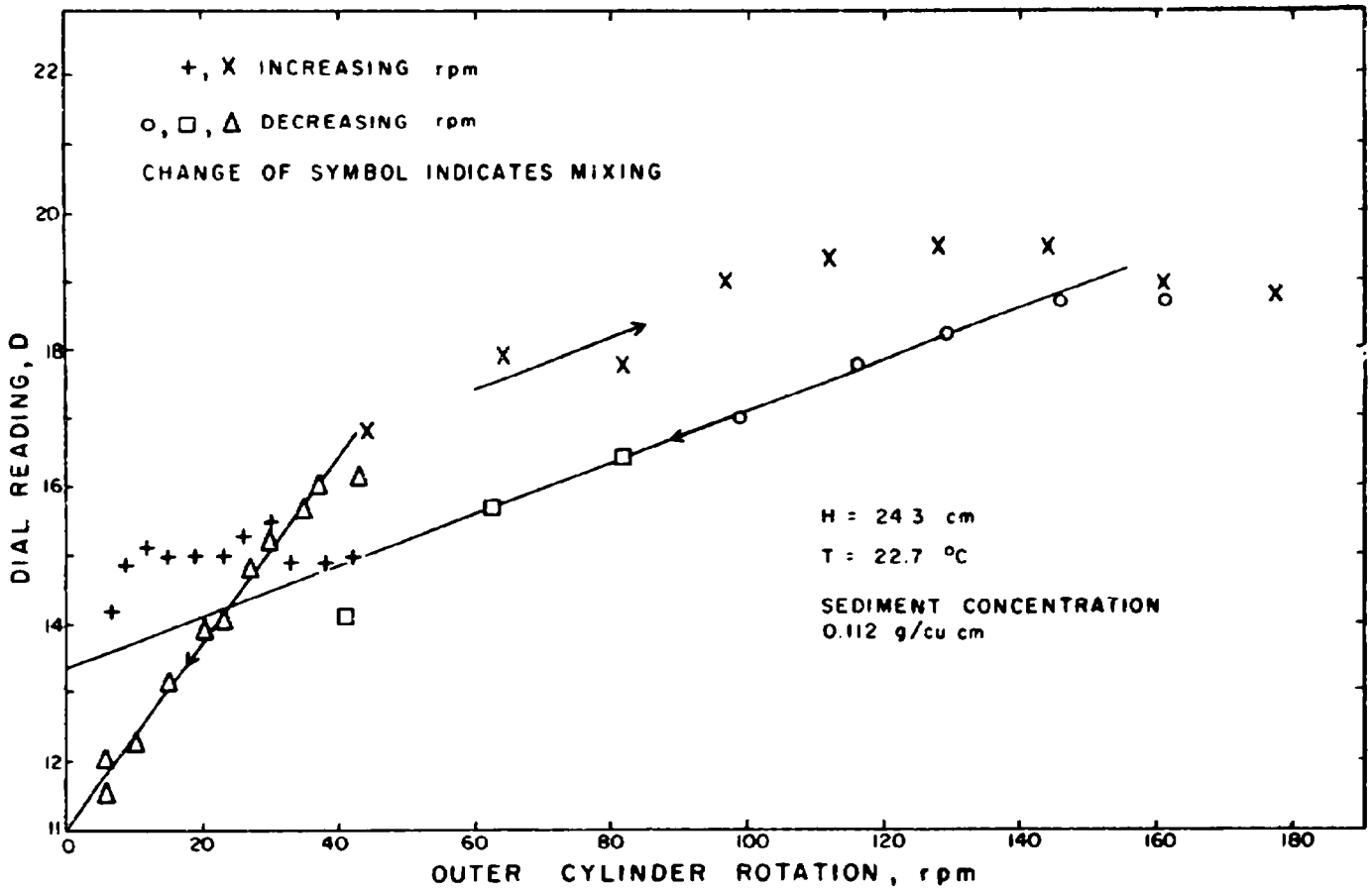

FIGURE 23. A PLOT OF RAW VISCOMETER DATA OBTAINED FROM THE WILMINGTON DISTRICT SAMPLE

were fitted to the decreasing rpm portions as shown in Figures 22 and 23. The plots usually had two such well-defined linear portions--one above, the other below 40 rpm. Occasionally, however, the one below was not well-defined and no line was fitted. The slopes and the intercepts on the zero rpm axis of the lines were tabulated, and the values of the differential viscosities, η_d, and of the Bingham shear strengths, τ_B, were calculated using the bracketed terms in Equation 9. The differential viscosities of the sediment suspensions, divided by published values for water at the same temperature, are plotted against the suspended sediment concentrations in Figures 24 through 29. The Bingham shear strengths are plotted in Figures 30 through 36. In all of these plots, circles denote relative differential viscosities determined from the higher rpm data, and triangles denote values calculated from the lower rpm data. Solid symbols represent points from a second set of measurements. The best straight lines were fitted to the plotted points by eye. Since the slopes of the η_d/η_ℓ curves are of interest, the lines were not forced to intercept the point 0,1. Deviations from such an intercept can be due to errors in measurement of the wire constant, the temperature, or the sediment concentration.

As shown in Figure 23, several slopes are possible for one sediment suspension. The slopes are related to the volume fraction of the sediment by Equation 5, and the several slopes indicate that several amounts of aggregation are possible in the same suspension. The three distinct lines evident by the points in Figure 24 show that only certain distinct volume fractions for a given amount of sediment occurred.

The distinctness of these volume fractions is not as clearly defined in the remaining relative differential viscosity plots. This is partly due to experimental imprecision, but is mostly due to crowding. In Figure 25 the lines terminate at the concentrations at which the space would be entirely filled with floc, as calculated by Equation 5. If the flocs are spherical, they would first all touch each other at $\pi/6$ of that concentration. In Figure 25 the sediment concentration at which the slope of the middle line would give a volume fraction of one is 0.067 g/cu cm. It can be seen that the circled points tend away from that line at half of that sediment concentration; they tend toward the line for the next lower volume fraction. Crowding tends to break up the less dense floc forms leaving the less viscous but more dense form. This factor, crowding, and the consequent adjustment of the volume fraction, are believed to account for much of the scatter in both the relative differential viscosity plots and the shear stress plots.

The bases for plotting the shear stress vs. concentration data on log-log coordinates are empirical. It was found that plots of shear strength data for each sediment produced a set of points that would fit a line with a slope of 5/2. The fit of this same function to all of the data indicates a relationship, but its theoretical bases are not apparent at this time.

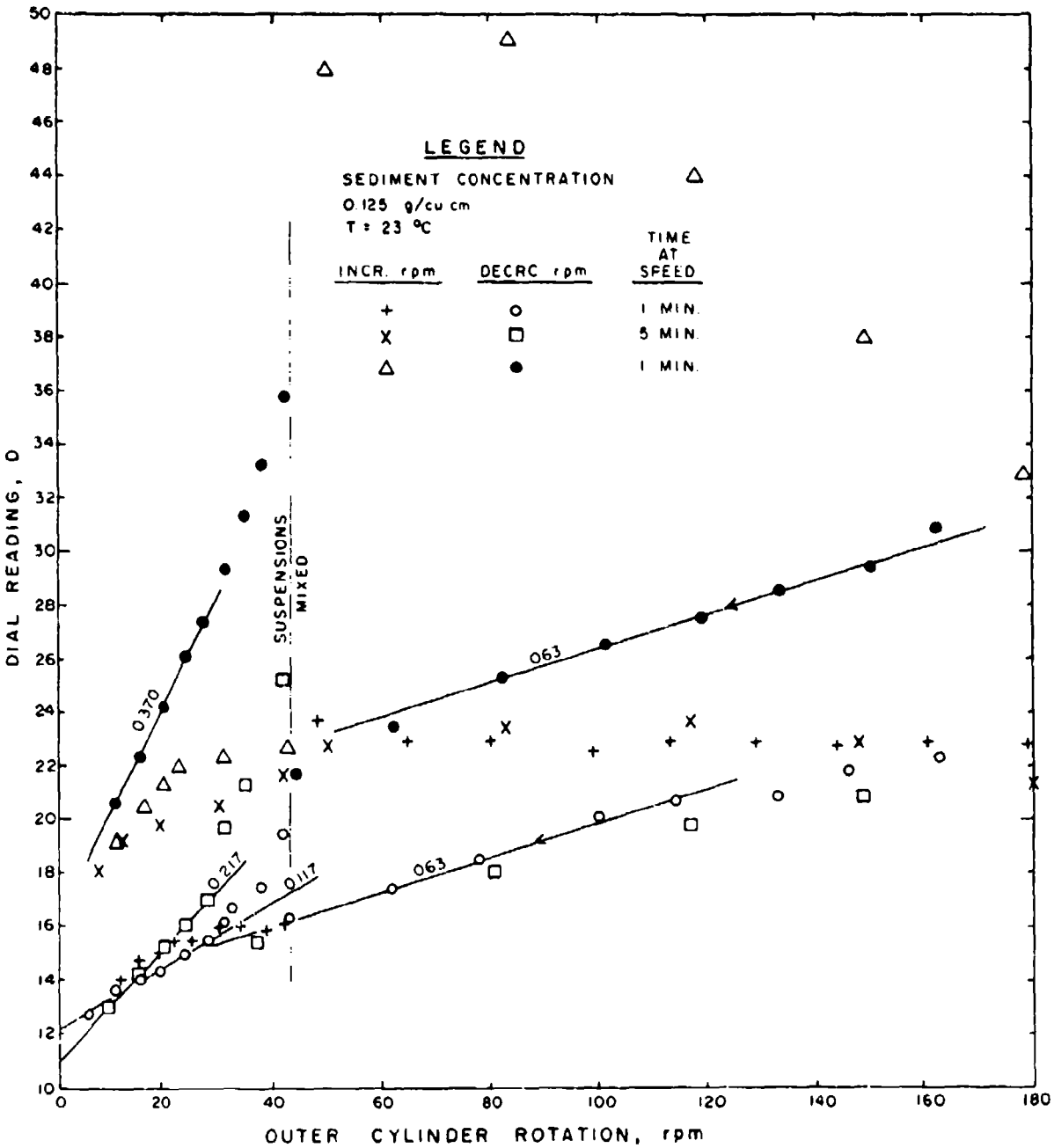

FIGURE 24. DATA OBTAINED FROM REPEATED SEQUENCES OF MEASUREMENTS ON A SAN FRANCISCO BAY SAMPLE

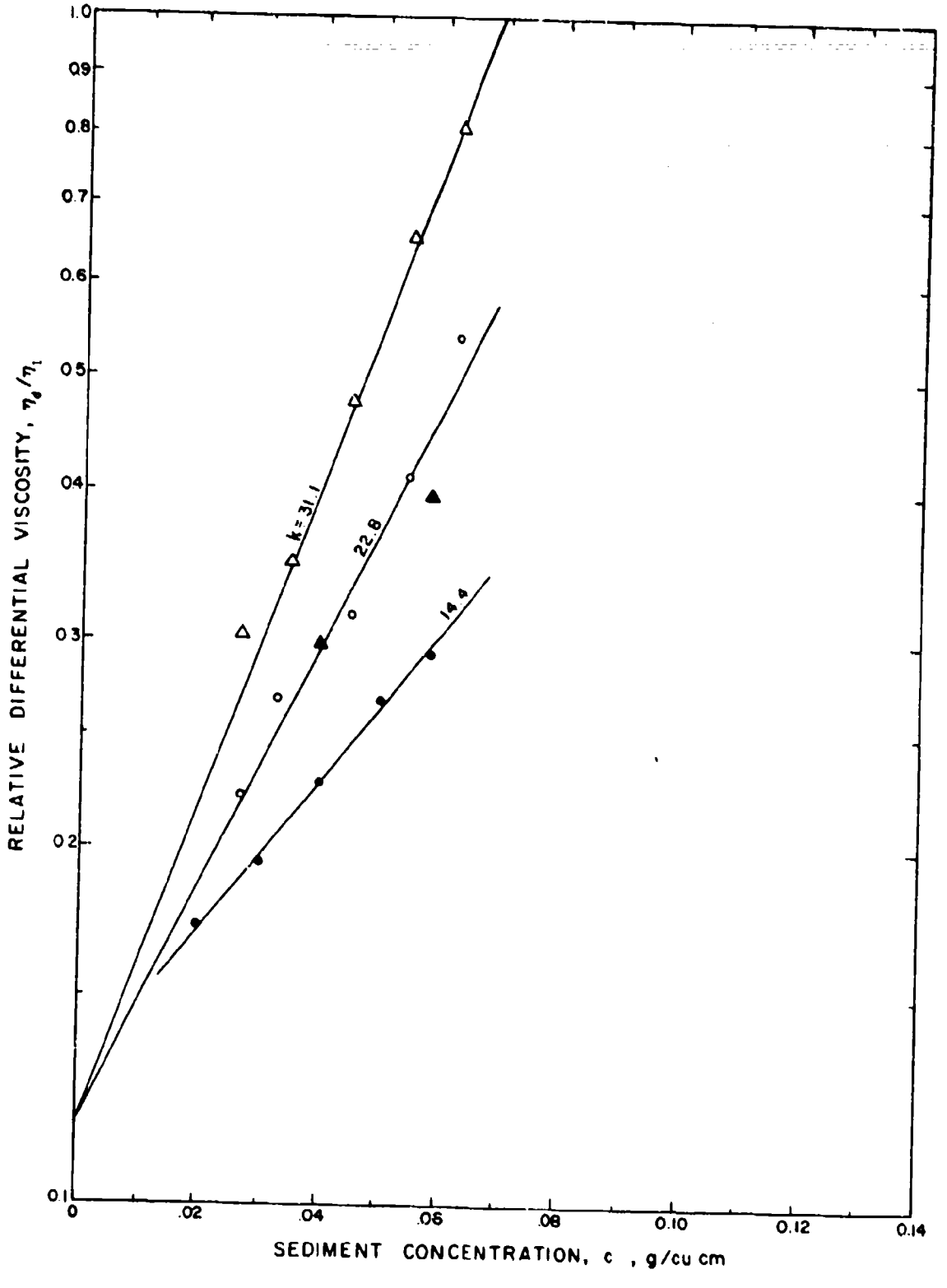

FIGURE 25. RELATIVE DIFFERENTIAL VISCOSITIES OF WILMINGTON DISTRICT SAMPLE FROM ROTATING CYLINDER VISCOMETER MEASUREMENTS

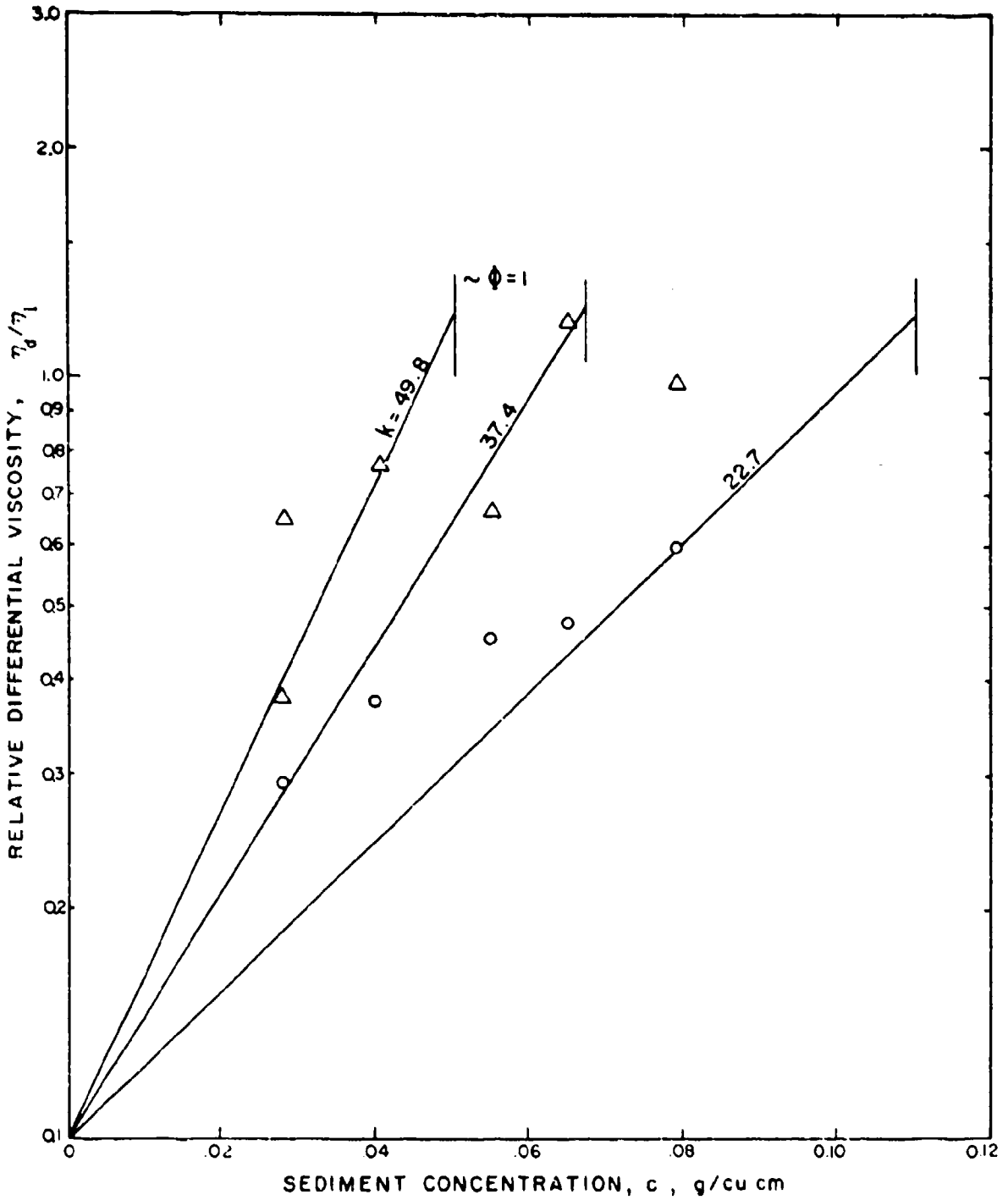

FIGURE 26. RELATIVE DIFFERENTIAL VISCOSITIES OF BRUNSWICK HARBOR SAMPLE FROM ROTATING CYLINDER VISCOMETER MEASUREMENTS

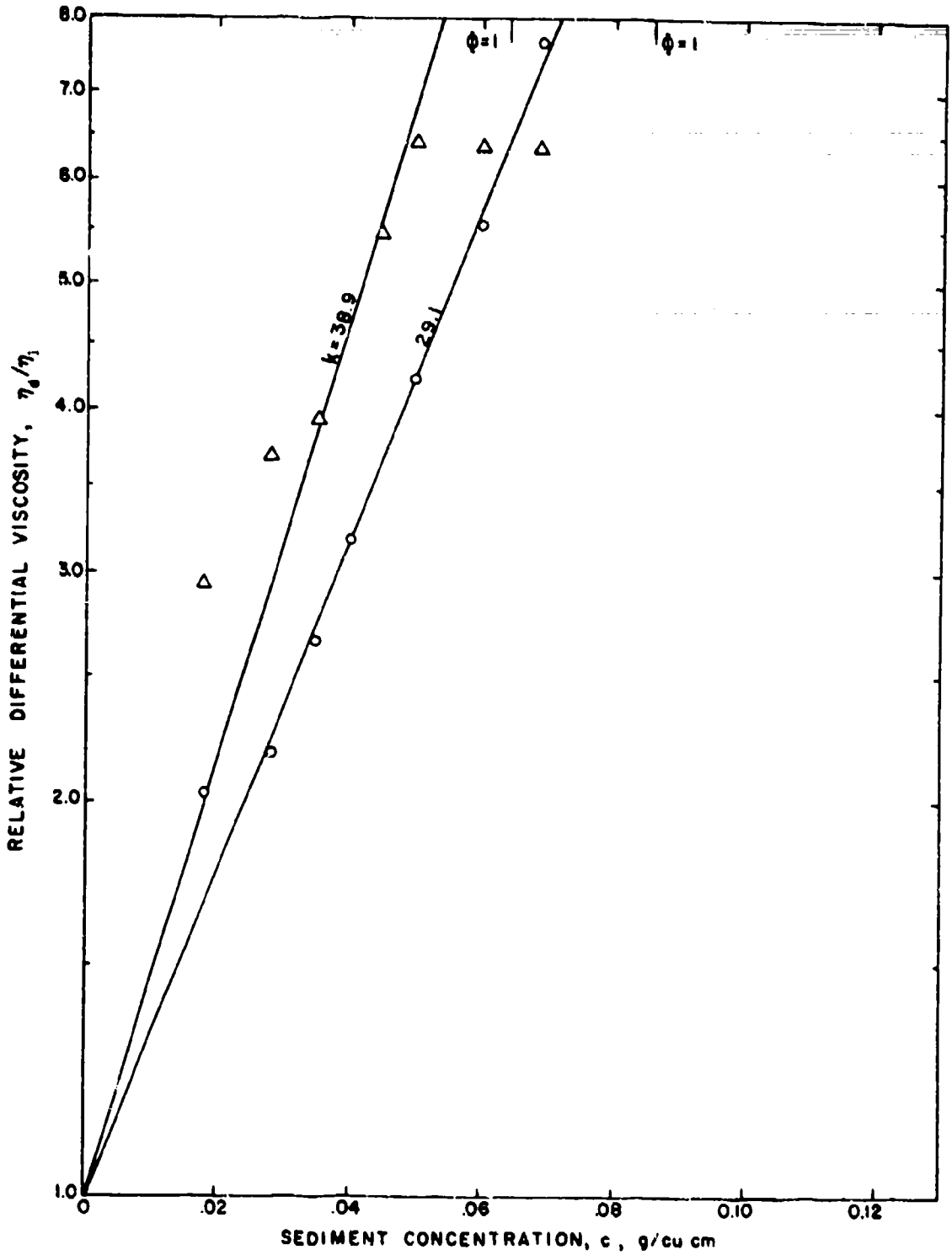

FIGURE 27. RELATIVE DIFFERENTIAL VISCOSITIES OF GULFPORT CHANNEL SAMPLE FROM ROTATING CYLINDER VISCOMETER MEASUREMENTS

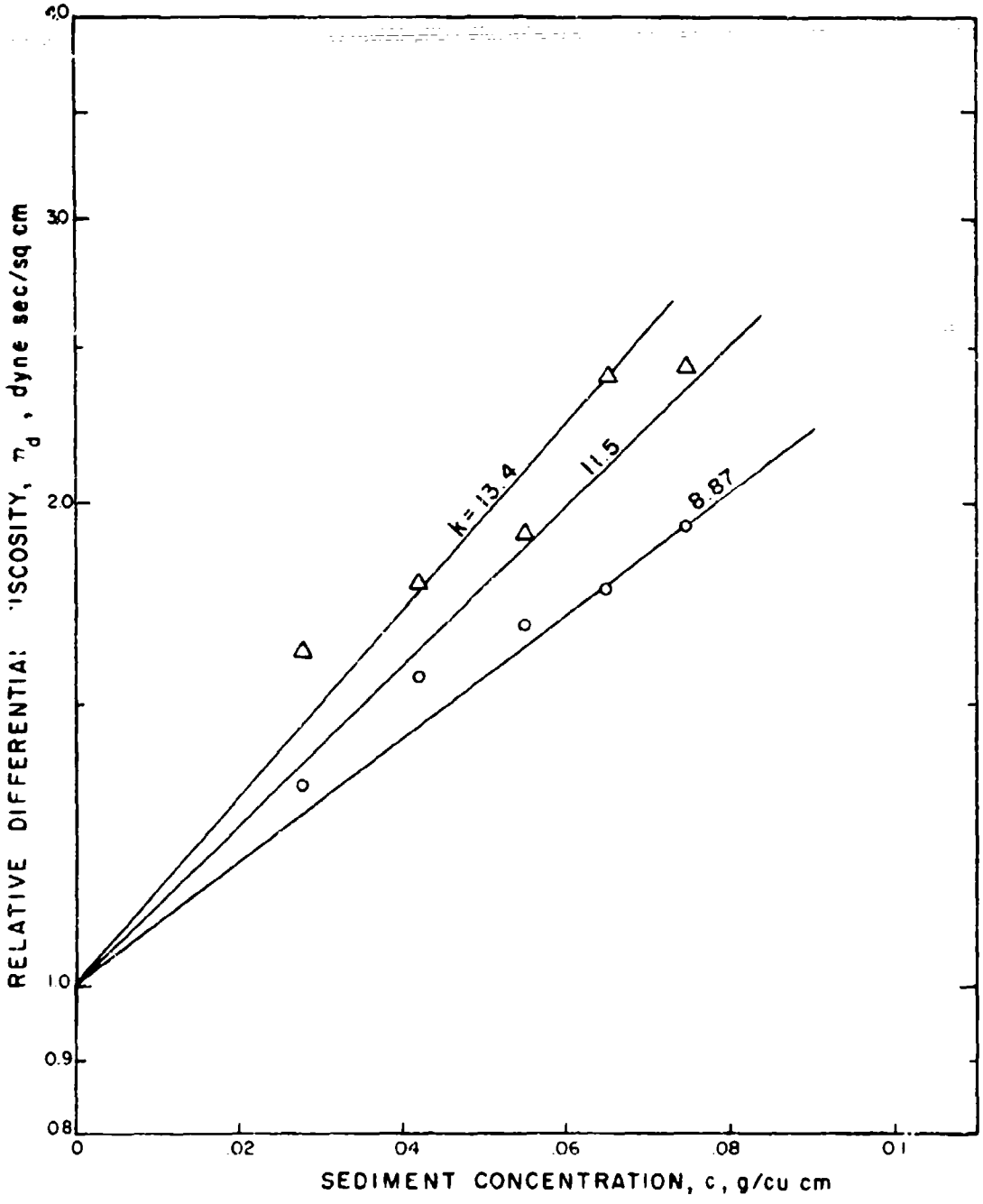

FIGURE 28. RELATIVE DIFFERENTIAL VISCOSITIES OF SAN FRANCISCO BAY, SAMPLE TWO, FROM ROTATING CYLINDER VISCOMETER MEASUREMENTS

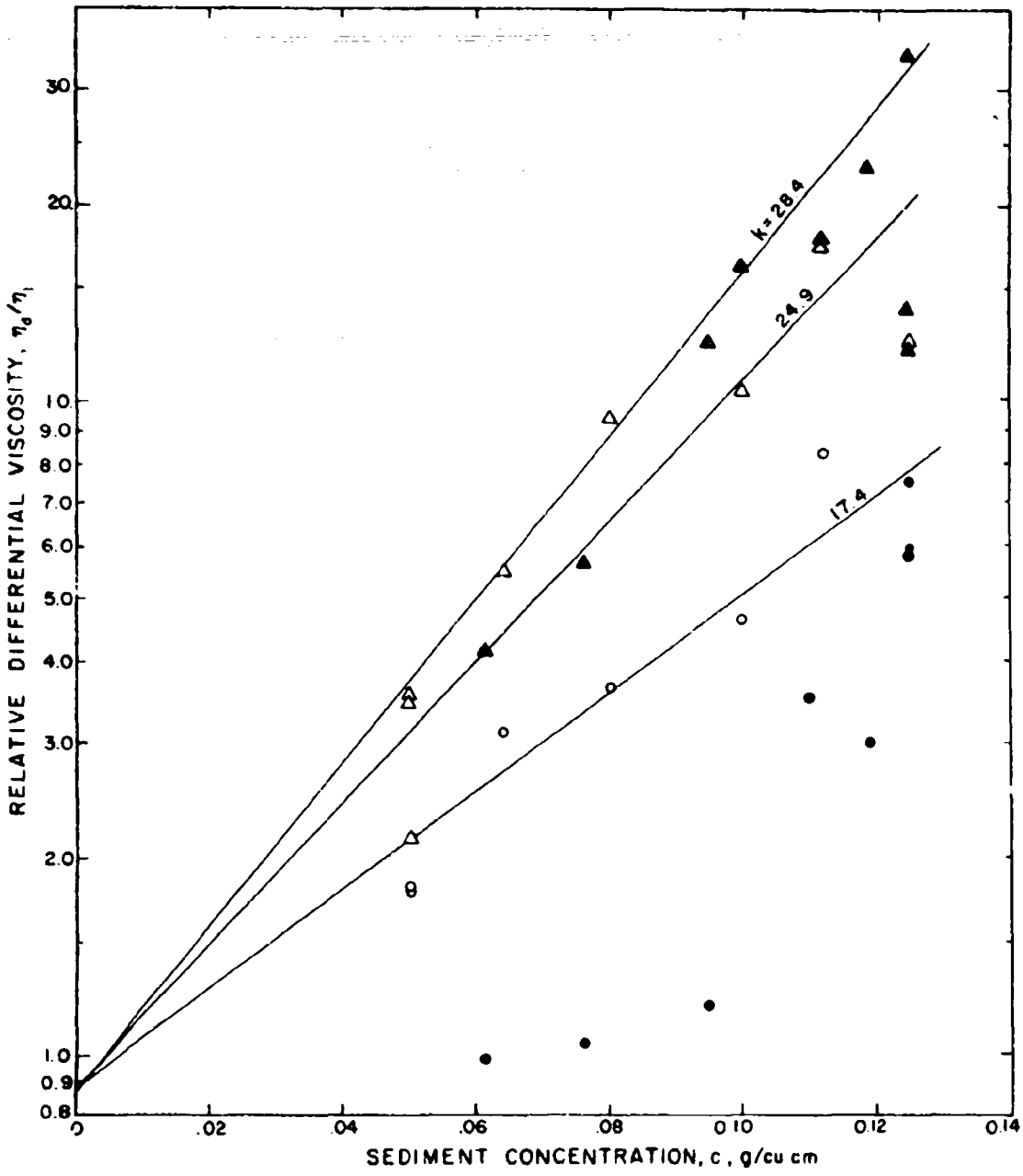

FIGURE 28A. RELATIVE DIFFERENTIAL VISCOSITIES OF SAN FRANCISCO BAY, SAMPLE ONE, FROM ROTATING CYLINDER VISCOMETER MEASUREMENTS

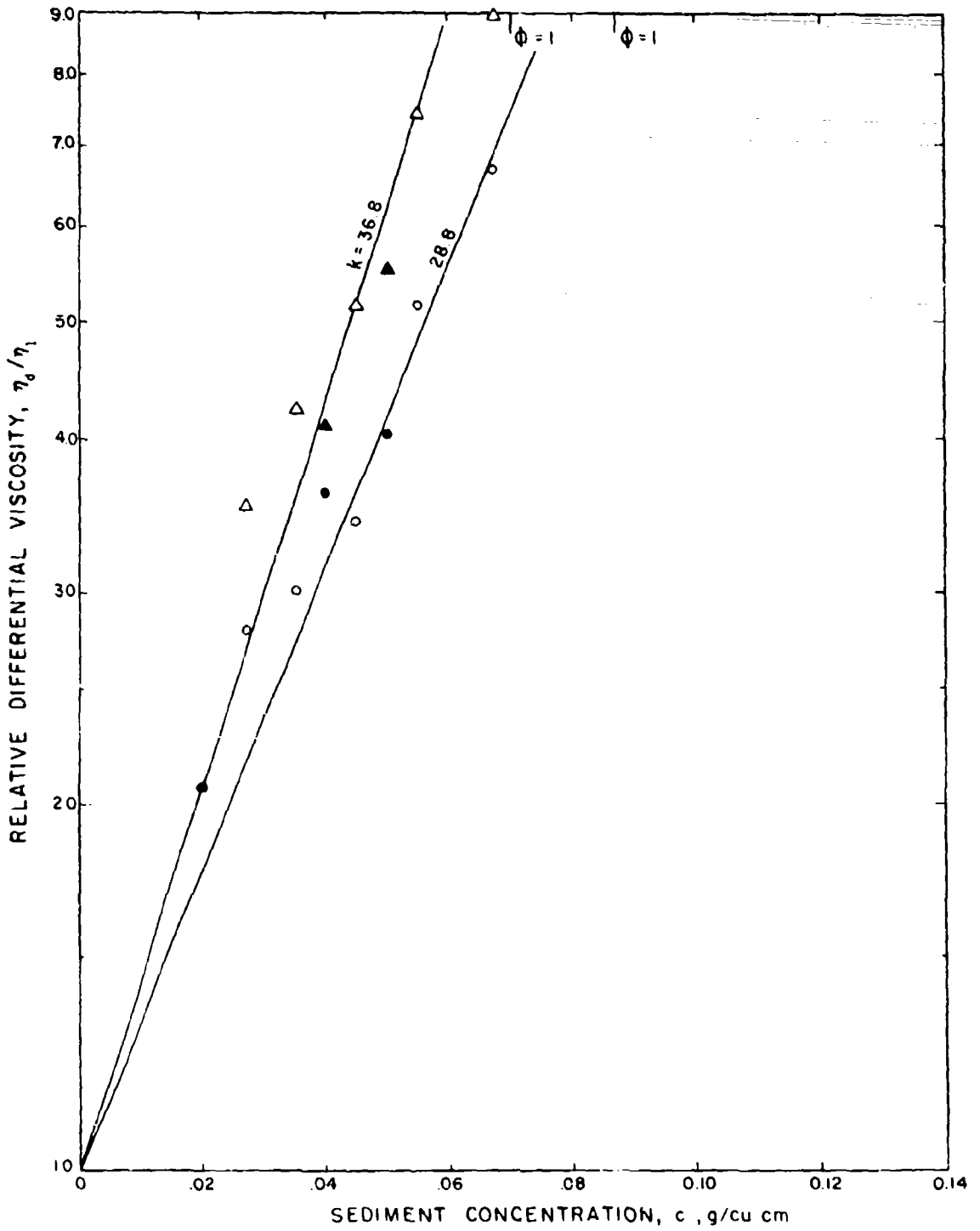

FIGURE 29. RELATIVE DIFFERENTIAL VISCOSITIES OF WHITE RIVER SAMPLE IN SALT WATER FROM ROTATING CYLINDER VISCOMETER MEASUREMENTS

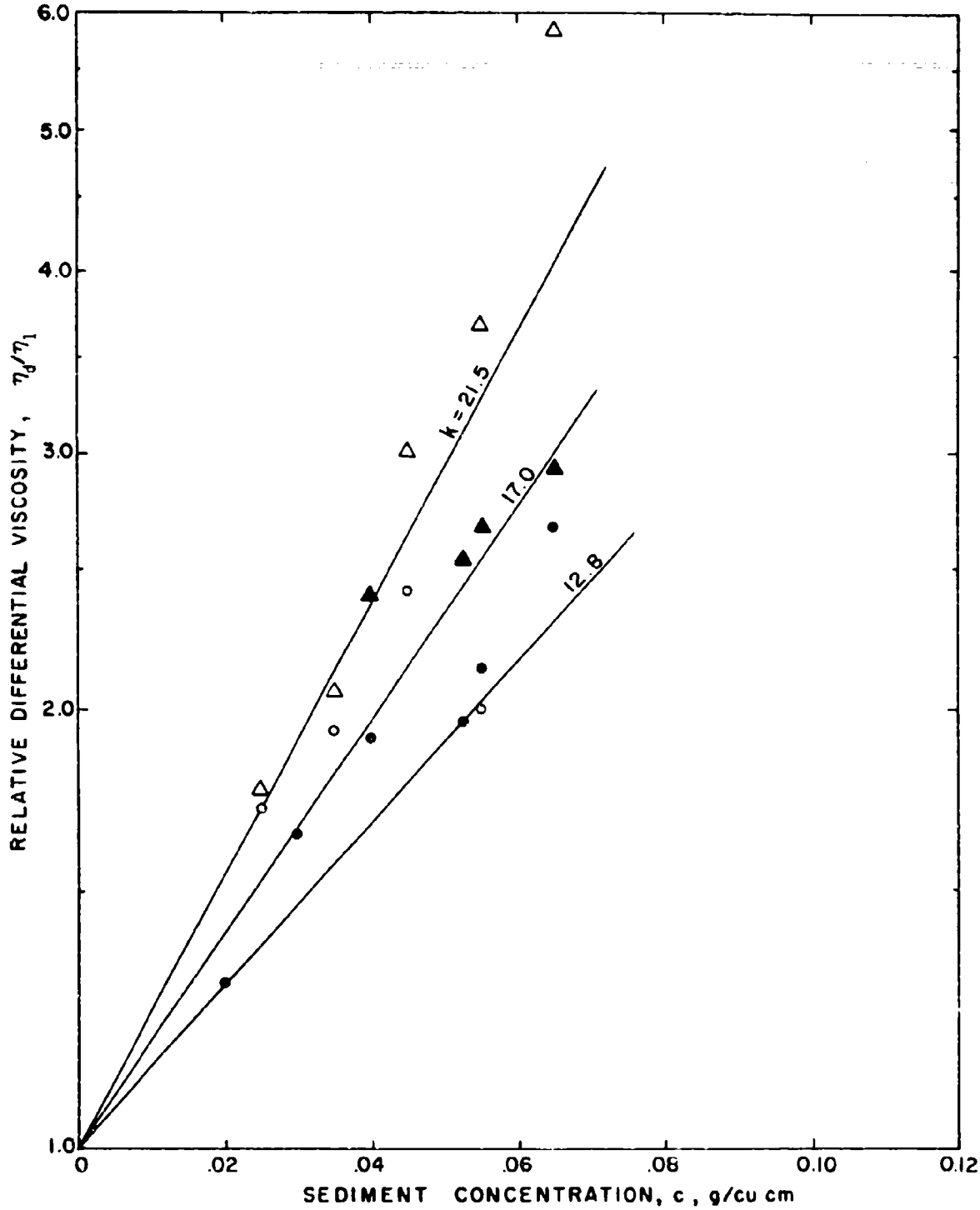

FIGURE 30. RELATIVE DIFFERENTIAL VISCOSITIES OF WHITE RIVER SAMPLE IN TAP WATER FROM ROTATING CYLINDER VISCOMETER MEASUREMENTS

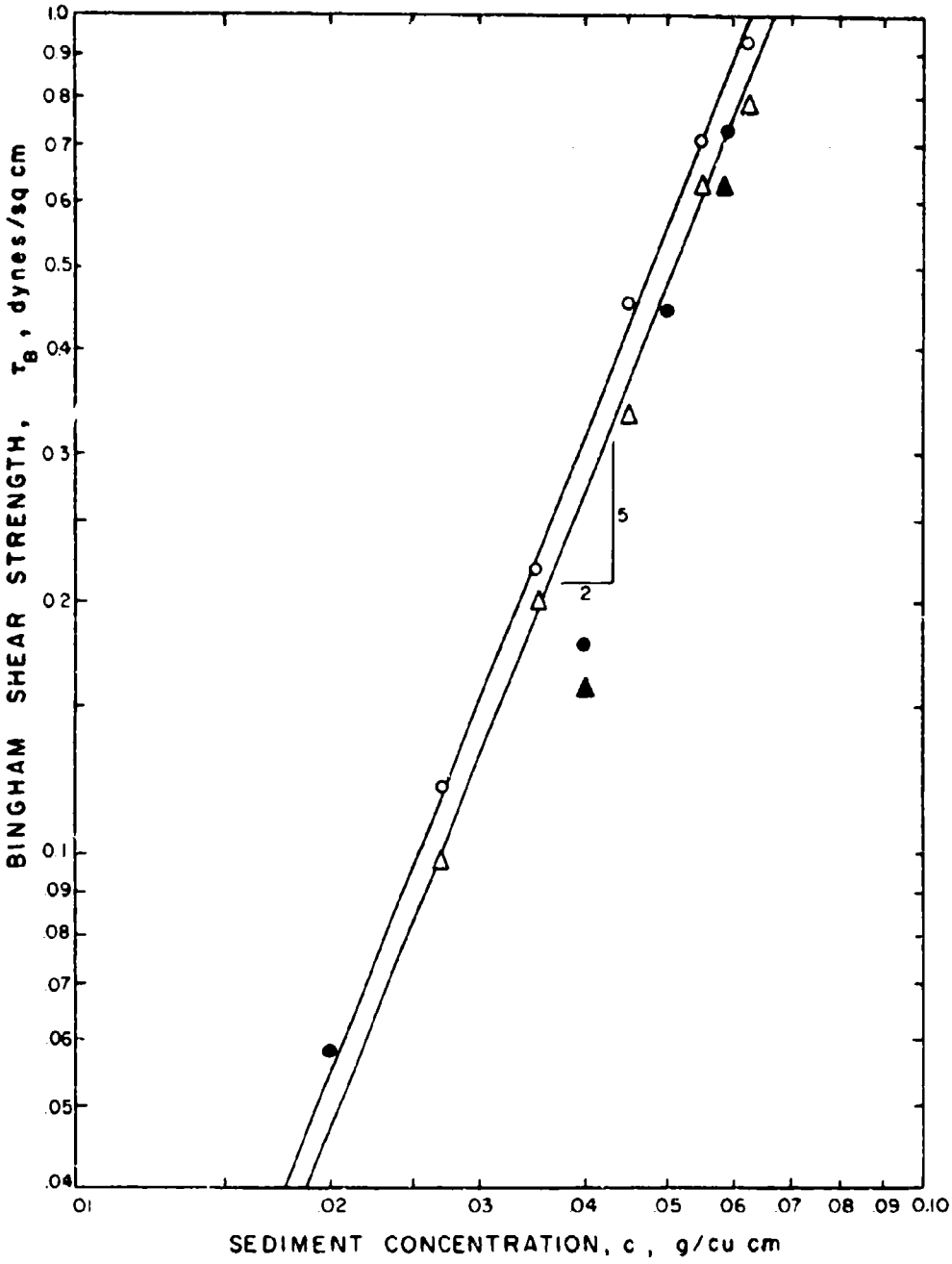

FIGURE 31. SHEAR STRENGTHS OF WILMINGTON DISTRICT SAMPLE FROM ROTATING CYLINDER VISCOMETER MEASUREMENTS

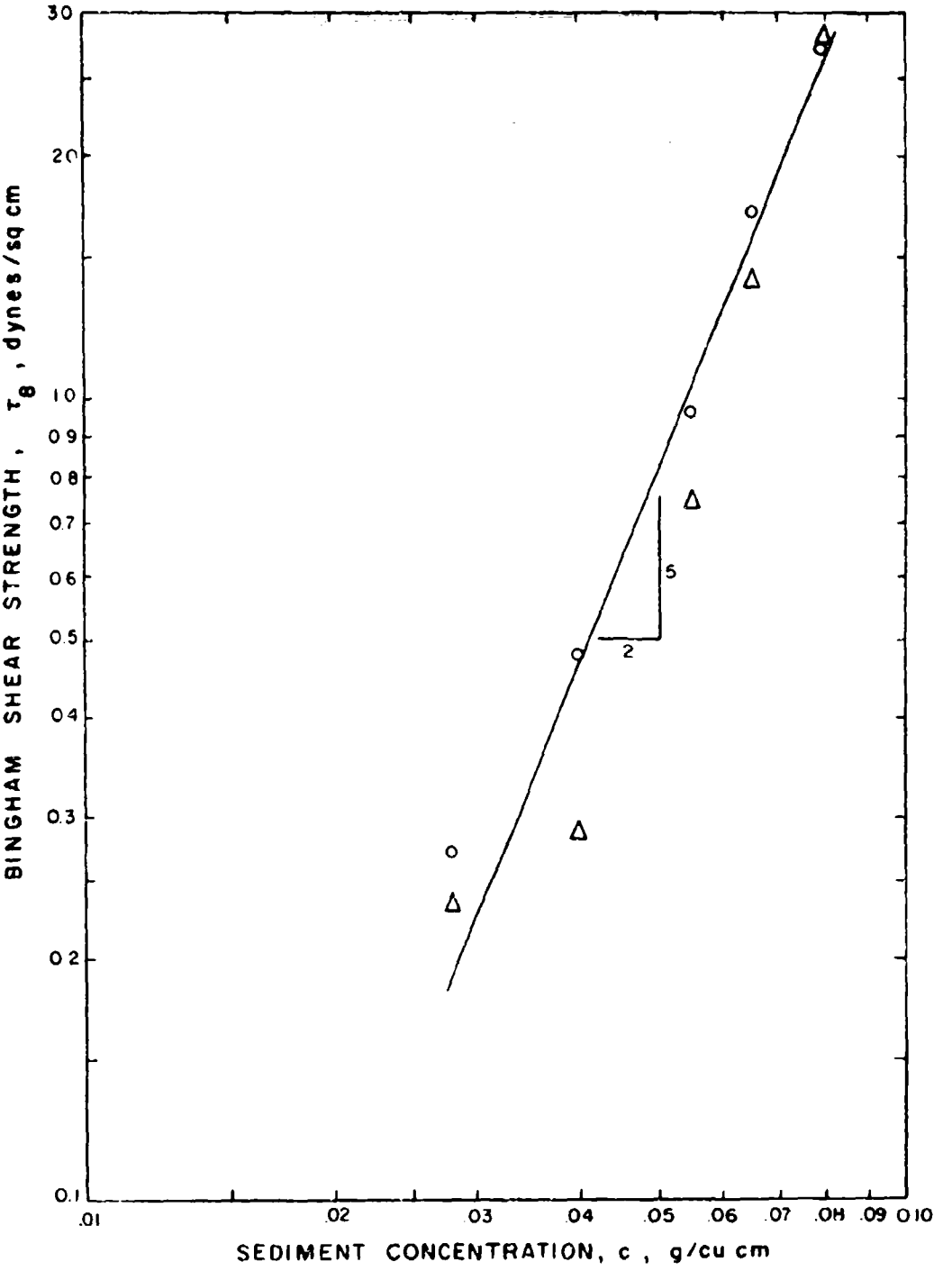

FIGURE 32. SHEAR STRENGTHS OF BRUNSWICK HARBOR SAMPLE FROM ROTATING CYLINDER VISCOMETER MEASUREMENTS

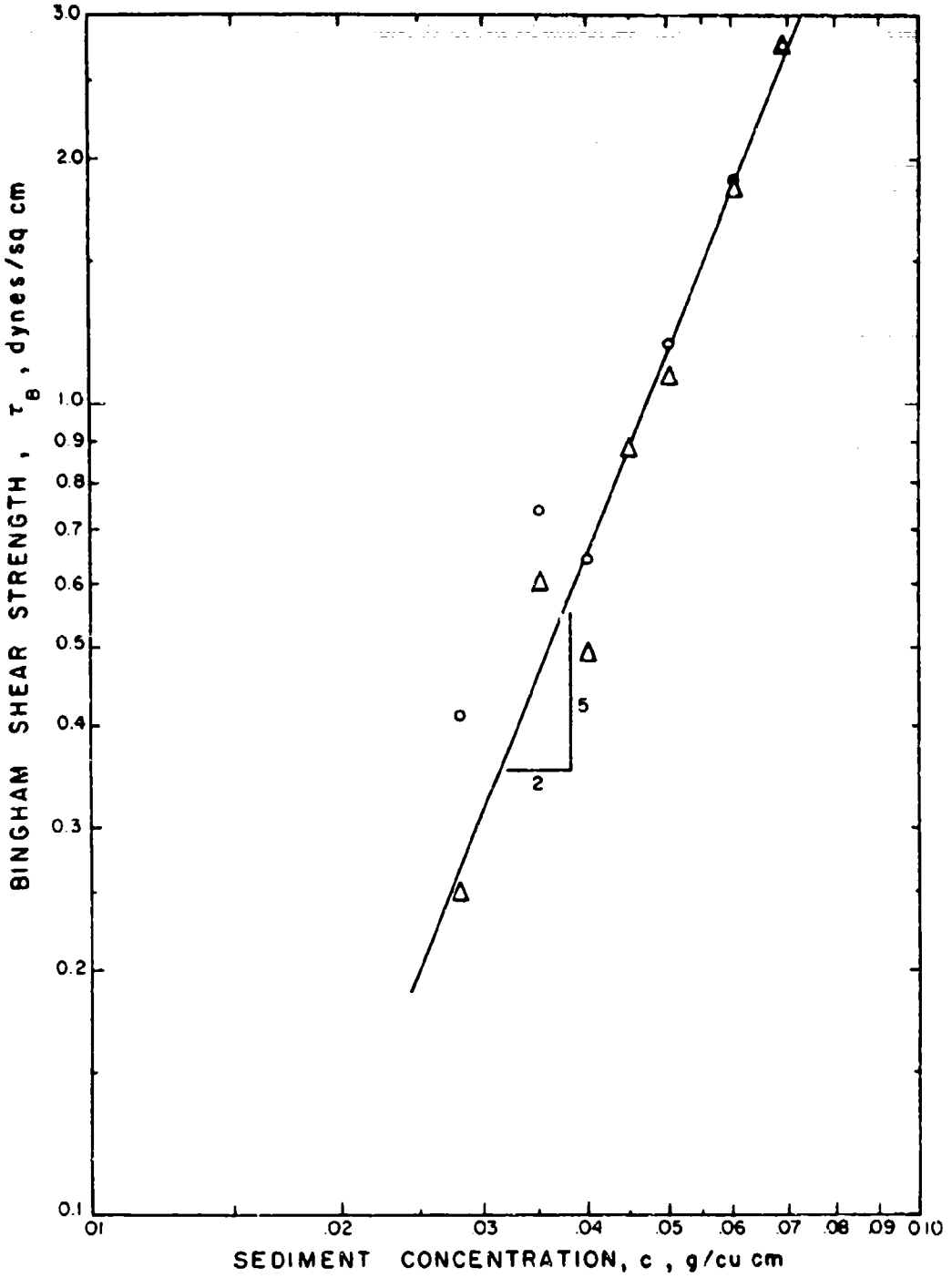

FIGURE 33. SHEAR STRENGTHS OF GULFPORT CHANNEL SAMPLE FROM ROTATING CYLINDER VISCOMETER MEASUREMENTS

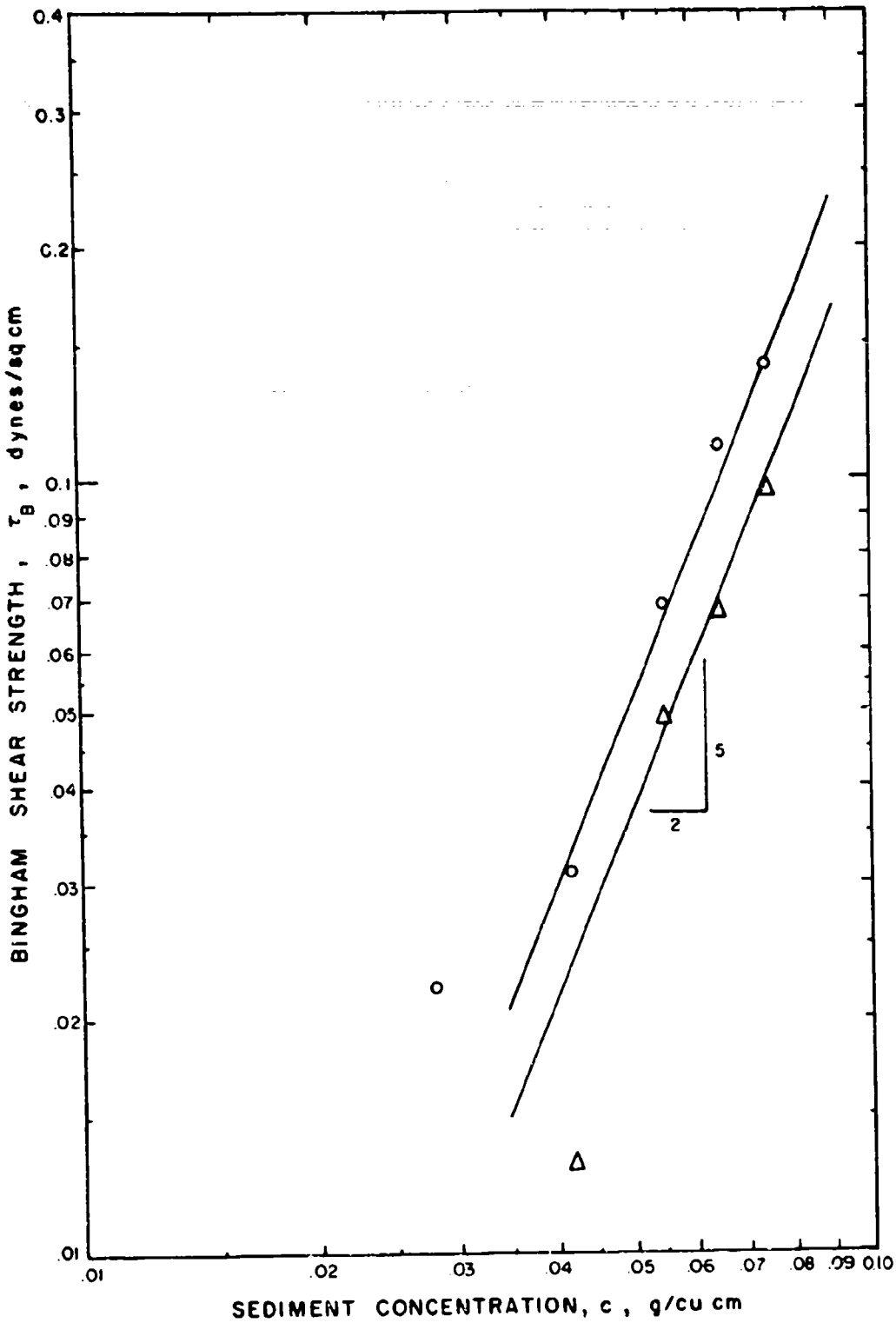

FIGURE 34. SHEAR STRENGTHS OF SAN FRANCISCO BAY, SAMPLE TWO, FROM ROTATING CYLINDER VISCOMETER MEASUREMENTS

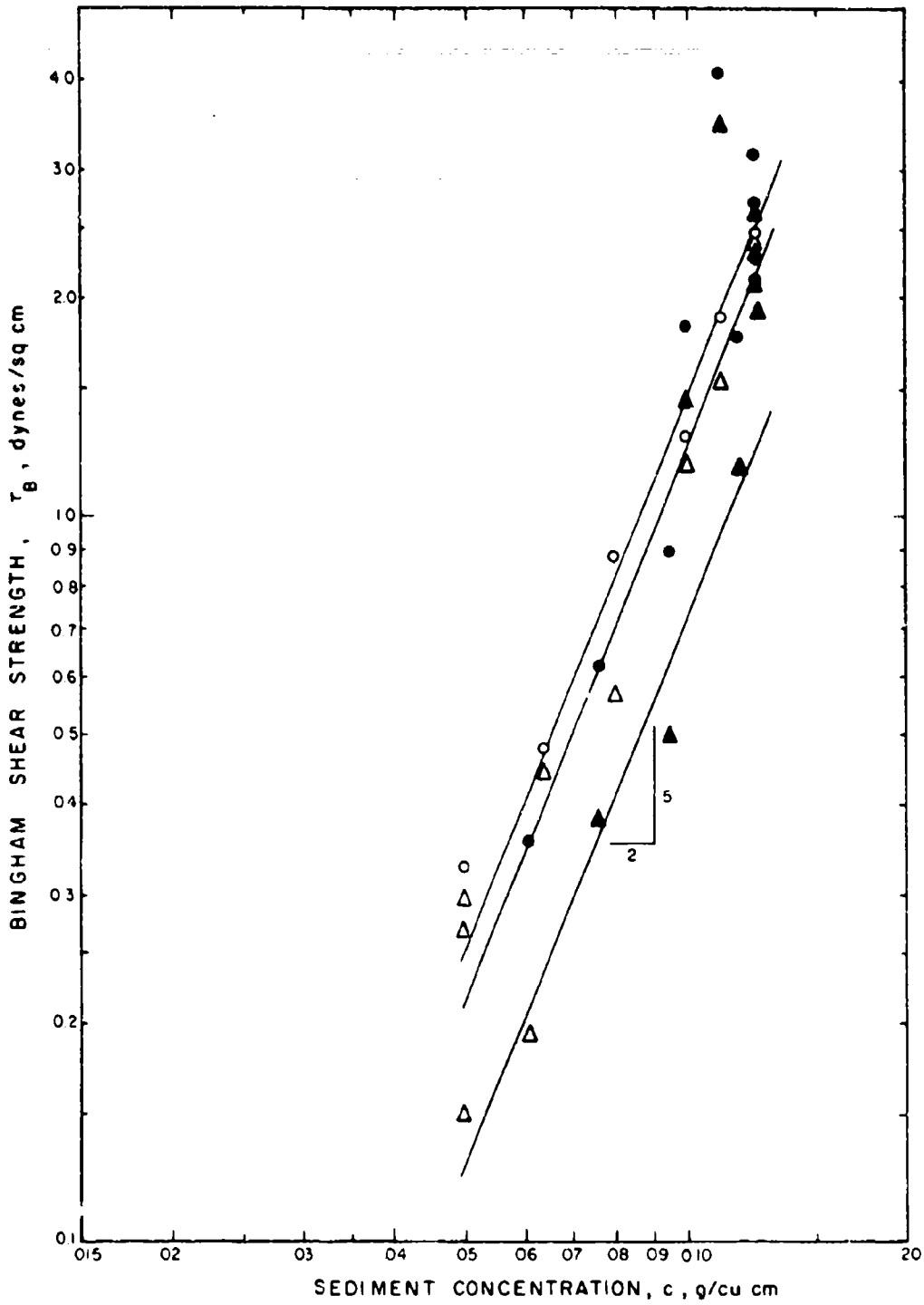

FIGURE 34A. SHEAR STRENGTHS OF SAN FRANCISCO BAY, SAMPLE ONE, FROM ROTATING CYLINDER VISCOMETER MEASUREMENTS

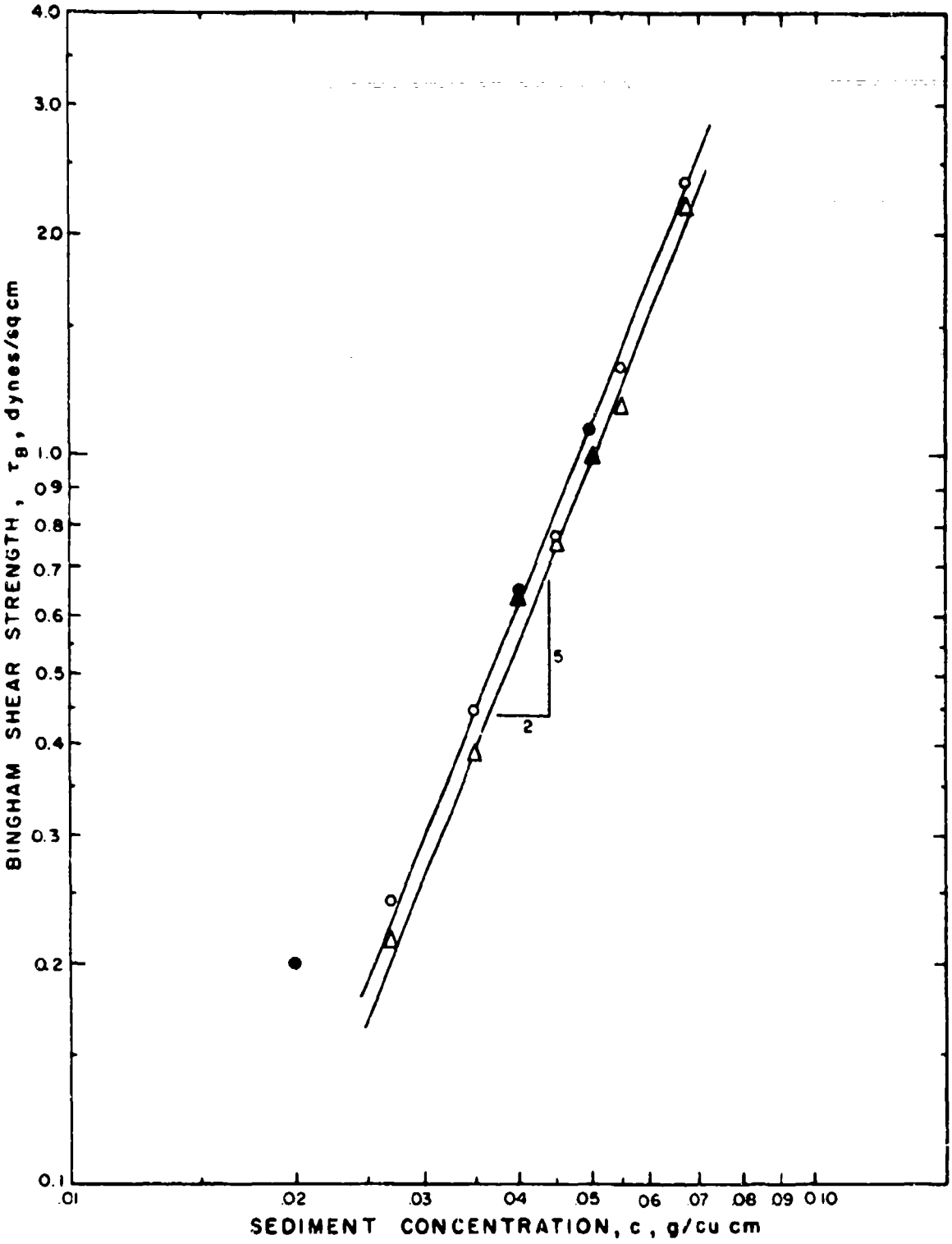

FIGURE 35. SHEAR STRENGTHS OF WHITE RIVER SAMPLE IN SALT WATER FROM ROTATING CYLINDER VISCOMETER MEASUREMENTS

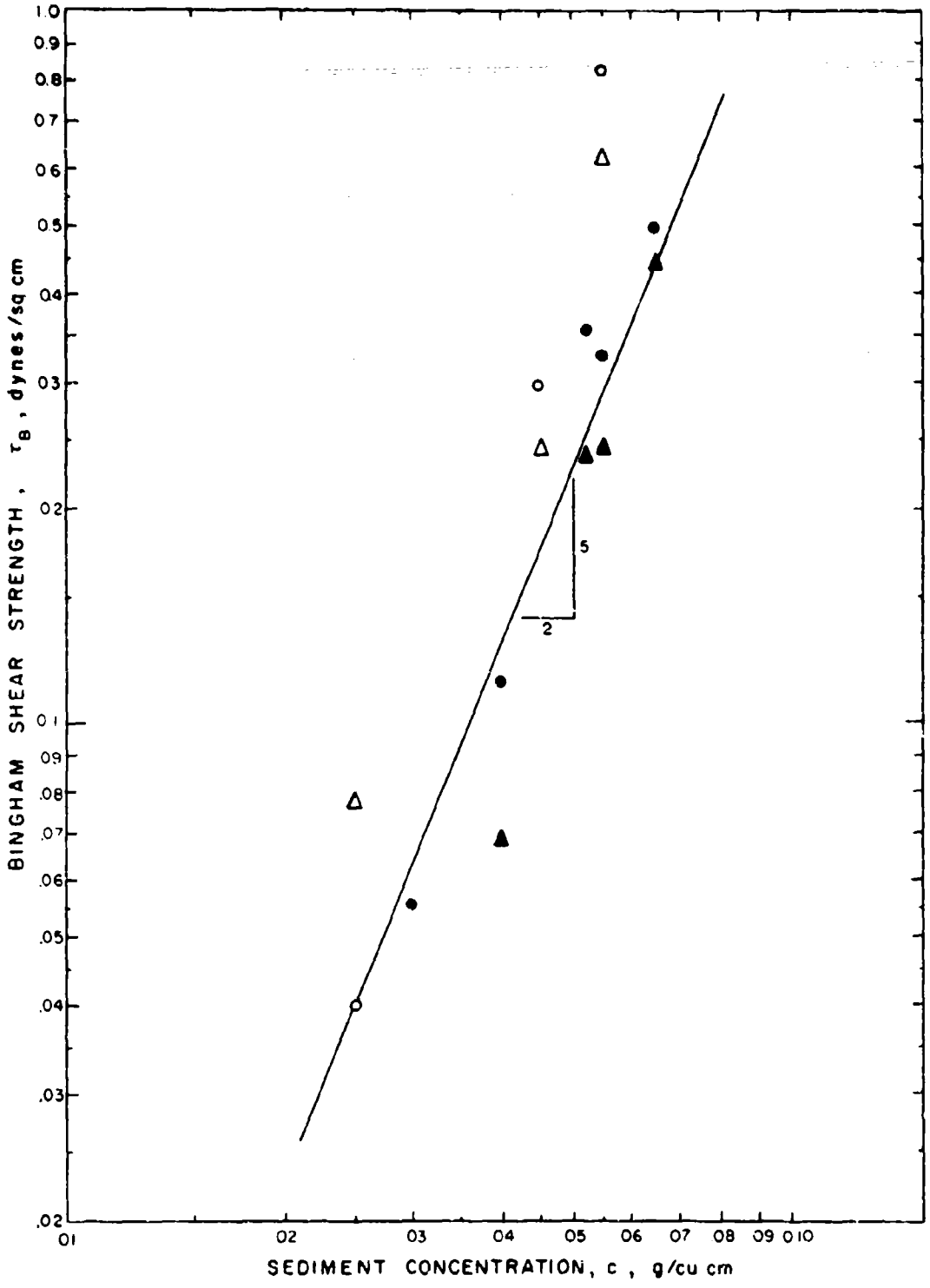

FIGURE 36. SHEAR STRENGTHS OF WHITE RIVER SAMPLE IN TAP WATER FROM ROTATING CYLINDER VISCOMETER MEASUREMENTS

Discussion

The occurrence of several curves in the relative differential viscosity plots indicates that the same suspension can aggregate in several ways, each of which has a different volume fraction. A description of aggregates is needed to interpret the data and to relate the behavior of the sediment in the viscometer to its behavior in the field. Such a description is presented next.

Consider the concept of aggregation of cohesive particles shown diagramatically in Figure 37. Mineral particles cohering in a cluster with uniform porosity are called a primary particle aggregate, with the symbol pa. Such an aggregate would form initially during flocculation of disperse particles, and might attain appreciable size if flocculation progressed slowly. An aggregation of a number of similar particle aggregates, with more or less uniform inter-aggregate porosity, is called a particle aggregate aggregate, designated symbolically as paa. When similar particle aggregate aggregates are joined together the resulting aggregation is called a particle aggregate aggregate aggregate, designated paaa. Increasing orders of aggregation are designated pna, with n indicating the number of successive aggregations.

The pore spaces in the aggregations can be described in the conventional ways, with the porosity meaning the ratio of pore volume to total volume and the voids ratio, e, meaning the ratio of pore volume to "solids" volume. Different kinds of pores can be identified in the floc construction described above. There are the pores between the primary particles in the primary particle aggregates, the pores between the primary particle aggregates in the particle aggregate aggregates, and so on. Each of these pores can be used to define a voids ratio, with the "solids" volume some lower order of aggregation. These are given the symbols and are defined, for example, as follows:

$$e_{(p)aa} = \frac{\Phi_{paa} - \Phi_p}{\Phi_p}$$

$$e_{(pa)a} = \frac{\Phi_{paa} - \Phi_{pa}}{\Phi_{pa}}$$

where Φ is the volume fraction of the particle or aggregation indicated by the subscript. The parenthesis in the subscript indicates the pores included in the void ratio.

If conservation of volume of solids and liquid is maintained, we can write

$$\Phi_{pna} - \Phi_p = \left(\Phi_{pa} - \Phi_p\right) + \left(\Phi_{paa} - \Phi_{pa}\right) + \ldots + \left(\Phi_{pna} - \Phi_{p(n-1)a}\right),$$

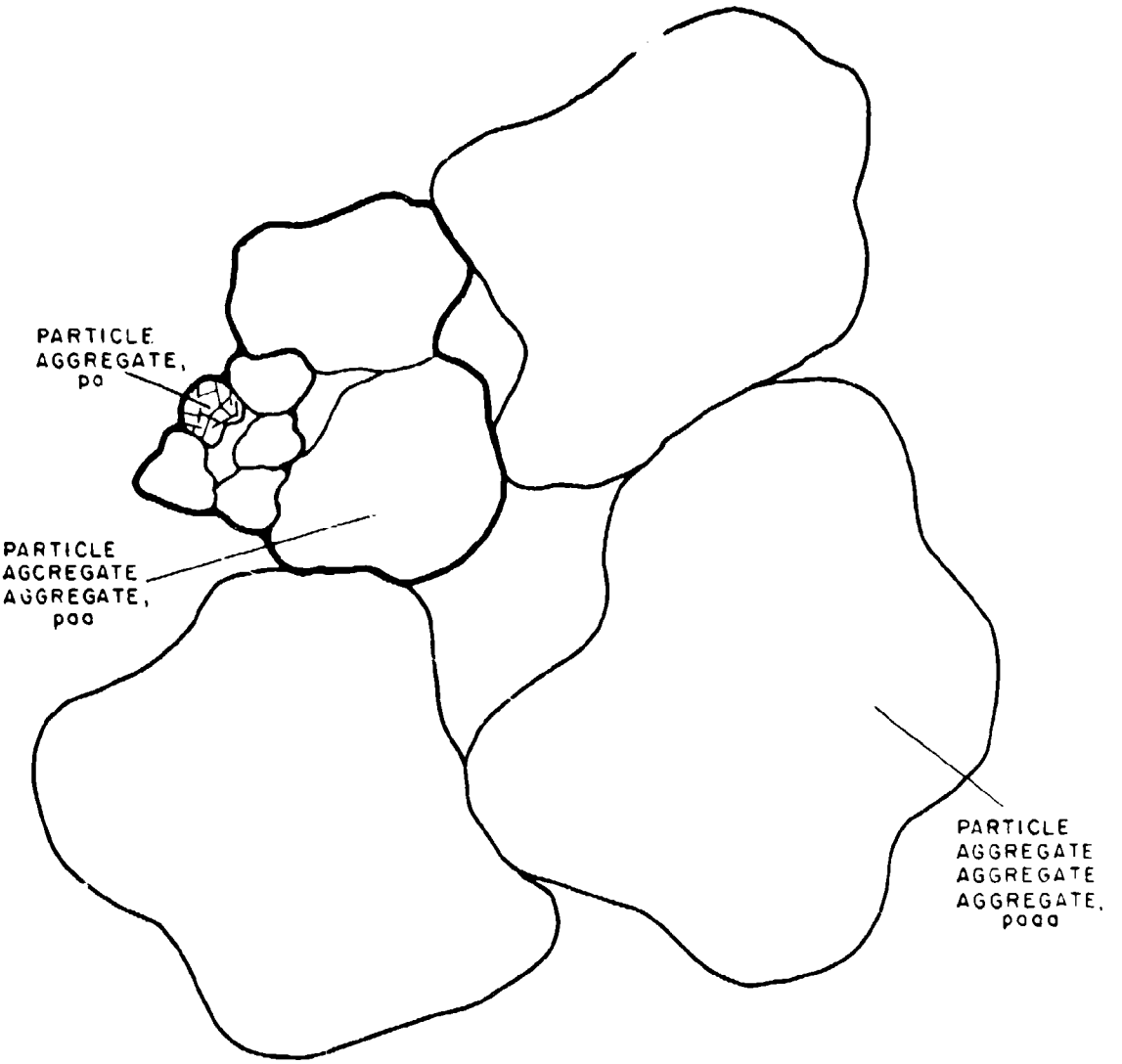

FIGURE 37. A TWO-DIMENSIONAL REPRESENTATION OF A PARTICLE AGGREGATE AGGREGATE AGGREGATE AGGREGATE, p4a

which is simply a statement that the total pore volume of a floc is the sum of the increments in pore volume gained at each stage of aggregation. Using the definition of voids ratio given above, then subtracting Φ_p from both sides gives

$$\Phi_{pna} = \Phi_{pa} + \epsilon_{(pa)a}\Phi_{pa} + \epsilon_{(paa)a}\Phi_{paa} + \cdot \cdot \cdot + \epsilon_{(p(n-1)a)a}\Phi_{p(n-1)a}. \quad (12)$$

If the successive terms on the right after the first term in Equation 12 are designated 1, 2, 3, . . . , we can write from the definitions

$$\Phi_{i+1} = \left(\epsilon_i + 1\right) \Phi_i \ , \quad (13)$$

by which successive terms can be related.

In order to apply these descriptions to clay flocs, assumptions are needed regarding the character of the material. It is assumed that:

1. The primary aggregates retain their density during aggregation. Primary particles do not themselves compress. It is assumed that no significant rearrangement of mineral particles within the primary aggregates occurs on successive aggregations.

2. Successive aggregations beyond primary particle aggregates require some intermeshing of the lower order aggregates. For a first estimate of the amount of intermeshing it was further assumed that the ratio of the increment in voids to the volume of the preceding aggregation is the same as the ratio of voids created during the preceding aggregation to the preceding aggregate volume. This assumption can be written

$$\epsilon_{i+1} = \frac{\epsilon_i}{\epsilon_i + 1} \ . \quad (14)$$

Combining Equations 13 and 14 yields

$$\epsilon_i \Phi_i = \epsilon_{i+1} \Phi_{i+1} \ ,$$

making all of the terms after the first in Equation 12 equal to one another. With these assumptions we now have

$$\Phi_{pna} = \Phi_{pa} + (n-1)(\epsilon_i \Phi_i), \quad n = 1, 2, 3, \ . \ . \ . \ , \quad (15)$$

which includes

$$\Phi_{pna} = \Phi_{pa}\left(1 + (n-1)\epsilon_1\right) \quad .$$

The term (n-1) is named here the <u>order</u> of aggregation of primary aggregates.

<u>Relative Differential Viscosity Data</u>. This description of clay flocs was tested by means of the relation $kc = 2.5\Phi$, and the values of k observed in both the capillary viscometer data and in Figures 24 through 29. Substituting for Φ_i in Equation 15 gives

$$k_n = k_1 + (n-1)(\epsilon_i k_i) \ , \tag{16}$$

which is independent of Einstein's constant and of c. Values of k were plotted against n-1 (integers) with the value of k determined by the capillary viscometer taken to be that for primary particle aggregates. These plots, presented in Figure 38, demonstrate the accuracy of the description of aggregations existing in the viscometer.

The slopes of the lines in Figure 38 are, for example, $\epsilon_1 k_1$. Dividing the slopes of the lines by their intercepts gives ϵ_1. Values of ϵ, thus obtained, are tabulated in Figure 38, and show that the first order aggregations of the clay sediments in sea water, except one from San Francisco, have initial voids ratios near 1.2. The remaining samples show an initial voids ratio near that for a close pack. Evidently the inter-aggregate cohesion for these remaining sediment suspensions was insufficient to maintain the open aggregate structure of the others. The voids ratio 1.2 is equivalent to a porosity of 0.55, which is a more open structure than commonly occurs in noncohesive materials.

The total extra-primary aggregate voids increase with each additional order of aggregation, even though the increment of porosity decreases. The successive voids ratios are, in general,

$$\epsilon_m = \frac{\epsilon_1}{1 + (m-1)\epsilon_1} \quad .$$

As the total voids increase, both the density and shear strength decrease.

An important feature of Equations 12 and 15 is their independence of floc size. The floc size depends both on the history of the suspension and on the prevailing shearing rate. If, for example, dispersed particles are slowly fed into a suspension containing only low numbers of

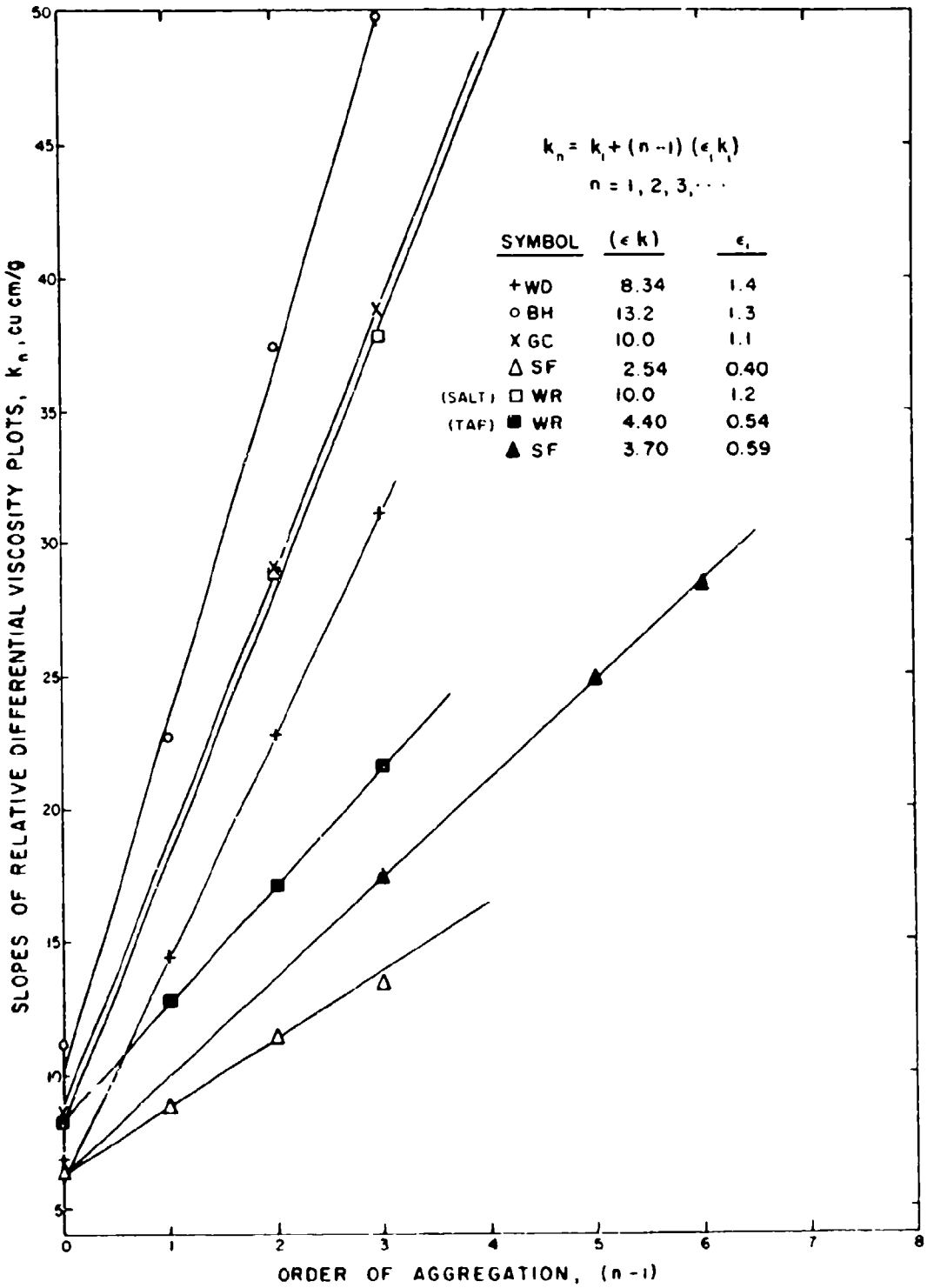

FIGURE 38. TEST OF EQUATION 16

primary aggregates, these primary aggregates might become large even at low shearing rates before first order aggregation becomes significant.

Bingham Shear Strength Data. Measurements of the shear strengths of primary particle aggregates, using the capillary viscometer, yielded shear strength—suspended sediment concentration relations that were linear after a sediment concentration sufficient to transmit shear was reached. Neglecting the conditions at low concentrations, the shear strengths of the primary particle aggregates can be written as

$$\tau_B \cong E_m c, \quad \text{or}$$

$$\tau_B \cong E_v \, \Phi_{pa} \, . \tag{17}$$

E_m has the units of dyne cm/g, and is interpreted as the energy required to disperse one gram of sediment material. E_v is the energy required to disperse a cubic centimeter of particle aggregate, and is numerically equal to the shear strength at $\Phi_{pa} = 1$. Since $\Phi_p = c/\rho_p$, $E_v = E_m \, \Phi_p \, \rho_p/\Phi_{pa}$. Values of E_v and E_m were presented in Table V.

The Bingham shear strength—suspended sediment concentration relations observed using the rotating cylinder viscometer have the form

$$\tau_B = K \, c^{5/2} \tag{18}$$

Equation 18 can be put into the same units as Equation 17:

$$\tau_B = E'_v \, \Phi_{pa}{}^{5/2} \, , \tag{19}$$

where E'_v is the energy to disperse a unit volume of aggregate.

The value of E'_v depends on the strength of the interparticle bonds in the primary aggregates, characterized by E_v, and by the floc structure in the region of failure. If the suspended particles exist as a number of flocs that collide, bond, then rupture during shearing, the region of bonding and failure is that of mutual interpenetration of the colliding flocs. Failure in such a region requires the simultaneous failure of the number of particle aggregate to particle aggregate bonds formed in the region. At the same time the volume of particle aggregates in the region is $\Phi_{pa}/\Phi_{p(n-1)a}$. Letting N be the number of simultaneous particle aggregate bonds ruptured, then

$$E_v' = NE_v \frac{\Phi_{pa}}{\Phi_{p(n-1)a}} = \frac{NE_v}{1+(n-2)\epsilon_1}, \quad n = 2, 3, 4, \ldots .$$

N should increase as the order of aggregation increases, but not necessarily uniformly.

Replacing E_v' in Equation 19 by the expression above, and putting Equation 19 in terms of sediment concentration gives

$$\tau_B = \frac{N}{1+(n-2)\epsilon_1} E_v \left(\frac{\Phi_{pa}}{\Phi_p \rho_p} c \right)^{5/2}, \quad n = 2, 3, 4, \ldots . \tag{20}$$

By comparison with Equation 18 it can be seen that

$$K = \frac{N}{1+(n-2)\epsilon_1} E_v \left(\frac{\Phi_{pa}}{\Phi_p \rho_p} \right)^{5/2} . \tag{21}$$

$N/(1+(n-2)\epsilon_1)$ can be evaluated with the available data. Values of Φ_{pa}/Φ_p and of E_v are presented in Tables IV and V, respectively. Taking $\rho_p = 2.65$ g/cu cm, finding ϵ_1 from Figure 38, and using values of K from Figures 30 through 36 enables calculation of $N/(1+(n-2)\epsilon_1)$. These calculated values, together with the values for N equal to an integer, are presented in Table VII. Integral values of N and (n-2) were sought to give the observed constant. Agreement between observed and calculated values in columns five and nine, and values in columns eleven and fourteen can be seen to be within seven per cent--well within the precision of the data. It can be concluded that this interpretation is consistent with the data from both viscometers, and that N is an integer.

Relations between integers N and n-2 of Equation 20 to order of aggregation are presented in Table VIII. The values of N in Table VIII show that N doubled for each of the sediments, and that all of the N values are equal to two raised to an integer. The missing values of N were inserted in Table VIII, shown in parentheses, as 2^m, and with the assumption that an increase in N would make itself apparent at as low an order as it occurred. Extension of the values of N, n-2 in Table VIII to those for orders higher than the observed ones will require additional knowledge of the intermeshing of flocs.

The observed values of the coefficients of Equation 20, together with the interpolated values of N, n-2 shown in Table VIII, enable the calculation of shear strengths of the aggregates. The aggregate densities can be calculated from the k values shown in Figure 38. Both of these aggregate properties are presented in Table IX.

TABLE VII

OBSERVED AND CALCULATED COEFFICIENTS FOR THE SHEAR STRENGTH–SEDIMENT CONCENTRATION RELATION

Sediment Sample	E_v	$\phi_{pa}\Phi_p\rho_p$	First Curve						Second Curve				
	dyne cm/cu cm	cu cm/g	$10^{-3}K$	$N/(1+(n-2)\epsilon)$	N	(n-2)	ϵ_1	Calculated $N/(1+(n-2)\epsilon_1)$	$10^{-2}K$	$N/(1+(n-2)\epsilon_1)$	N	(n-2)	Calculated $N/(1+(n-2)\epsilon)$
Wilmington District	21.0	2.74	1.01	3.87	4	0	1.37	4.00	8.65	3.32	8	1	3.38
Brunswick Harbor	33.7	4.44	1.47	1.05	1	0	1.29	1.00	--	--	-	-	--
Gulfport Channel	45.9	3.43	2.10	1.99	2	0	1.14	2.00	21.0	1.99	2	0	2.0
San Francisco Bay	21.8	2.52	0.453	2.06	2	0	0.586	2.00	2.93	1.34	2	1	1.26
White River (salt)	48.6	3.28	1.96	2.06	2	0	1.20	2.00	17.5	1.85	4	1	1.82

TABLE VIII

INTEGERS N AND (n-2), SHOWN AS N,(n-2)

Sediment Sample	Order of Aggregation[a]					
	1	2	3	4	5	6
Wilmington District	4,0	8,1	8,1			
Brunswick Harbor	1,0	1,0	1,0			
Gulfport Channel	(1,0)[b]	2,0	2,0			
San Francisco Bay	(1,0)	(1,0)	2,0	(2,0)	2,1	2,1
White River (salt)	(1,0)	2,0	4,1			

[a]Determined from Figure 38.

[b]( ) Not observed.

The aggregate densities can be seen to diminish rapidly toward the density of the liquid, and the shear strengths to decrease rapidly as the order of aggregation increases. Even one order of aggregation reduces the shear strength to as little as one-eighth of that of the particle aggregates themselves. Such a change agrees with soils experience, and is the reason an earth fill is compacted when strength is desired.

The shear strengths of the second and third order aggregates of San Francisco Bay sediment shown in Table IX have the same value. The second was calculated with $N = 1$ and the third with the observed $N = 2.06$. The high sediment concentrations and the shearing in the viscometer caused rapid growth, while failure of interaggregate bonds reduced the aggregate growth. If failure of the third order aggregates is no more probable than failure of second order aggregates, the higher order aggregations would be favored. This consideration accounts for the lack of observed values for second order aggregations.

The sediment properties shown in Table IX summarize the results of measurements on aggregate properties made during this study. Applications of floc densities and shear strengths are made in the next chapter.

Conclusions

The measurements of sediment properties made with the large annular gap rotating cylinder viscometer provided information on properties of flocs that complemented the information obtained using the capillary viscometer. In particular it was found that:

TABLE IX

PROPERTIES OF SEDIMENT AGGREGATES

Sediment Sample	Order of Aggregation	k_n,[a] cu cm/g	Density[b] g/cu cm	Shear Strength dynes/sq cm
Wilmington District	0	6.0	1.250	21
	1	14.4	1.132	9.4
	2	22.7	1.093	2.6
	3	31.1	1.074	1.2
Brunswick Harbor	0	10.2	1.164	34
	1	23.5	1.090	4.1
	2	36.7	1.067	1.2
	3	49.8	1.056	0.62
Gulfport Channel	0	8.8	1.205	46
	1	18.9	1.106	6.9[c]
	2	29.0	1.078	4.7
	3	39.0	1.065	1.8
San Francisco Bay	0	6.3	1.269	22
	1	10.0	1.179	3.9[c]
	2	13.7	1.137	1.4[c]
	3	17.5	1.113	1.4
	4	21.1	1.098	0.82[c]
	5	24.8	1.087	0.36
	6	28.5	1.079	0.20
White River (salt)	0	8.2	1.212	49
	1	18.2	1.109	6.8[c]
	2	28.2	1.079	4.7
	3	38.2	1.065	1.9

[a]The value k_n taken from curves in Figure 38.

[b]Density in sea water, ρ_ℓ = 1.025 g/cu cm.

[c]Based on N,(n-2) values shown in parentheses in Table VIII.

1. Aggregations of distinct character occurred in the viscometer at different ranges of shearing rates for any one sediment sample. Each kind of aggregation produced a linear shear—shearing rate plot characteristic of a Bingham fluid.

2. The distinct aggregations can be described as aggregations of primary particle aggregates, aggregations of primary particle aggregate aggregates, and so on. Primary particle aggregates are designated as zero order aggregates, aggregations of primary particle aggregates are designated as first order aggregates, aggregation of these are called second order aggregates, and so on. The volume fraction of any aggregation, $\Phi_{pna} = \Phi_{pa}(1+(n-1)\epsilon_1)$, $n = 1, 2, 3, \ldots$, where Φ_{pa} is the volume fraction of the particle aggregates, $(n-1)$ is the order of aggregation, and ϵ_1 is the ratio of interparticle aggregate pore volume to the volume of the particle aggregates in a first order aggregation.

3. The ratios of voids between particle aggregates to volume of particle aggregates, in first order aggregation, range from 1.0 to 1.4 for all of the sediments suspended in sea water except the samples from San Francisco Bay.

4. The shear strengths of the sediments suspended in sea water, τ_B, are

$$\tau_B = E_V' \, \Phi_{pa}^{5/2} ,$$

where E_V' is the energy per volume of particle aggregate required to disperse the mineral particles. E_V' depends on the order of aggregation and the character of the aggregates.

V. APPLICATIONS OF RHEOLOGICAL DATA

The formation of cohesive sediment shoals in an estuary depends on the rate of subsidence of suspended sediment material to the shoal surface, the adhesion of subsiding particles to the shoal surface and the stability of the shoal surface under subsequent flows. The rheological data presented in the preceding chapters bear directly on these processes of shoaling through their characterization of floc density and shear strength. Application of these data to descriptions of shoaling processes is the subject of this chapter.

The most general conditions of cohesive sediment shoaling appear to be those wherein flocs settle independently from a flowing suspension to the bed. Independent settling occurs at suspension concentrations less than about 0.01 g/cu cm. Suspended sediment concentrations above 0.01 g/cu cm are unlikely except in the vicinity of a working dredge, or in a turning basin or protected area where ships churn up sediment. Under these conditions "hindered" settling occurs. The consolidation of sediment by hindered settling has been described [2,10]. The shoaling processes described in this chapter are those in which the settling velocity of individual flocs, the flow near the bed, and the properties of the bed surface determine shoaling.

The Shoal Surface

It is evident that the shoal surface plays a central role in the interchange of sediment between a shoal and the suspension above. The properties of even a very thin layer on the shoal surface determine the properties of the shoal so far as a suspended particle is concerned, whereas the thickness of a weak surface layer can determine the amount of material that will be resuspended when the bed shear is increased by increasing flow.

The maximum thickness of a surface layer weaker than lower layers, such as those previously illustrated [2, Figure 28], can be calculated from the shear strengths presented in Table IX. The maximum thickness is determined by the depth at which the weight of the overlying particle skeleton can just crush the flocs. The downward stress, σ_1, at this depth is

$$\sigma_1 = \frac{\Phi_p}{\Phi_{pna}} (\rho_p - \rho_\ell) \, g \, h \, , \qquad (22)$$

where h is the thickness of the layer. Recalling that $\Phi_p/\Phi_{pna} = 2.5/\rho_p k_n$ for spherical flocs, Equation 22 can be replaced by

Preceding page blank

$$\sigma_1 = \frac{2.5(\rho_p - \rho_\ell)\ g\ h}{\rho_p k_n} \quad . \tag{22a}$$

For a cohesive material σ_1 is close to $\tau_{111} + 2\tau$, where τ_{111} is the lateral compressive stress. From consideration of Poisson's ratio, $\tau_{111} = K_s\tau_1$ [11], where K_s is called the "hydrostatic pressure ratio." Combining these relations lead to

$$\tau_1 = 2\tau/(1 - K_s) \ . \tag{23}$$

Combining Equations 22a and 23, and rearranging, gives

$$h = \frac{2\rho_p\ k_n\ \tau_B}{2.5(1 - K_s)(\rho_p - \rho_\ell)g} \quad . \tag{24}$$

A depth of 2.5 cm was observed for a surface layer on a bed of San Francisco Bay sediment [2, p. 72]. As indicated by penetrometer measurements, the shear strength increases to that of the next lower order at the bottom of the layer while the density changes only slightly. Assuming a 2.5 cm layer of first order aggregates on a zero order bed, and using the appropriate shear strength and density values shown in Table IX, Equation 24 yields a value for K_s of 0.93. If the surface layer is composed of successive higher orders, each having the same value for K_s, the calculated value would be slightly lower. Equation 24, together with the shear strength and density values given in Table IX, show that the thickness of flocculent layers having orders higher than zero should be no more than a few centimeters.

Since τ_B decreases rapidly and k_n increases linearly, the maximum thicknesses of layers having orders higher than the first should diminish with increasing order. After an accumulation of aggregates to the depth at which the deepest aggregates fail is reached, further accumulation will simply cause further failure at the bottom of the layer. The more consolidated material at the bottom of the layer is stronger and is better able to withstand erosion by later increased flows.

If a flocculent layer is left for a long period partial consolidation of the layer will occur, because of thermal activity of the particles, by a process of creep. The weight of overlying particles will aid the thermal energy, and consolidation at the bottom will proceed at a faster rate than that near the surface. This process is slow at normal temperatures, and probably is insignificant within normal tidal periods. For infrequent occurrences of high-bed shear, however, deposits formed between these occurrences can consolidate by this process. An excellent paper describing creep of clays has been presented by Mitchell [12].

Both of these mechanisms, crushing and slow rearrangement of deposited aggregates, account for continued accumulation of flocculent material under conditions of variable flows. During periods of low bed shears, some of the deposited material is crushed and forms a bed that is resistant to the subsequent higher bed shears. Even when the bed shear-time relation is symmetrical these mechanisms can facilitate deposition if the deposited layer is thick enough.

The shoal surface material, under conditions of deposition, will depend on the state of aggregation of the depositing particles, and on the applied shear. If the particles join the bed without breaking up, the bed surface is an aggregation one order higher than that of the settling aggregate. The highest order of aggregation a bed surface can have is determined by the bed shear existing during the period of deposition, so that, as shown in Table IX and demonstrated by the flume studies, the deposition of high order aggregates requires low-bed shears.

The Suspended Aggregate

Understanding of the transport of cohesive sediments in estuaries is made difficult by the alterations of the transported material resulting from local changes of hydraulic and suspended sediment conditions. These alterations consist of the growth or deterioration of aggregations, or flocs, of mineral particles. As shown in the last chapter, a floc of a given size can have several densities and shear strengths. Its resistance to erosion, its settling velocity, and its adherence to the bed depend on its size and order of aggregation. This section consists of a discussion of the effects of local hydraulic conditions on the suspended sediment aggregate.

Aggregation. In the portion of an estuarial region where the salinity is greater than one part per thousand, approximately, any collision of suspended mineral particles can result in a bond. Successive collisions of suspended particles result in a suspended particle composed of cohering mineral particles. The frequency of collisions on a suspended particle depends on the absolute temperature, the number of particles per unit volume, the sizes of the colliding particles, the local shearing rate, and on the difference of settling velocities of the colliding particles [13]. The absolute temperature changes only slightly in an estuary, and its effect can be considered constant. The frequency of collisions on a suspended floc is directly proportional to the number of flocs per unit volume. When collision results from the difference in velocity of two particles in a shearing fluid, the frequency of collision is also proportional to the sum of the two colliding particle radii cubed and to the local shearing rate. Because of the great effect of particle radii, larger particles tend to gather up smaller ones. As they continue to enlarge by this process they become increasingly effective. For this reason flocculation by internal shearing of the suspending water and the resuspension of flocculated particles are especially effective in promoting flocculation. When collision of particles results from their differences in settling velocities, the

differences in radii and densities are important. It is difficult to separate the effects of this mechanism from the effects of the others.

These processes and their importance in estuaries have been discussed in detail in an earlier report [2]. For this discussion it is sufficient to point out the importance to the rate of aggregation of suspended particles of particle concentration by number, the particle size, and the local shearing rate.

The concept of aggregation presented in the last chapter of this report leads to further descriptions of aggregates. These descriptions can be summarized in a few short statements:

1. When particles of the same order combine a homogeneous aggregate having the next higher order is formed.

2. When particles of adjacent orders combine a homogeneous aggregate having the higher order is formed.

3. When particles having more than one order difference combine the order at the surface can be lower than the order on the interior of the aggregate.

4. When any combination of cohesive particles occurs the resulting aggregate has a volume greater than the sum of the particle volumes, and the size is greater than the size of the largest particle.

5. When particles of different orders combine, the shear strength of the bond will probably be as great as that of the bond between particles of the lower order.

Statements one through four are direct consequences of the concept of aggregate construction presented in the last chapter. Statement five results from consideration of the exposure of the lower order aggregates in the surface of the higher order particle.

Particle Size. While the local internal shearing promotes aggregation, it also has a limiting effect when the shearing rate is high. An aggregate suspended in a shearing fluid rotates because of the velocity gradient. When the shear at the contact of two colliding particles, due to the force of the rotation, is greater than the shear strength of the material, the bond fails [2, p. 15]. A relation has been derived [2, p. 105] for estimating the particle radius at which the bond fails. Its derivation, with a correction, is outlined here for later use.

Consider a sphere radius R suspended in a fluid having a linear velocity gradient, du/dz. If the free stream velocity u at any distance from the center of the sphere normal to the direction of flow is z(du/dz), and the unit drag on any infinitesimal strip around the sphere is $3\eta u/2R$ (calculated by Stokes for a particle moving through a still fluid), then the torque available to rotate the sphere is

$$T = 2 \int_0^R \frac{3\eta}{2R} z \frac{du}{dz} 2\pi R dz \cdot z$$

from which

$$T = 2\pi\eta R^3 du/dz \ . \tag{25}$$

The shear force at the particle surface is T/R. For small interpenetrations, $2\Delta R$, of colliding spherical flocs the area of contact is $2\pi R\Delta R$. The shear, τ_{max}, for the maximum sized floc that will stick to another is the shear force divided by the contact area. Neglecting the loss of T due to mutual shielding, this calculation leads to

$$R = \frac{\tau_{max} \Delta R}{\eta \ du/dz} \ . \tag{26}$$

Values of τ_{max} are presented in Table IX.

When a floc attains the radius given by Equation 26 it should no longer be able to attach itself to larger flocs but should continue to gather much smaller ones. As more of the flocs approach this size the number of collisions resulting in bonds should fall, and the flocs should become more uniform in size.

The derivation above is based on the assumption that Stokes' traction is valid in a shearing region and that the bond failure follows the idealized mechanism for a spherical floc. Such an application of Stokes' relation has not been demonstrated directly. It does lead to a dimensionally correct relation, Equation 26, that has been found to describe observed sizes [2, p. 18] with reasonable values of ΔR.

Particle Shear Strength. The shear strength of a suspended floc is at least great enough to resist the drag of water on its surface. The surface drag on a suspended floc can be illuminated by the following argument:

A sphere suspended in water undergoing shear will rotate about an axis in the plane of shearing and normal to the direction of flow. The rotation results from the differences in velocity above and below the axis of rotation. The rotation will be resisted by drag of the water on the upstream and downstream faces of the sphere because of the difference between its surface movement and that of the liquid. This drag will produce a disturbance in the velocity distribution over the entire surface of the sphere so that the drag causing the rotation just equals the drag resisting it. The disturbance in flow pattern due to

the resistance to rotation can be taken to be the flow pattern around a slowly rotating sphere in an infinite still fluid. Lamb [14] gives the torque necessary to maintain rotation of a sphere in an infinite still fluid as

$$T = 8\pi\eta\, R^3\omega \ , \tag{27}$$

where ω is the angular velocity of rotation of the sphere.

Equating 25 and 27 yields

$$\omega = \frac{1}{4}\frac{du}{dz} \ , \tag{28}$$

showing that the rotation rate depends only on the shearing rate. This result can be approximated by inspection. If only the shears at the top and bottom and front and back extremities of the sphere are considered, ω would be half of the shearing rate. Since the drag of the shear on the remainder of the sphere is less than this, the coefficient should be less than one half.

The maximum shear on a floc surface due to the drag from rotation can be calculated by considering the drag on the edge of a thin disc at the equator. Following the procedure for deriving Equation 9, the shear around the disc is

$$\tau = T'/2\pi r^2 dy \ . \tag{29}$$

The shear in the fluid is

$$\tau = \eta\left(\frac{dq}{dr} - \frac{q}{r}\right)$$

with

$$q = 0 \text{ at } r = \infty$$

$$q = \omega R \text{ at } r = R \ . \tag{30}$$

Combining Equations 29 and 30 and solving yields

$$T' = \pi\eta dy\ \omega\, R^2 \ . \tag{31}$$

Substituting the right hand side of Equation 31 for T' in Equation 29 leads to

$$\tau = \eta\, \omega/2 \ .$$

Using the ω shown in Equation 28 gives

$$\tau = \frac{1}{8}\, \eta\, \frac{du}{dz} \qquad (32)$$

for the maximum shear stress on a suspended floc. Equation 32 is dimensionally correct. The coefficient is reasonable in view of the freedom a suspended floc has to move so that the drag forces can adjust to the minimum over its surface. The linear superpositions used in obtaining Equation 32 are less crude than the assumption of spherical shape.

The argument above emphasizes the fact that a suspended floc can have a lower shear strength than does a fixed bed exposed to water having the same shearing rate. It also shows that the floc size is independent of the shearing rate provided that its shear strength is sufficient to allow its growth. A floc grown in water having a low shearing rate then moved into a region having a significantly higher one, however, could be broken up if a higher order, weaker floc had grown at the lower shearing rate.

Particle Density. The density of a floc is shown in the last chapter to depend on the particle aggregate density, the porosity increase on the first aggregation of particle aggregates, and on the order of aggregation. The difference in density between a spherical suspended flocculent particle and the suspending liquid can be found, by combining Equations 6 and 16, to be

$$\rho_f - \rho_\ell = 2.5(\rho_p - \rho_\ell)/\rho_p\, k_1\, (1 + (n-1)\epsilon_1) \ . \qquad (33)$$

Both k_1 and ϵ_1 can be found in Figure 38. The order of aggregation, however, will be limited by the prevailing shearing rate, as described above.

Particle Settling Velocity. Because of the small size and low density the settling velocity, v_s, of a spherical floc in still water is usually given by Stokes' Law:

$$v_s = 2\left(\rho_p - \rho_\ell\right) g\, R^2/9\eta \ . \qquad (34)$$

The difference between particle and water densities, and the particle radius are given in terms of particle properties and the hydraulic conditions in the paragraphs above. Following custom and the procedure used in this report, R is the radius of an equivalent sphere. Examples of application of Stokes' law are given below.

Shoaling

The understanding of shoaling processes provided by knowledge of floc properties can be presented best with the aid of an example. Consider a uniform channel 30 feet deep with uniform open-channel flow. Typical characteristics of flow in such a channel at average velocities in areas of shoaling [2] are given in Table X.

TABLE X

AVERAGE SHEARING RATES IN A CHANNEL 30 FEET DEEP

Average Velocity fps	Average Shearing Rate sec^{-1}	Shearing Rate[a] at Bed sec^{-1}	Shear on Bed[a] dynes/sq cm
0.1	0.56	0.93	0.0093
0.2	0.16	3.7	0.037
0.5	0.62	23	0.23
1.0	1.8	93	0.93
2.0	5.0	370	3.7
3.0	8.8	780	7.8
4.0	14	1500	15

[a] $\tau = \eta_\ell \, du/dz$.

The second column in Table X shows that the average shearing rate in the flow is low; even at the flow rate of 4 ft/sec the average shearing rate is only 14/sec. Most of the shearing occurs close to the bed, so that the shearing in a large portion of the flow is much less than the average given in column two. Since the flocculation of sediment at the concentrations normally existing in estuaries is directly proportional to the shearing rate, sediment suspended in such flow is reasonably stable. When the shearing rate in the flow is increased, such as by passing the flow through pilings or by mixing due to density changes in the profile or by sudden enlargements in a channel, flocculation is accelerated and settling velocities of the sediment are increased. Once flocs have grown they will not be ruptured so long as they stay sufficiently high above

the bed, even at high flows. The shearing rate at the bed, shown in column three, increases much faster with increasing flow. High order aggregates settling into this shearing would be broken up, at least at the higher flows.

Consider a channel in San Francisco Bay, with the flow characteristics shown in Table X, that carries tidal flows with a maximum velocity of 3.0 ft/sec. At this maximum flow the shearing rate in most of the flow will be less than 8.8/sec. By Equation 32 the shear on the suspended floc will be less than 0.011 dynes/sq cm. According to Table IX this floc can have an order of six or perhaps seven. If it settled to the viscous layer at the bed surface, where the shear stress on a suspended floc is one dyne/sq cm, it would be broken into third-order pieces.

The third-order aggregates that find their way back up into regions having lower shearing rates can recombine if they are sufficiently small. By Equation 26, with a shearing rate of 8.8/sec, and a ΔR of 2μ, the largest particle that could combine with a larger particle has a radius of 32μ. Growth to more than twice this size seems unlikely at low suspended sediment concentrations. The 32μ third-order particle would have a settling velocity, by Equation 34, of 0.0196 cm/sec. A fourth-order aggregation of the third-order flocs having twice the radius would settle at 0.065 cm/sec. When such a floc settled to the boundary layer it would break to third-order fragments again. It is evident that the viscous boundary layer establishes a base order for subsequent floc formation above it, and that recombination above the boundary layer increases the rate an aggregation would return to be disrupted.

Base order aggregates can grow from lower order aggregates. In the example above, the third-order aggregates can become larger by accumulating second or lower order aggregates. Such growth would occur only on the addition of sediment material to the flow.

The two effects of shearing rate on suspended cohesive particles should be recalled when considering transport of such particles. While low shearing rates permit the existence of large, high order aggregates, they provide little opportunity for flocs to combine. Unless the time for recombination is long or unless the suspended sediment concentration is high, large aggregates will not form. A region having a transition from high to low shearing rates, such as that in a channel as a particle moves upward from the bed, however, provides both shearing to promote flocculation and a diminishing shearing rate as the floc grows. If the concentration of suspended sediment is sufficiently large, flocs can form. Shearing due to the bed promotes the regrowth of flocs that settle back into the region of high shearing and most of the transition in shearing occurs in only a small portion of the flow near the bed. In a uniform open channel flow of a dilute sediment suspension both the disruption and formation of flocs takes place near the bed, with relatively inactive flocs suspended higher in the flow.

The discussion above emphasizes the importance of shearing near the bed in limiting the aggregation of particles. Shearing at the bed similarly determines the character of a bed surface. As shown in

column four, Table X, typical bed shears in a navigable estuarial channel can exceed the strength of all but zero order beds. (A bed is an aggregation of particles. The concept of order was extended to the bed surface in deriving Equation 24, and is supported by photomicrographs [2].) The order of a bed is one higher than the order of the particles making it up. If flocculent particles simply settle in still water the order of the bed surface would be one higher than that of the particles.

When the bed is undergoing shear, however, the order of the bed surface during deposition is at least low enough to withstand the shear. The order of the bed surface will be even lower if the suspended flocs have orders two or more lower than that of the highest order bed that will resist the shear. If the suspended particles have an order higher than that of the bed, contact with the bed can leave a portion of the particle on it or take some of the bed back into suspension. Interchange of suspended and deposited material was demonstrated using radioactive tracers [2, p. 45]. As postulated by Statement 5 in the paragraph on aggregation, above, a bond between a bed and a higher order floc can have the strength of the bed. Interchange would selectively leave the more strongly bonded material on the bed.

This description of bed formation is supported by data obtained during scour of beds that had been deposited under a variety of flow conditions in a recirculating flume [2, p. 79]. These data were obtained long before the concept of orders of aggregation was found, and they show the concentrations of suspended sediment at various bed shears. The concentration is roughly proportional to the total depth of bed scour. Plots of these data can be fitted by several straight lines that intersect the zero concentration line, the abscissa, at the shear strengths of first, second or third, fourth, and the fifth order aggregates. The lines show increasing strength with depth, which would result from floc deformation due to skeletal overburden pressure.

It appears from these data that the rate of scour reflects the properties of the bed. Interchange of suspended material and material in the bed surface was observed during scour, as well as during deposition. Evidence of armoring, or development of an increasingly resistant surface, during scour was also observed. These observations, together with the observations of floc properties, lead to the conclusion that scour of a bed is resisted by filling pores in the surface of the bed with suspended material. This process can be viewed as a tendency toward the formation of a lower order bed as required by the higher bed shear, and it accounts for the slow rates of scouring observed at moderate shears.

Conclusions

Application of the information on floc properties to any particular system will require information on the hydraulic regime and the suspended sediment concentration and properties. The foregoing discussion leads, however, to several conclusions that apply generally to transport and shoaling processes. They can be summarized as follows:

1. A suspended floc can have any one of several orders. The order is determined by the growth history or the shearing, whichever is limiting.

2. The size of a suspended floc is independent of its order, except that an increase in order requires an increase in size, and conversely.

3. An increase in order produces an increase in settling velocity, and conversely.

4. During deposition the bed surface strength is determined by the bed shear or by the order of aggregation of the depositing floc.

5. The strength of the bed below the surface is determined by the order formed during deposition and by the subsequent deformation or collapse resulting from overburden pressure.

6. The shearing rates in normal flows, except those near interfaces, are low compared to that shearing rate necessary to disrupt flocs of high order.

7. The relatively high shearing rates near the bed limit the order of aggregation of flocs suspended in flowing water.

8. At low bed shears high order flocs can deposit. If the deposit is sufficiently thick the increase in strength due to overburden pressure can prevent subsequent resuspension by increased flows.

VI. SUMMARY AND CONCLUSIONS

Conclusions appropriate to the material in each chapter are presented at the ends of the chapters. In this chapter a summary of the methods of study and the results are presented, together with recommendations for subsequent investigations.

Sediments from deposits in several representative estuaries were examined for mineral content and particle size distribution, and were found to contain large amounts of clay minerals. The clay mineral composition varied among the sediments in relative abundance of the principal minerals montmorillonite, kaolinite, and illite. The clay minerals account for the cohesive character of the sediments studied, and their relative abundances determine the porosities and strengths of aggregations of the mineral particles.

The porosities and shear strengths of sediment aggregations were obtained from measurements of rheological properties of suspensions over a range of sediment concentrations, and at varying shearing rates. An Ostwald-type capillary viscometer, equipped with variable driving pressures, was used for measurements at high shearing rates, and a concentric cylinder viscometer with a wide annular gap was constructed for measurements at low shearing rates.

Interpretation of the data from the rheological measurements was facilitated by Bingham's hypothesis and Einstein's viscosity relation. A relation was derived by H. A. Einstein based on Bingham's hypothesis, for relating the drag and rotation speeds in a wide-gap concentric cylinder viscometer to the shear strength and differential viscosity of a suspension. Separation of fluid from solid friction by Bingham's hypothesis allowed separate interpretations of shear strengths of the suspended aggregates and of the viscosities of the suspensions. Einstein's relation, derived for an infinitely dilute suspension, was extended to a logarithmic form to accommodate the concentrations of suspended particles of interest to this study. The data support the extension, and with it was obtained information on densities and porosities of sediment aggregates. Both the shear strengths and the densities of the suspended aggregates of estuarial sediments were thereby obtained.

Measurements with the wide annular gap concentric cylinder viscometer showed that each of the suspended sediments can aggregate in several ways, depending on the shearing rate and the history of the suspension. A description of aggregates was devised that is based on the concept of combinations of simple aggregations of primary mineral particles. When such clusters of mineral particles, designated zero order aggregates, combine with one another they form first order aggregates that have larger volume or lower density because of the pore space between the zero order aggregates. Second order aggregates, formed by combination of the first order aggregates, have an even lower density.

Preceding page blank

Successive orders have successively lower densities and, because the shear strength depends on the interaggregate bonds within a higher order aggregate, the shear strength also decreases with increasing order of aggregation. A quantitative relation, based on this concept and with assumptions regarding intermeshing of joining aggregates, was derived and was found to describe the porosity or density for any order of aggregation in terms of the zero order aggregate density and the void ratio for first order aggregates.

The shear strengths for primary aggregates, measured using the capillary viscometer, were found to relate to the shear strengths of higher order flocs measured using the concentric cylinder viscometer when the character of the interaggregate contact was taken into consideration. This relation facilitated construction of a table of shear strengths for several orders of aggregation of each of the estuarial sediments (Table IX, p. 74).

Finally, a short chapter describes methods and examples of applications of floc shear strength and density data to suspended flocs and to cohesive sediment beds. The information on flocculent sediment properties obtained in this study was found to explain properties of sediment beds observed during an earlier study.

The conclusions and other material presented in each chapter can be summarized by the following:

1. Cohesive sediment aggregates can occur in distinct orders. The shear strength and density of the aggregates are reduced as order is increased.

2. Rheological measurements on sediment suspensions can provide aggregate shear strengths and densities provided that a viscometer with a sufficient thickness of shearing fluid, sufficient sensitivity, and an adequate range of shearing rates is used.

3. The shear strengths of sediment aggregates are very weak, but are adequate to make aggregates the significant form of sediment in estuarial transport processes.

Measurements of rheological properties of cohesive materials should continue until experience with a wider range of materials and a thorough understanding of the process of flow of such materials are obtained. A program of measurements of properties of suspended and deposited sediments in estuaries is needed also to establish the local hydraulic and sediment conditions around shoals and to relate sediment properties to shoaling. Knowledge of such relations will enable the best designs of harbors and channels, and will provide guides for economical maintenance of waterways.

REFERENCES

1. First Annual Progress Report on the Silt Transport Studies Utilizing Radioisotopes. Univ. of Calif., Hydraulic Eng. Lab., and Sanit. Eng. Research Lab., December 1957.

2. Flume Studies of the Transport of Sediment in Estuarial Shoaling Processes. Univ. of Calif., Hydraulic Eng. Lab., and Sanit. Eng. Research Lab., June 1962.

3. Einstein, H. A. The viscosity of highly concentrated underflows and its influence on mixing. Trans. Amer. Geophys. U., Hydrology, p. 597, 1941.

4. Poiseuille, J.L.M. Experimental researches on the motion of liquids in tubes of very small diameter. Mem. Acad. Roy. Sci. 9:433-543, 1846.

5. Bingham, E. C. Fluidity and Plasticity. New York: McGraw-Hill Book Co., Inc., 1922.

6. Einstein, A. A new determination of molecular dimensions. Ann. Phys. 19:289-306; 34:591-92, 1911.

7. Van Olphen, H. Forces between suspended bentonite particles, Clays and Clay Minerals, Pub. 456, NAS-NRC, pp. 204-24, 1956.

8. Mallock, H.R.A. Experiments on fluid viscosity. Trans. Roy. Soc. London A187:41-56, 1896.

9. Taylor, G. I. Fluid friction between two rotating cylinders. Proc. Roy. Soc. London A157:546-73, 1936.

10. Michaels, A. S., and Bolger, J. C. Settling rates and sediment volumes of flocculated kaolin suspensions, I&EC, Fund. 1:24-33, 1962.

11. Krynine, D. P. Soil Mechanics. New York. McGraw-Hill Book Co., Inc., 1941.

12. Mitchell, J. K. Shearing resistance of soils as a rate process. ASCE J. Soil Mech. and Foundations, SMI, Div. 90:29-61, January 1964.

13. Kruyt, H. R. (editor). Colloid Science, VI, Irreversible Systems, Elsevier, 1952.

14. Lamb, H. Hydrodynamics, Cambridge Univ. Press, 1906.